(2)

A Final Report
Contract No. N00014-85-K-0526

October 1, 1987 - December 24, 1990

PLASTIC BEHAVIOR OF Al-Li-X ALLOYS

Submitted to:

Office of Naval Research
800 N. Quincy Street
Arlington, VA 22217-5000

Attention:

Dr. George R. Yoder, Program Manager
Materials Division, Code 1131

Submitted by:

E. A. Starke, Jr.
Earnest Oglesby Professor of
Materials Science and Dean

Report No. UVA/525400/MS92/103
July 1991

DEPARTMENT OF MATERIALS SCIENCE

SCHOOL OF
ENGINEERING
& APPLIED SCIENCE

University of Virginia
Thornton Hall
Charlottesville, VA 22903

UNIVERSITY OF VIRGINIA
School of Engineering and Applied Science

The University of Virginia's School of Engineering and Applied Science has an undergraduate enrollment of approximately 1,500 students with a graduate enrollment of approximately 600. There are 160 faculty members, a majority of whom conduct research in addition to teaching.

Research is a vital part of the educational program and interests parallel academic specialties. These range from the classical engineering disciplines of Chemical, Civil, Electrical, and Mechanical and Aero-.pace to newer, more specialized fields of Applied Mechanics, Biomedical Engineering, Systems Engineering, Materials Science, Nuclear Engineering and Engineering Physics, Applied Mathematics and Computer Science. Within these disciplines there are well equipped laboratories for conducting highly specialized research. All departments offer the doctorate; Biomedical and Materials Science grant only graduate degrees. In addition, courses in the humanities are offered within the School.

The University of Virginia (which includes approximately 2,000 faculty and a total of full-time student enrollment of about 17,000), also offers professional degrees under the schools of Architecture, Law, Medicine, Nursing, Commerce, Business Administration, and Education. In addition, the College of Arts and Sciences houses departments of Mathematics, Physics, Chemistry and others relevant to the engineering research program. The School of Engineering and Applied Science is an integral part of this University community which provides opportunities for interdisciplinary work in pursuit of the basic goals of education, research, and public service.

A Final Report
Contract No. N00014-85-K-0526

October 1, 1987 - December 24, 1990

PLASTIC BEHAVIOR OF Al-Li-X ALLOYS

Submitted to:

Office of Naval Research
800 N. Quincy Street
Arlington, VA 22217-5000

Attention:

Dr. George R. Yoder, Program Manager
Materials Division, Code 1131

Submitted by:

E. A. Starke, Jr.
Earnest Oglesby Professor of
Materials Science and Dean

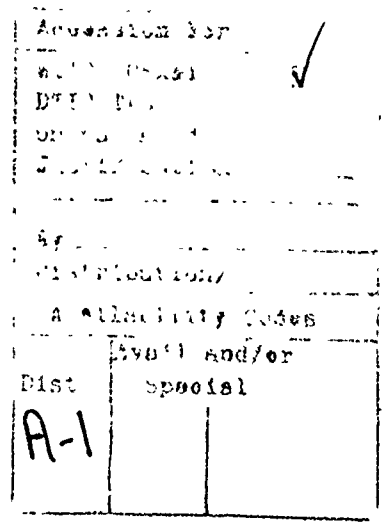

Department of Materials Science
SCHOOL OF ENGINEERING AND APPLIED SCIENCE
UNIVERSITY OF VIRGINIA
CHARLOTTESVILLE, VIRGINIA

Report No. UVA/525400/MS92/103
July 1991

Copy No._____

REPORT DOCUMENTATION PAGE

Form Approved
OMB No. 0704-0188

1. AGENCY USE ONLY (Leave blank)	2. REPORT DATE	3. REPORT TYPE AND DATES COVERED
	July 1991	Final Report - 1 Oct. 87 - 24 Dec. 90

4. TITLE AND SUBTITLE
Plastic Behavior of Al-Li-X Alloys

5. FUNDING NUMBERS
N00014-85-K-0526

6. AUTHOR(S)
E. A. Starke, Jr.

7. PERFORMING ORGANIZATION NAME(S) AND ADDRESS(ES)
University of Virginia
School of Engineering and Applied Science
Department of Materials Science
Thornton Hall
Charlottesville, VA 22903-2442

8. PERFORMING ORGANIZATION REPORT NUMBER
UVA/525400/MS92/103

9. SPONSORING/MONITORING AGENCY NAME(S) AND ADDRESS(ES)
Department of the Navy
Office of the Chief of Naval Research
800 North Quincy Street
Arlington, VA 22217-5000 Code 1513:BSM

10. SPONSORING/MONITORING AGENCY REPORT NUMBER

11. SUPPLEMENTARY NOTES

12a. DISTRIBUTION/AVAILABILITY STATEMENT
Unlimited

12b. DISTRIBUTION CODE

13. ABSTRACT *(Maximum 200 words)*

The major objectives of this program were to characterize the microstructure, strengthening, deformation and fracture modes of Al-Li-X alloys with emphasis on determining the relationships between alloying elements, processing parameters, microstructure, deformation modes and fracture behavior. In order to reach these objectives the following tasks were undertaken. (A) The literature on Al-LI alloys was reviewed and major problem areas were identified. (B) Since one of the advantages of Al-Li alloys is their higher modulus, a study was conducted on the dependence of the modulus on the various types of precipitates that occur in these age-hardenable alloys. (C) One major problem area associated with Al-Li alloys has been their low fracture toughness in the short transverse direction. The low fracture toughness and ductility in this direction also appears to cause delamination along the high angle grain boundaries which are parallel to the processing direction. The effects of texture, deformation mode, and precipitate free zones on this phenomenon at both room and cryogenic temperatures were examined. (D) It has been shown that in order to maximize the strength-fracture toughness properties of Al-Li-X alloys, cold work prior to aging is necessary in order to provide nucleation sites for the strengthening precipitates, to accelerate aging and to minimize the detrimental grain boundary precipitates and associated precipitate free zones. One alternative method of accomplishing the same result is to add trace alloy additions. The role that the trace addition plays on the precipitation in age-hardenable aluminum alloys was examined.

14. SUBJECT TERMS
Al-Li-X alloys, age hardening fracture trace additions effects

15. NUMBER OF PAGES
18 plus appendix

16. PRICE CODE

17. SECURITY CLASSIFICATION OF REPORT	18. SECURITY CLASSIFICATION OF THIS PAGE	19. SECURITY CLASSIFICATION OF ABSTRACT	20. LIMITATION OF ABSTRACT
Unclassified	Unclassified	Unclassified	UL

TABLE OF CONTENTS

PLASTIC BEHAVIOR OF Al-Li-X ALLOYS

I. ABSTRACT

The major objectives of this program were to characterize the microstructure, strengthening, deformation and fracture modes of Al-Li-X alloys with emphasis on determining the relationships between alloying elements, processing parameters, microstructure, deformation modes and fracture behavior. In order to reach these objectives the following tasks were undertaken. (A) The literature on Al-Li alloys was reviewed and major problem areas were identified. (B) Since one of the advantages of Al-Li alloys is their higher modulus, a study was conducted on the dependence of the modulus on the various types of precipitates that occur in these age-hardenable alloys. (C) One major problem area associated with Al-Li alloys has been their low fracture toughness in the short transverse direction. The low fracture toughness and ductility in this direction also appears to cause delamination along the high angle grain boundaries which are parallel to the processing direction. The effects of texture, deformation mode, and precipitate free zones on this phenomenon at both room and cryogenic temperatures were examined. (D) It has been shown that in order to maximize the strength-fracture toughness properties of Al-Li-X alloys, cold

work prior tc aging is necessary in order to provide nucleation sites for the strengthening precipitates, to accelerate aging and to minimize the detrimental grain boundary precipitates and associated precipitate free zones. One alternate method of accomplishing the same result is to add trace alloy additions. The role that the trace addition plays on the precipitation in age-hardenable aluminum alloys was examined.

II. INTRODUCTION

Many alloys derive their strength in part from the homogeneous distribution of coherent or non-coherent second-phase particles. Accurate predictions of the yield strengths of precipitate hardened alloys are based on the well understood interaction of a dislocation with a particle at the microscopic level. However, precipitate hardened alloys also exhibit low ductility and low fracture toughness, features that also must depend on the presence of the second-phase particles. This problem is less well understood.

Age hardenable aluminum alloys in particular may undergo relatively brittle intergranular fracture at strains from 2 to 10 times smaller than the strain to fracture for pure aluminum. This phenomenon can be explained in broad terms as follows. Within a grain, an advancing dislocation either bypasses the coherent particles it encounters or cuts through them; cutting reduces the effective size of the obstacle, while bypassing the obstacle effectively enlarges it. If the obstacles are cut, the weakened plane will continue to slip and deformation will be localized. As a result, dislocations pile up at the grain boundaries at isolated points; the large associated tensions across the grain boundaries open intergranular cracks that propagate without absorbing much energy. Slip becomes more localized as the size of the included particles increases and as the grain size increases. Aluminum-lithium alloys are

particularly prone to strain localization because of the shearable nature of some of the strengthening precipitates and grain-refining dispersoids, the very sharp deformation texture that develops in these alloys, and the presence of grain boundary precipitates and associated precipitate free zones.

This document is our Final Report on Office of Naval Research Contract No. N00014-85-5-0526 (85-K-0526), "Plastic Behavior of Al-Li-X Alloys." The major objectives of this program have been to characterize the microstructure, deformation, and fracture modes of Al-Li-X alloys with emphasis on determining the relationships between the alloying elements, processing parameters, microstructure, and deformation and fracture behavior. The research results obtained on this program should aid in the development of Al-Li-X (or other high strength aluminum alloys) having density, strength, stiffness, ductility and high temperature combinations needed for high performance naval aircraft.

III. ACCOMPLISHMENTS

A. A Review of the Microstructure and Properties of Aluminum-Lithium Alloys: The advantages to be gained by weight reduction of aerospace structures have encouraged the aluminum industry to develop a family of aluminum alloys which contain lithium as one of the alloying elements. When alloyed with aluminum, lithium can reduce the density by approximately three percent and increase the elastic modulus by six percent for every weight percent added. A new series of aluminum alloys, typified by 2090, 2091, 8090, and 8091, have been developed and are currently being produced in commercial quantities. These alloys have densities between 7% and 10% lower than the conventional alloy 7075 with correspondingly higher stiffness. Although a combined set of specific properties of the Al-Li-X alloys often exceeds those of the conventional aluminum materials used in aerospace, these properties seem to be much more sensitive to processing parameters. The strong processing-property relationship is associated with sharp crystallographic textures that are develcped during primary processing and very complex precipitate microstructures whose distributions are sensitive to quench rates and degree of deformation prior to aging. Our review of this topic resulted in the following two publications which are included in the Appendix:

1. Edgar A. Starke, Jr., and William E. Quist, "The Microstructure and Properties of Aluminum-Lithium Alloys," AGARD

Lecture Series No. 174, New Light Alloys, North Atlantic Treaty Organization, 1990, p. 2-1.

2. E.A. Starke, Jr. and H.G.F. Wilsdorf, "New Low Density and High Temperature Aluminum Alloys," presented at the First Thermal Structures Conference, November 13-15, 1990, University of Virginia, Charlottesville, Virginia. To appear in the AIAA Progress Series in Aeronautics and Astronautics (1992).

B. **Dependence of Elastic Modulus on Microstructure in 2090-Type Alloys:** The Young's modulus, shear modulus and Poisson's ratio were determined using an ultrasonic pulse echo technique. Three commercially fabricated aluminum-copper-lithium alloys and an aluminum-lithium binary alloy were examined. The elastic properties were measured as a function of aging time, aging temperature, amount of stretching and testing direction. An increase in Young's modulus due to δ' and T_1 precipitation has been measured and treated quantitatively including precipitation kinetics. A significant decrease of about 5% in the modulus of elasticity was found in the peak-aged condition. This decrease can be attributed to precipitation of the T_2 phase. The shear modulus behaves similar to Young's modulus while the Poisson's ratio remains unchanged. There is no significant orientation dependence of the elastic properties on testing direction despite the fact that a typical rolling texture was present. This study resulted in the following publications which are included in the Appendix:

3. E. Agyekum, W. Ruch, E.A. Starke, Jr., S.C. Jha and

T.H. Sanders, Jr., "Effect of Precipitate Type on Elastic Properties of Al-Li-Cu and Al-Li-Cu-Mg Alloys," Aluminum-Lithium Alloys III, ed. by C. Baker, P.J. Gregson, S.J. Harris and C.J. Peel, The Institute of Metals, London, 1986, p.448.

4. M.E. O'Dowd, W. Ruch and E.A. Starke, Jr., "Dependence of Elastic Modulus on Microstructure in 2090-Type Alloys," Journal de Physique, Colloque C3, September, 1987, p. C3-565.

C. **Fracture Toughness and Delamination Behavior of Al-Li-X Alloys:** Rolled plate of 2090- and 8090-type Al-Li alloys may have a tendency to form delamination cracks extending in the rolling direction during fracture. Some authors have suggested that the delamination phenomena increases the conventional fracture toughness due to 'delamination toughening', i.e. the L-T, L-S and T-S oriented specimens show higher fracture toughness than S-L and S-T specimens. Moreover, recent research indicates that the cryogenic fracture toughness in the L-T orientations is higher than at room temperature and is accompanied by an increase in the yield strength, UTS, strain to fracture and strain hardening exponent. We have investigated the effect of aging treatment on the fracture toughness of 2090 and 8090 at room temperature and liquid nitrogen temperature. The fracture toughness samples at liquid nitrogen temperature exhibited deeper and larger numbers of delaminations normal to the crack plane at all aging conditions and in both alloys. Fractography of the samples revealed the fracture mechanism to be slip band decohesion at both ambient and liquid nitrogen temperatures.

However, the transgranular shear band facets were observed to be consistently wider at 77K. Transmission electron microscopy of thin foils obtained from fractured tensile samples showed wider slip bands and smaller slip band spacing at 77K. These results are consistent with the observations made by other researchers who observed higher strain hardening exponents and wider slip bands with small spacing associated with higher fracture toughness.

Our results suggest that the fracture toughness improvement at liquid nitrogen temperature could be explained by the deformation processes that occur in the Al-Li-X alloys. We observed that the increase in strain hardening capacity and total elongation at 77K is related to wider slip bands and smaller slip band spacings. At 300K where slip localization is more prevalent, i.e. narrower slip bands and larger spacings, a decrease in the strain hardening exponent and fracture strain occurs. In notched specimens, such as a compact tension specimen, the crack initiation process is controlled by the deformation process ahead of the crack tip. For a critical strain controlled fracture process, the ability to concentrate strain in the slip bands is a critical factor. When slip is dispersed, such as at 77K, larger numbers of wider slip bands accommodate strain whereas at 300K when slip is localized, fewer and narrower slip bands accommodate strain. Thus at 77K, the critical strain in one of the potential slip bands where cracks initiate is reached at a later stage when compared to that at

300K. Our first attempt to develop a model to describe this phenomenon (K.V. Jata and E.A. Starke, Jr., "Fatigue Crack Growth and Fracture Toughness Behavior of an Al-Li-Cu Alloy", Met. Trans. A. 17A, 1986, p. 1101) resulted in the equation

$$K_{1c} = [8\ Sin\ \alpha E \sigma_{ys} W (\frac{D}{d}) \gamma_{SB}^{c}\ ]^{1/2}$$

where K_{1c} is the plane strain fracture toughness, α the angle between the stress axis and the slip band, E is Young's modulus, σ_{ys} is the yield strength, W the width of the slip band, D the plastic zone size, γ_{SB}^{c} the critical strain to fracture in the slip band, and d the slip band spacing. This expression has recently been modified (H.J. Roven and E.A. Starke, Jr., "Microstructural Effects on Fatigue and Fracture Behavior at Cryogenic and Room Temperature of an Al-Li 8090 Alloy", to be presented at the 6th ICM, Japan, August, 1991, and published in the proceedings of the conference) to the following expression:

$$K_{1c} = (\frac{2\ D^2\ W\ \sigma_{ys}\ E}{M \tan\alpha\ d^2})^{1/2}$$

where D is now the average grain diameter, M the crystallographic orientation factor, and α the average angle between the macroscopic crack path and the direction of the slip

bands extending from the crack tip. The other parameters are as described previously. Both of these expressions appear to describe the experimental results.

We have also examined the influence of precipitate free zones and variations in the relative misorientations between grains in the S-direction on the delamination behavior of an 8090-type alloy at cryogenic and room temperature. Two conditions were investigated, i.e., one condition having a wide PFZ and the other condition with no PFZ. We used the EBSP technique in the SEM for micro-texture measurements. Again our study showed that the tensile, fracture and strain hardening properties increase as the test temperature decreases from room temperature to 77K. The delamination behavior could be characterized by (i) a 'fine delamination' whose spacing depends on both the aging condition and test temperature, and (ii) a 'coarse delamination' whose spacing varied both with aging condition and test temperature. However, the coarse spacing was roughly equal for the two conditions at 77K. The spacing of the 'fine delamination' correlated very closely to periodical events of high to low relative misorientations of grains in the S direction, which suggests that the grain boundaries which represent high misorientations across the grains serve as barriers to the dislocations in the slip bands and thus aid in the initiation of cracks at the boundaries. The fracture process of the PFZ-containing condition included slip localization both in slip bands and in the PFZs giving

intergranular failure. In the PFZ-free condition the fracture process was dominated by slip localization in slip bands which also resulted in slip band decohesion. The latter condition had better cryogenic properties than the PFZ-containing microstructure.

This study resulted in the following publications which are included in the Appendix:

5. K.V. Jata and E.A. Starke, Jr., "Fracture Toughness of Al-Li-X Alloys at Ambient and Cryogenic Temperatures," Scripta Metallurgica, Vol. 22, 1988, p. 1553.

6. H.J. Roven, E.A. Starke, Jr., O. Sodahl, and J. Hjelen, "Effects of Texture on Delamination Behavior of a 8090-Type Al-Li Alloy at Cryogenic and Room Temperature," Scripta Metallurgica, Vol. 24, 1990, p. 421.

7. C.P. Blankenship, Jr., H.J. Roven and E.A. Starke, Jr., "The Fracture and Fatigue Behavior of Al-Li-X Alloys," Fatigue 90, ed. by H. Kitagawa and T. Tanaka, Materials and Component Engineering Publications Ltd, Birmingham, England, 1990, p. 937.

D. **The Role of Trace Alloy Additions on Precipitation in Age-Hardenable Aluminum Alloys:** The application of most age-hardenable aluminum alloys requires that they have both high strength and fracture toughness. Studies have shown that this is best accomplished when the strengthening phases are fine and uniformly distributed throughout the matrix and there is a minimum of coarse grain boundary precipitates. Often a preaging deformation is applied to promote nucleation of the

strengthening phases by providing nucleation sites in the form of dislocation structures. The preaging deformation also affects the aging kinetics in such a way that the time at the aging temperature can be reduced which reduces the volume fraction and size of the deleterious grain boundary precipitates. For some alloy systems and/or product forms a preaging deformation is impractical and other methods must be utilized. In many aluminum alloys trace element additions may stimulate nucleation of finer dispersions of strengthening precipitates. Such potential benefits have been known for many years although there is no consistent theory to explain the effects of such additions to aluminum alloys.

We have reviewed the literature on this topic and have conducted our own experiments on the affect of trace element additions on precipitation in aluminum alloys. The results of this task confirms that trace element additions in aluminum alloys can have a profound effect on the rates at which precipitates form. Also, the effect on nucleation rates is not due to a single mechanism but involves augmenting several heterogeneous sites in the matrix simultaneously. One of the primary mechanisms associated with the trace element effects in Al-based alloys is that the trace elements first precipitate out early in the heat treatment cycle as elemental, or as binary or ternary precipitates (depending on the alloy systems) and these precipitates in turn act as the potential heterogeneous nucleation sites for the intermediate phases of interest during

the aging heat treatments. This can allow the bypass of one or more metastable precipitates and thus a more rapid decrease in the supersaturation.

This is demonstrated in the role of In in Al-Cu-Li based alloys together with the earlier results of the trace element effects in Al-Cu-Cd(/In or Sn) and in Al-Cu-Mg-Si (/Ge). Results show that aging enhancement in alloys containing trace elements is caused by the preferential nucleation of the intermediate phases of interest at numerous fine trace-element-bearing precipitates which form at the early stages of the aging cycle.

Trace additions can alter nucleation rates through electronic contributions (e/a ratios). In Al-Cu-Mg alloys Ag additions promote ordering in GPB zones as well as inducing nucleation of the T phase over the S phase, while the effect of Ag in Al-Zn-Mg alloys is to enhance both the nucleation rate, as well as the stability of η' precipitates through modification of the electronic structure. This study resulted in the following publication which is included in the Appendix:

8. A.K. Mukhopadhyay, G.J. Shiflet and E.A. Starke, Jr., "The Role of Trace Alloy Additions on Precipitation in Age-Hardenable Aluminum Alloys," Morris E. Fine Symposium, ed. Peter K. Liaw, Julia R. Weertman, Harris L. Marcus and Joseph S. Santer, The Metallurgical Society of AIME, 1990, p. 283.

IV. LIST OF PARTICIPANTS

1. J.M. Duva, Assistant Professor of Applied Mathematics
2. K.V. Jata, Research Assistant Professor of Materials Science
3. H. Roven, Post-Doctoral Research Associate
4. C.P. Blankenship, Jr., graduate student (Ph.D.)
5. A.K. Mukhopadyay, Post-Doctoral Research Associate
6. W. Ruch, Research Assistant Professor of Materials Science
7. M.E. O'Dowd, graduate student (M.S., 1986)
8. E.A. Starke, Jr., Oglesby Professor of Materials Science and Dean

V. LIST OF PRESENTATIONS

A. Invited:

1. "Overview on Aluminum-Lithium Alloys: The State of the Art - 1989," E.A. Starke, Jr., and W.E. Quist, presented at the ASM International World Metal Congress, Chicago, IL, September 26-29, 1988.

2. "Aluminum Alloys for Aerospace: Current Developments and Future Trends," E.A. Starke, Jr., Alpha Sigma Mu Lecture presented at the ASM International World Metal Congress, Chicago, IL, September 26-29, 1988.

3. "The Microstructure and Properties of Aluminum-Lithium Alloys," E.A. Starke, Jr., and W.E. Quist, presented at the AGARD/NATO Specialist's Meeting and New Light Alloys, Mierlo, Netherlands, October 3-5, 1988.

4. "Microstructure and Properties of Al-Li Alloys," NADC Advanced Aluminum Alloys for Naval Aircraft Symposium, E.A. Starke, Jr., Valley Forge, PA, October 25-27, 1988.

5. "The Physical Metallurgy of Al-Li Alloys - A Review," T.H. Sanders, Jr., and E.A. Starke, Jr., 5th International Aluminum-Lithium Conference, Williamsburg, VA, March 27-31, 1989.

6. "The Use of Fundamental Concepts in the Design of Al Alloys," E.A. Starke, Jr., 1989 Physical Metallurgy Gordon Conference, Tilton, NH, August 7-11, 1989.

7. "An Overview of Al-Li Alloys," T.H. Sanders, Jr., and E.A. Starke, Jr., 1990 Advanced Aerospace Materials/Processes Conference, Long Beach, CA, May 21-24, 1990.

8. "The Sensitivity of Al-Li Alloys to Microstructure," T.H. Sanders, Jr., and E.A. Starke, Jr., ASM International Conference on Advanced Aluminum and Magnesium Alloys, Amsterdam, The Netherlands, June 20-22, 1990.

9. "The Fracture and Fatigue Behavior of Al-Li-X Alloys," C.P. Blankenship, Jr., H.J. Roven, and E.A. Starke, Jr., Fourth International Conference on Fatigue and Fatigue Thresholds, Fatigue '90, Honolulu, Hawaii, July 15-20, 1990.

10. "The Role of Trace Alloy Additions on Precipitation in Age-Hardenable Aluminum Alloys," A.K. Mukhopadhyay, G.J. Shiflet, and E.A. Starke, Jr., Morris E. Fine Symposium, TMS-AIME Fall Meeting, Detroit, MI, October 7-11, 1990.

11. "New Low Density and High Temperature Aluminum Alloys," E.A. Starke, Jr., and H.G.F. Wilsdorf, First Thermal Structures Conference, Charlottesville, VA, November 13-15, 1990.

B. Contributed:

1. "Intergranular Fracture Caused by Non-Equilibrium Eutectic Melting in an Al-Li-Cu-Mg Alloy," P. Bourgasser, J.A. Wert and E.A. Starke, Jr., TMS-AIME Fall Meeting, Cincinnati, Ohio, October 12-14, 1987.

2. "The Effects of the PFZ and Texture on Delamination of 8090-Type Al-Li Alloys at Cryogenic and Room Temperature," H.J. Roven and E.A. Starke, Jr., 1990 Advanced Aerospace Materials/Processes Conference, Long Beach, CA, May 21-24, 1990.

APPENDIX

Publications

Publications

1. Edgar A. Starke, Jr., and William E. Quist, "The Microstructure and Properties of Aluminum-Lithium Alloys," AGARD Lecture Series No. 174, New Light Alloys, North Atlantic Treaty Organization, 1990, p. 2-1.

2. E.A. Starke, Jr. and H.G.F. Wilsdorf, "New Low Density and High Temperature Aluminum Alloys," presented at the First Thermal Structures Conference, November 13-15, 1990, University of Virginia, Charlottesville, Virginia. To appear in the AIAA Progress Series in Aeronautics and Astronautics (1992).

3. E. Agyekum, W. Ruch, E.A. Starke, Jr., S.C. Jha and T.H. Sanders, Jr., "Effect of Precipitate Type on Elastic Properties of Al-Li-Cu and Al-Li-Cu-Mg Alloys," Aluminum-Lithium Alloys III, ed. by C. Baker, P.J. Gregson, S.J. Harris and C.J. Peel, The Institute of Metals, London, 1986, p.448.

4. M.E. O'Dowd, W. Ruch and E.A. Starke, Jr., "Dependence of Elastic Modulus on Microstructure in 2090-Type Alloys," Journal de Physique, Colloque C3, September, 1987, p. C3-565.

5. K.V. Jata and E.A. Starke, Jr., "Fracture Toughness of Al-Li-X Alloys at Ambient and Cryogenic Temperatures," Scripta Metallurgica, Vol. 22, 1988, p. 1553.

6. H.J. Roven, E.A. Starke, Jr., O. Sodahl, and J. Hjelen, "Effects of Texture on Delamination Behavior of a 8090-Type Al-Li Alloy at Cryogenic and Room Temperature," Scripta Metallurgica, Vol. 24, 1990, p. 421.

7. C.P. Blankenship, Jr., H.J. Roven and E.A. Starke, Jr., "The Fracture and Fatigue Behavior of Al-Li-X Alloys," Fatigue 90, ed. by H. Kitagawa and T. Tanaka, Materials and Component Engineering Publications Ltd, Birmingham, England, 1990, p. 937.

8. A.K. Mukhopadhyay, G.J. Shiflet and E.A. Starke, Jr., "The Role of Trace Alloy Additions on Precipitation in Age-Hardenable Aluminum Alloys," Morris E. Fine Symposium, ed. Peter K. Liaw, Julia R. Weertman, Harris L. Marcus and Joseph S. Santer, The Metallurgical Society of AIME, 1990, p. 283.

AGARD

ADVISORY GROUP FOR AEROSPACE RESEARCH & DEVELOPMENT

7 RUE ANCELLE 92200 NEUILLY SUR SEINE FRANCE

Paper Reprinted from
Lecture Series No. 174

New Light Alloys

(Les Nouveaux Alliages Légers)

NORTH ATLANTIC TREATY ORGANIZATION

THE MICROSTRUCTURE AND PROPERTIES OF ALUMINUM-LITHIUM ALLOYS

Edgar A. Starke, Jr.
School of Engineering and Applied Science
University of Virginia
Charlottesville, Virginia 22901

William E. Quist
Boeing Commercial Airplane Company
P.O. Box 3707, M/S 73-43
Seattle, Washington 98124

ABSTRACT

The advantages to be gained by weight reduction of aerospace structures have encouraged the aluminum industry to develop a family of aluminum alloys which contain lithium as one of the alloying elements. When alloyed with aluminum, lithium can reduce the density by approximately three percent and increase the elastic modulus by six percent for every weight percent added. A new series of aluminum alloys, typified by 2090, 2091, 8090, and 8091, have been developed and are currently being produced in commercial quantities. These alloys have densities between 7% and 10% lower than the conventional alloy 7075 with correspondingly higher stiffness. Although a combined set of specific properties of the Al-Li-X alloys often exceeds those of the conventional aluminum materials used in aerospace, these properties seem to be much more sensitive to processing parameters. The strong processing-property relationship is associated with sharp crystallographic textures that are developed during primary processing and very complex precipitate microstructures whose distributions are sensitive to quench rates and degree of deformation prior to aging. This paper describes the processing-microstructure-property relationships of the new Al-Li-X alloys and focuses on strength, ductility, fracture toughness, fatigue and stress corrosion properties.

INTRODUCTION

The development of Al-based alloys containing lithium began in Germany in the 1920's and was primarily concerned at first with additions of very small amounts of lithium to Al-Zn-Cu alloys to increase their strength (1,2). However, the development of modern aluminum-lithium alloys can be traced to the discovery by Le. .ron in 1942 that lithium could be a major strengthening element in aluminum-copper alloys (3). Subsequent work by Hardy and Silcock (4,5) identified the lithium-containing strengthening phases in Al-Cu-Li alloys and contributed significantly to the scientific understanding of these complex materials. In the 1950's metallurgists at Alcoa recognized that lithium also increased the elastic modulus of aluminum and developed the high strength Al-Cu-Li alloy 2020. Later, metallurgists in Russia (6) developed the Al-Mg-Li alloy 01420 which had a considerable density advantage over other medium strength aluminum alloys. However, production problems combined with marginal engineering properties inhibited the widespread use of these lithium-containing aluminum alloys.

In the early 1970's escalating fuel costs and the desire to develop more fuel-efficient and high-performance aircraft generated a major interest in materials that would reduce weight and thereby increase structural efficiency. Reducing the density, without compromising strength, toughness, and corrosion resistance, has been shown to be the most efficient way to accomplish this goal (7). Although carbon fiber and boron fiber non-metallic composites offer a considerable density advantage over all other structural materials used in aircraft, improvements in the properties of aluminum alloys seemed desirable due to their relatively low acquisition cost and the aircraft community's extensive design and manufacturing experience with these materials. Aluminum-lithium alloys appeared attractive since lithium can reduce the density of aluminum by three percent and increase the elastic modulus by six percent for every weight percent added (8). These advantages have encouraged every major aluminum alloy producer in the U.S. and abroad to develop alloys containing lithium, usually at levels of 2.0 weight percent and higher. Both ingot metallurgy (I/M) and powder metallurgy (P/M) approaches were used during the alloy development programs; however, most major advances were made using the former technique.

Alloy designations and compositions of the new lithium-containing aluminum alloys are listed in Table 1. Many of these alloys possess good combinations of strength, damage tolerance and durability, in general are quite weldable, and several have demonstrated excellent cryogenic and elevated temperature properties. In addition, to those listed in Table 1, alloys are under development which show improved corrosion resistance and post-weld properties. One of these, a high strength, weldable Al-5.0Cu-1.3Li-0.4Mg-0.4Ag-0.1Zr alloy, Weldalite 049, was developed specifically for cryogenic tanks associated with launch vehicles (9). The properties of most of the new aluminum-lithium alloys appear particularly sensitive to small variations in composition and processing. This sensitivity seems to be associated with the difficulty in maintaining metal quality during casting, the presence of recrystallization inhibiting elements, and the complexity of the microstructure after primary processing and heat treatment. As with most aluminum alloys, microstructural features of importance for property control of Al-Li alloys include: (a) cast structure, (b) grain structure and crystallographic texture, (c) volume fraction, size and distribution of insoluble intermetallic particles and grain boundary precipitates and (d) coherency, volume fraction and distribution of strengthening precipitates.

TABLE 1. Current Al-Li Alloys and Compositions.

Alloy / Element*	2090 Alcoa 8/6/84	2091 C Pechiney 4/8/85	8090 Alcan and C Pechiney May 1985	8090A Alcoa (Late 1985)	8091 Alcan 3/29/85	X8092 Alcoa May 1985	X8192 Alcoa Aug 1985
Si	0.10	0.20	0.20	0 10	0 30	0 10	0 10
Fe	0 12	0 30	0 30	0.15	0 50	0 15	0 15
Cu	2 4-3 0	1.8-2.5	1 0-1.6	1.1-1 6	1 8-2 2	0 5-0 8	0.4-0.7
Mn	0 05	0.10	0 10	0 05	0 10	0 05	0 05
Mg	0.25	1 1-1 9	0 6 to 1 3	0.8-1 4	0.5-1 2	0 9-1 4	0 9-1 4
Cr	0 05	0 10	0.10	0 05	0 10	0.05	0.05
Ni	—	—	—	—	—	—	—
Zn	0.10	0.25	0.25	0.10	0.25	0.10	0.10
Ti	0.15	0.10	0.10	0 15	0.10	0.15	0.15
Li	1.9-2.6	1.7-2.3	2 2-2.7	2.1-2.7	2.4-2.8	2.1-2.7	2.3-2 9
Zr	0.08-0.15	0.04-0.16	0 04-0.16	0 08-0.15	0.08-0.16	0 08-1 5	0 08-1.5
Other: Each	0.05	0.05	0.05	0 05	0.05	0 05	0 05
Total	0.15	0.15	0.15	0 15	0.15	0 15	0 15

*Numbers Shown Are Either Maximums or Ranges

MICROSTRUCTURE AND DEFORMATION BEHAVIOR

Cast Structure:

Casting problems have been associated with the development of Al-Li alloys since Alcoa's entry with alloy 2020. Some of these are related to the reactivity of lithium-containing aluminum alloys and associated safety problems which have necessitated the use of modified refractories and degassing procedures, protective inert cover gases and/or surface fluxes during melting and casting, and special ingot cooling techniques (some employing organic coolants in place of water). These techniques have minimized the hazards of casting Al-Li alloys and current work is focusing on improving the quality of the as-cast product. The "as-cast quality" of ingot depends on both the surface quality, which determines the amount of scalping prior to further processing, and the internal structure which determines the processing steps necessary to produce the desired microstructure-property relationship. There can be, of course, some casting defects which are impossible to remove during subsequent processing. In addition to having a high surface quality and a crack-free ingot, the ingot should be free of spherical voids and blisters and have a medium-fine grain structure, a consistent composition throughout, a low inclusion and alkali impurity content, and a low gas content (10).

A fine cast grain structure reduces porosity and the tendency for ingot cracking. Aluminum-lithium alloys have been found to be more difficult to grain refine than conventional aluminum alloys (11). The difficulty has been partly associated with the presence of zirconium which is used to control the wrought grain structure, since zirconium enhances the formation of twinned columnar grains (TCG) (12). Zirconium has beneficial effects, of course, since it forms the coherent Al_3Zr during ingot preheat which is very efficient in inhibiting recrystallization without the adverse effects on fracture toughness that are sometimes associated with large $Al_{12}(Fe,Mn)_3Si$, Al_9Mn_3Si, and $Al_{20}Cu_2Mn_3$ particles present in many 2XXX alloys. During normal ingot breakdown, hot working and subsequent heat treatment, the Al_3Zr dispersoids inhibit recrystallization although the cast grains do elongate in the direction of metal flow. Consequently, in the final product most Al-Li alloys are unrecrystallized, and the cast grain structure relates directly to the grain structure.

Typical grain refining problems include a non-uniform grain size and the formation of twinned columnar grains (TCG) which not only result in increased cracking during processing but also reduce the elongation of the final product as shown in Figure 1. The as-cast grain size correlates well with both the toughness and the stress corrosion resistance of the final product. A fine as-cast grain size reduces fracture toughness, and fatigue crack growth resistance, since it minimizes the beneficial crack branching and the tortuous crack path often observed in larger-grained aluminum alloys. However, a fine as-cast grain size has been shown to have beneficial effects on the stress corrosion resistance of aluminum-lithium alloys, Figure 2. A reduction in grain size decreases the slip length and reduces the stress concentrations at grain boundaries thus reducing the mechanical component of stress corrosion cracking.

Inclusions may originate from the lining of the furnace, the flux, or from the presence of certain impurities, e.g., iron and silicon. The effect of iron content on the strength/toughness of alloy 2020 aged to the T8 temper (13) is shown in Figure 3. Molten metal filtering, fluxless or inert gas casting, and high purity starter materials are

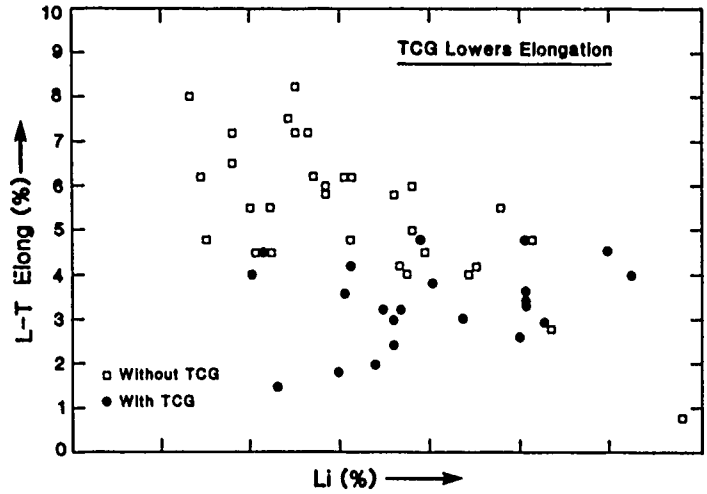

Figure 1. The effect of twin columnar grains and lithium content on the elongation of Al-Li alloys (From Labarre et al., reference 11).

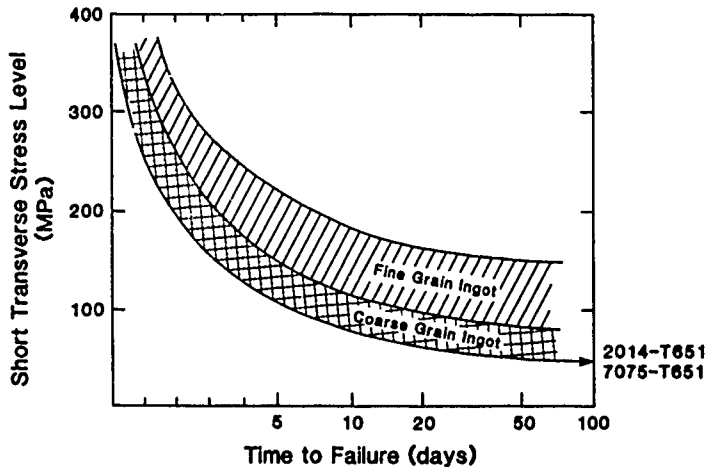

Figure 2. The effect of as-cast grain structure on the stress corrosion behavior of 8090-T851 plate. Base-line data of 2012-T651 and 7075-T651 is shown for comparison (Courtesy of A. Gray, Alcan International).

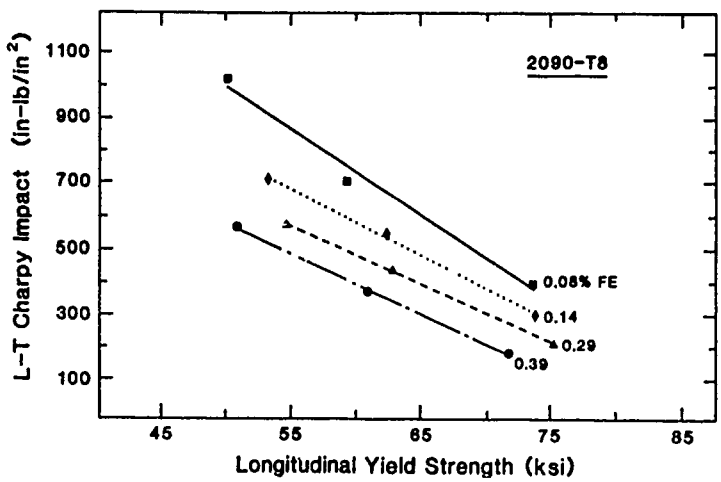

Figure 3. The effect of iron content on the strength/toughness relationship of 2090 (From Ashton et al., reference 1.).

common methods used to minimize inclusion problems. Besides the well-known relationship between inclusion content and fracture toughness, a high silicon content is believed to have a detrimental effect on the corrosion properties of Al-Li alloys (14). For compositions containing greater than 0.08 wt.% Si, the equilibrium AlLiSi phase forms upon solidification and is retained through all subsequent thermal mechanical treatments. This phase serves as an active nucleation site for surface pitting upon exposure to salt water, and greatly diminishes the material's resistance to stress corrosion cracking.

Precipitate Structure, Deformation Behavior and Fracture:

Al-Li: When binary Al-Li alloys containing more than 1 wt.% lithium are quenched from the single-phase field and aged at a temperature below the solvus, homogeneous precipitation of the metastable ordered phase δ' (Al_3Li) occurs. For alloys containing more than 1.7 wt.% Li it may be impossible to suppress δ' formation during quenching even when using ice water as the quenching medium (15). These precipitates have an $L1_2$ type superlattice structure, a spherical shape, and a cube/cube orientation with the aluminum matrix (16,17). High temperatures and/or long aging times at normal aging temperatures result in the heterogeneous precipitation of the equilibrium δ (AlLi) phase at grain boundaries and other planar interfaces. These precipitates consume lithium from the surrounding region and produce a lithium-depleted precipitate-free-zone (PFZ) adjacent to the grain boundary. The microstructural features just described are shown in the transmission electron micrographs (TEM's) of Figure 4a. In commercial Al-Li alloys that contain zirconium the small ($\approx$ 50 nm) coherent, ordered Al_3Zr dispersoids that form during the ingot preheat are isostructural with Al_3Li and can act as nucleation sites for these precipitates. These composite precipitates are often observed coexisting with the homogeneously nucleated δ'. Although the δ' precipitates can be sheared by moving dislocations, Figure 4b, they impede their motion and, consequently, greatly improve the strength over that of unalloyed aluminum. During artificial aging the δ' precipitates coarsen but retain their coherency and spherical morphology to relatively large sizes (>50 nm). A change in deformation mode from shearing to Orowan looping does not occur during practical heat-treatment times and temperatures.

When the δ' precipitates are sheared by dislocations during deformation, their strengthening effect is reduced as both the degree of order and the precipitate size on the glide plane is reduced when the precipitate is sheared. Although dislocations move in pairs (superdislocations) in order to minimize the creation of antiphase domain boundaries in the δ', their shearing results successively in a local decrease in resistance to further dislocation motion, a concentration of slip into intense shear bands, Figure 5 (15), and a reduction in ductility and fracture toughness. Cassada et al. (18) have shown how the deformation can be homogenized and ductility improved by the addition of non-shearable precipitates. Since PFZ's are weaker than the precipitation-hardened matrix they can also lead to strain localization, thus further lowering the ductility and fracture toughness. This adverse effect is enhanced by the presence of the coarse grain boundary precipitates which may fracture or act as stress risers and preferential sites for microvoid nucleation and growth. Because of the severe strain localization effects associated with δ' and PFZ's, all aluminum alloys containing lithium that are being developed for commercial use contain other alloying elements in order to modify the precipitate types and sequences and thereby develop acceptable combinations of strength and toughness.

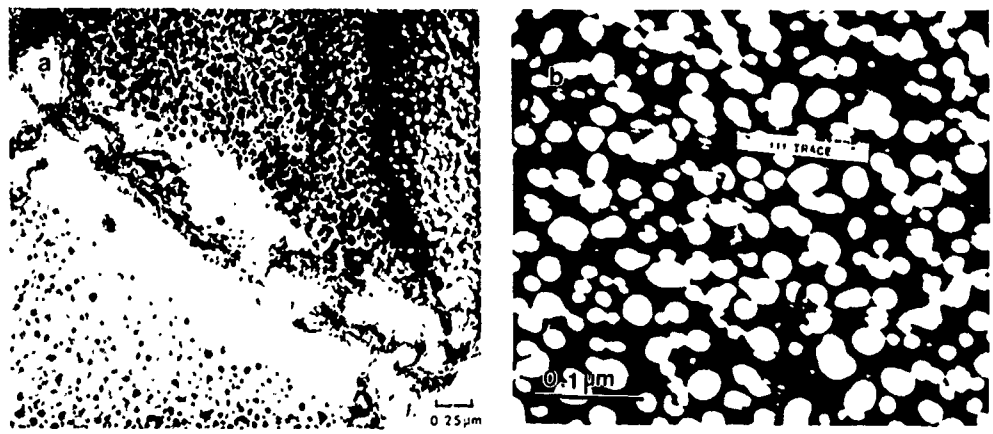

Figure 4. TEM's of an Al-Li alloy aged 24 h at 363K: (a) Bright-field image showing Al_3Li in the matrix, AlLi at grain boundaries and PFZ. (b) Dark field image showing the shearing of Al_3Li that occurs during deformation.

Figure 5. TEM showing intense shear bands in an Al-Li binary alloy.

Al-Li-Mg: The effect of magnesium additions on the phase equilibria of Al-Li alloys has been reported by a number of investigators (6,19,20). Magnesium decreases the solubility of lithium in aluminum at all temperatures below about 425°C (21). Similarly, the solubility of magnesium in aluminum is drastically reduced by the presence of lithium. Beyond the region of solid solution, in Al-Li-Mg ternary alloys with compositions close to the Al-Li binary, the decomposition of the supersaturated solid solution occurs via the δ' to δ precipitation sequence. However, as the composition of the ternary alloy is varied from the Al-Li binary towards the Al-Mg binary by increasing the magnesium to lithium ratio, the phase that is in equilibrium with the α solid solution changes from δ to Al_2MgLi. When supersaturated Al-Li-Mg alloys of practical interest are aged at temperatures below about 240°C, the precipitation sequence occurs as follows:

$$\alpha_{ss} \rightarrow \alpha_m + \delta' \rightarrow \alpha_m + \delta' + Al_2MgLi \rightarrow \alpha_e + Al_2MgLi$$

where α_{ss}, α_m, and α_e, refer to the supersaturated, the metastable and the equilibrium α solid solutions, respectively.

The δ' phase that forms in Al-Mg-Li alloys is similar to that which occurs in the Al-Li binary. Al_2MgLi has a cubic α-Mn crystal structure and forms as rods along the <110> directions of the matrix (20). This phase is incoherent with the matrix, and nucleates predominately along the grain boundaries, dislocations and other structural inhomogeneities. Consequently, it does not contribute to precipitation hardening. Al_3Li is the only phase responsible for the strength of Al-Li-Mg alloys, with the magnesium contributing to some solid solution hardening (22). Therefore, the deformation behavior is coarse-planar, similar to that which occurs in Al-Li binary alloys, and the extensive strain localization that develops during deformation leads to premature failure. The lithium-rich Al_2MgLi phase that precipitates along grain and subgrain boundaries results in the formation of δ' PFZ's during prolonged artificial aging. As discussed previously, these zones, and their associated coarse grain boundary precipitates, have deleterious effects on ductility, fracture toughness, and possibly corrosion resistance (19).

Al-Li-Cu: The addition of copper decreases the maximum solid solubility of lithium in aluminum at all temperatures (5). Copper in solid solution does not influence the basic character of the δ' precipitation reaction (23), but it does introduce additional beneficial precipitation reactions that occur independent of the δ' reaction. The natures of the metastable and equilibrium phases that form within this alloy system have been shown to be dependent on the Cu:Li ratio and the aging temperature (5). For example, during aging at temperatures typical of commercial aging practices (120° to 200°C) the decomposition of the solid solution in a 2090 type alloy (Al-2.2Li-2.7Cu-0.12Zr) results in the formation of the metastable θ' (Al_2Cu-the primary strengthening phase in Al-Cu alloys) and the equilibrium T_1 phase (Al_2CuLi)(5,24,25). Al_2Cu has not been observed for Cu:Li ratios less than approximately 1.3. Al_2Cu has a tetragonal crystal structure and the precipitates form as platelets parallel to the {100} planes of the matrix. T_1 has a hexagonal crystal structure with a = 0.497 and c = 0.934 nm and also forms as thin platelets but with a {111} habit plane. In commercial Al-Li-Cu alloys such as 2090, T_1 is the predominant copper bearing strengthening phase present after artificial aging to the near peak strength condition, although θ' may be present to a lesser degree. Figures 6a and 6b are TEM's of a 2090-type alloy showing the complex precipitate structure after aging to peak strength.

Both T_1 and θ' nucleate heterogeneously on dislocations and low angle grain boundaries, and other substructural features. Al_3Li normally is the first precipitate that forms during the aging of Al-Li-Cu alloys having compositions of commercial interest. Subsequent precipitation of T_1 and θ' may reduce the volume fraction and alter the distribution of δ' since T_1 incorporates lithium and artificial aging may result in some

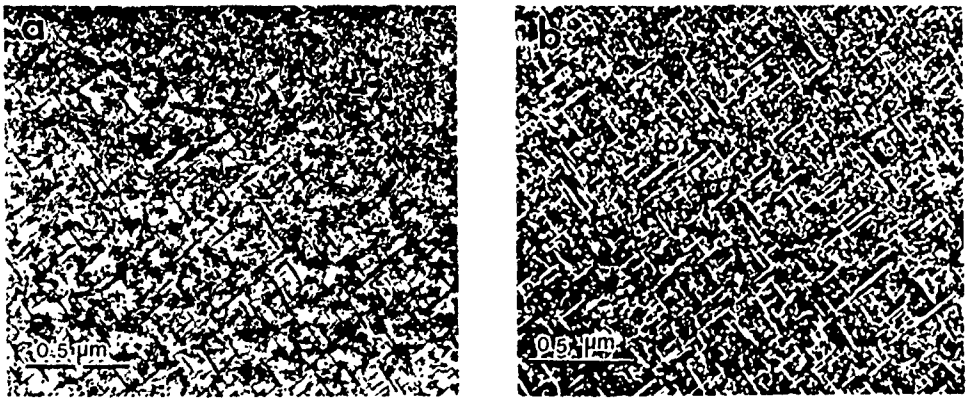

Figure 6. TEM's of the 2090 alloy solution heat treated showing a complex precipitate structure tnat includes θ', T_1, δ', and Al_3Zr (β'). (a) Bright field, (b) dark field.

reversion and reprecipitation of δ'. Although Noble and Thompson (24) and Gregson and Flower (26) have suggested that growth of the T_1 platelets is sustained by lithium from solid solution rather than dissolution of the δ' particles, Sanders (27) has clearly shown that during growth the T_1 precipitates cut through the δ' precipitates and may consume them, Figure 7. Reducing the volume fraction of δ' is beneficial in reducing the degree of strain localization (15).

Apart from the metastable θ' and equilibrium T_1 precipitates, the addition of copper also introduces another copper-containing phase, T_2, having the stoichiometry of Al_6CuLi_3 (5) which nucleates predominately on high angle boundaries. Electron (28-31) and x-ray diffraction (29) analyses of this phase provide strong evidence that T_2 displays five fold icosahedral symmetry. The formation of the T_2 phase particles (which are richer in lithium than δ') along the grain boundaries lead to the development of δ' PFZ's adjacent to these boundaries, Figure 8, with concomitant reduction in ductility and fracture toughness. Cassada et al. (30) have shown that in 2090-type Al-Li alloys the T_2 phase is stable over the temperature range of 170°-520°C. Consequently, grain boundary precipitation of this phase should be anticipated in products that are slowly cooled or aged at temperatures above 170°C.

Early work by Price and Kelly (32) on Al-Cu single crystals aged to precipitate θ' indicated that θ' was not sheared but was looped and bypassed by moving dislocations in accordance with the Orowan model of strengthening. However, Starke and Lin (33) clearly showed that when the Al-Cu-Li alloy 2020 was aged to peak strength, where both θ' and δ' were present, deformation occurred by coarse planar slip. Huang and Ardell (34) obtained indirect evidence that T_1 is looped and bypassed by glissile dislocations, confirming an earlier suggestion by Sainfort and Guyot (35). The former authors aged an Al-Li-Cu alloy to produce δ' and T_1 and then applied a reversion treatment to eliminate δ'. However, Jata and Starke (36) showed direct evidence of T_1 shearing in an Al-Li-Cu alloy which also contained θ' and δ' precipitates. Howe et al. (37) used high resolution electron microscopy to study the structure and deformation behavior of T_1 plates in an Al-2Li-1Cu alloy and showed conclusively that T_1 plates are cut by dislocations during deformation and that such cutting leads to a disruption of nearest-neighbor bonding in the plates. Shearing of T_1 and θ' when δ' is present may result from the superdislocations associated with δ' having a pileup force sufficient to shear these partially coherent precipitates.

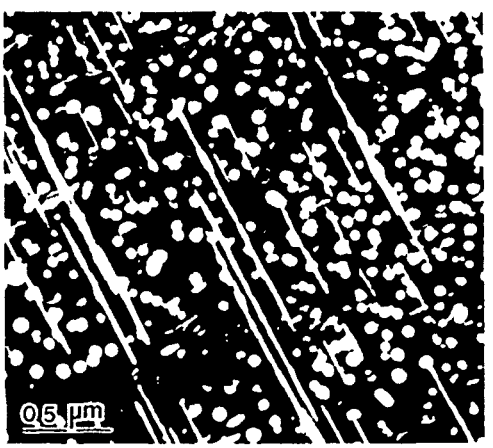

Figure 7. Dark-field micrograph showing T1 precipitates cutting through and consuming Al_3Li precipitates (Courtesy of T.H. Sanders, Jr.).

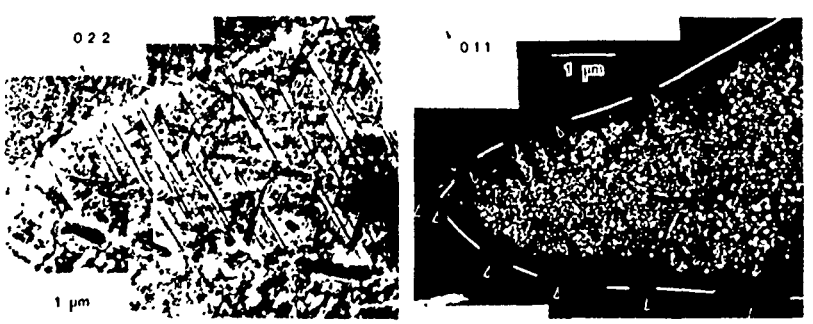

Figure 8. Micrographs illustrating grain boundary precipitates and associated PFZ: (a) Bright-field micrograph with T_2 grain boundary precipitates with five-fold diffraction symmetry arrowed. (b) Al_3Li dark field showing the location of grain boundary and grain boundary precipitates (Courtesy of W.A. Cassada).

Although both θ' and T_1 may be sheared in the presence of δ', they do appear to decrease the extent of strain localization that occurs in binary Al-Li alloys. The resistance that a shearable strengthening precipitate offers to a glissile dislocation depends on a number of factors which include the coherency strain field, the interfacial energy, the internal structure of the precipitate, etc. For ordered precipitates, such as δ', the strengthening mechanism associated with the internal structure is reduced by shearing. The small lattice misfit (-0.18%)(16) and the small interfacial energy (180 ergs/cm^2) (38) between δ' and the matrix suggest that these strengthening mechanisms are not important for δ'. However, the much larger misfits and interfacial energies between θ', T_1 and the matrix suggest that these strengthening mechanisms do operate when these precipitates are present. Neither strengthening mechanism is as effectively destroyed by particle shearing as is order strengthening and, therefore, the tendency for strain localization by work softening on the glide plane is reduced when θ' and T_1 are present. The alloy Weldalite may be used to illustrate the effect of δ' and T_1 on the deformation behavior of Al-Li-Cu alloys (39). Weldalite-T3 is characterized by fine GP zones and δ' particles and deforms by intense localized planar slip, Figure 9a. When aged to the T8 temper, T_1 is the only strengthening phase and deformation is more homogeneous, Figure 9b, indicating that there is no significant loss in strength on the slip plane during deformation (39) and supporting the contention that T_1 is difficult to shear in the absence of δ'.

Al-Li-Cu-Mg: When magnesium is added to Al-Li alloys containing copper, matrix precipitation of S' (Al_2CuMg) occurs. The exact nature of the phase equilibria of the quaternary Al-Li-Cu-Mg alloys depends on the relative concentrations of all three alloying elements. For example, the addition of small amounts (0.5 to 1.0 wt.%) of magnesium to a high copper alloy such as 2090 suppresses the formation of θ' and introduces the S' phase (40). Since S' contains no lithium, δ' precipitation is not markedly influenced by the magnesium addition and T_1 remains the dominant secondary phase in such an alloy. For alloys such as Al-3Cu-1.6Li-0.8Mg little or no δ' forms and there appears to be equal amounts of T_1 and S' (40). In higher lithium - lower copper alloys such as 8090, S', which precipitates with δ' and a small amount of T_1, becomes the dominant Cu-bearing phase (26,41). As the magnesium to copper ratio is progressively increased, the precipitation of T_1 is fully suppressed and S' becomes the primary Cu-bearing strengthening phase. This is the case for 2091 which has a nominal composition of Al-2Li-2.2Cu-1.5Mg-0.8Zr (42,43). When the concentration of magnesium exceeds that of copper the Al_2MgLi phase may precipitate in addition to S' (44).

The S' phase has an orthorhombic crystal structure (a = 0.405 nm; b = 0.905 nm; c = 0.72 nm) and forms initially as rods or needles aligned along the <100> directions in the matrix. The precipitates are partially coherent with the matrix and show a strong tendency for heterogeneous nucleation along matrix dislocations, low angle grain boundaries and other structural inhomogeneities, Figure 10. However, unlike the case of T_1 precipitation, the heterogeneous precipitation of S' does not result in PFZ's along either low or high angle grain boundaries. A T_2-type phase (possibly $Al_6Cu(LiMg)_3$) has been observed on grain boundaries of 8090-type alloys and, similar to such precipitation in Al-Li-Cu alloys, it does result in PFZ's. The combination of these microstructural features may lead to low ductility, fracture toughness, and corrosion resistance although the presence of S' in the matrix certainly minimizes these effects. Crooks et al. (45) and Crooks and Starke (40) have clearly shown that when S' is present in Al-Li-Cu-Mg alloys strain localization is suppressed indicating that the precipitate is not sheared by glissile dislocations. These observations were later confirmed by Gregson and Flower (26). The S' precipitates do not have densely packed slip planes parallel to the matrix slip planes and are, therefore, unlikely to be penetrated by dislocations (26).

A schematic representation of the various phases found in basic as well as the more complex Al-Li-X systems that encompass modern Al-Li alloys is shown in Figure 11.

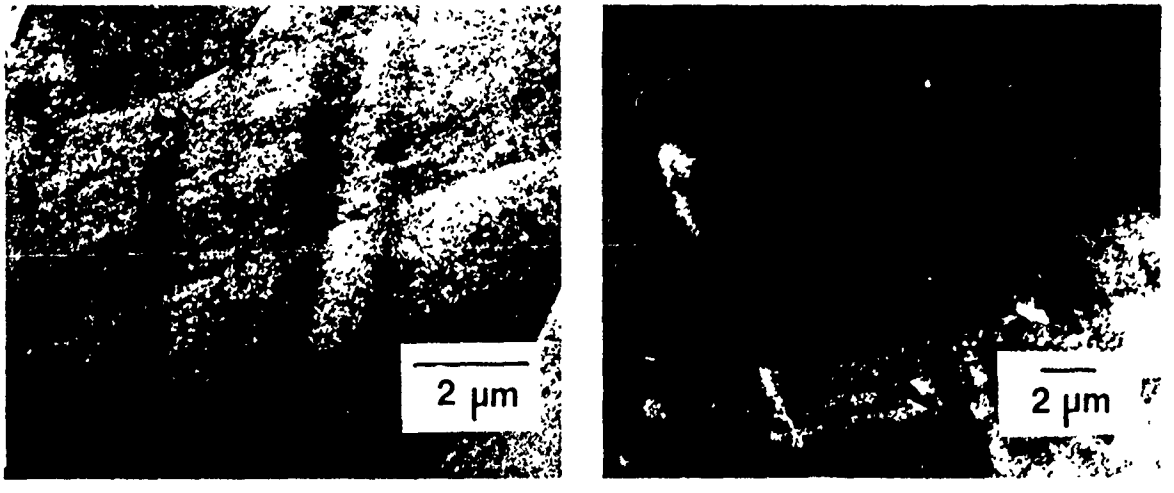

Figure 9. TEM showing deformation behavior in Weldalite (a) aged to the T3 temper, (b) aged to the T8 temper after 2% plastic strain.

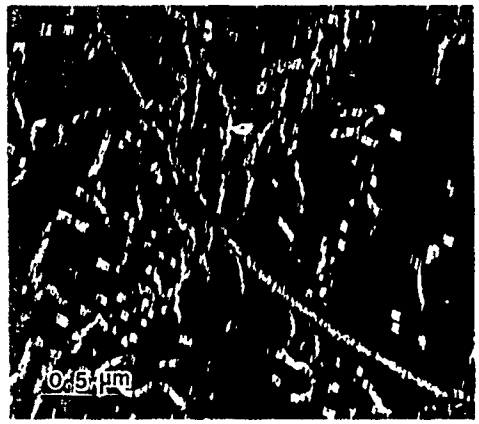

Figure 10. Dark field TEM showing δ' precipitation on matrix dislocations and low angle boundaries in an Al-2.7Li-1.5Cu-1Mg-0.15Zr alloy.

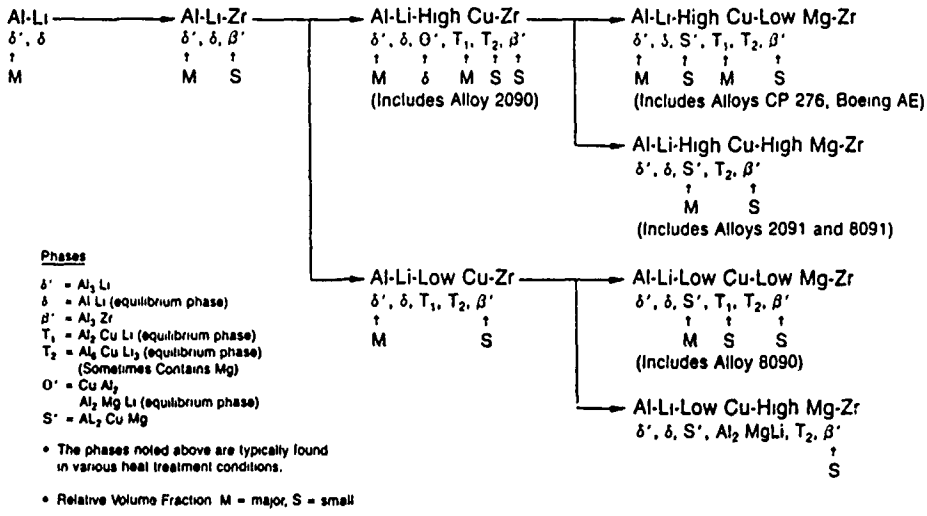

Figure 11. A schematic illustration of the precipitate phases that form in Al-Li-X alloys (from Narayanan and Quist).

EFFECT OF PROCESSING ON MICROSTRUCTURE DEVELOPMENT AND PROPERTIES

As mentioned previously, the first Al-Li-X alloys that were developed for commercialization suffered from low ductility and fracture toughness. These problems were primarily associated with strain localization and grain boundary precipitates, and alloying additions and processing methods were selected to minimize these problems. A variety of production methods, including rapid solidification and powder metallurgy consolidation, mechanical alloying, and ingot casting have been used for the development of the new Al-Li alloys. Rapid solidification and mechanical alloying were used as a means of reducing the grain size and extending solid solubility; however, ingot casting has proven to be the most feasible method for the production of large plate and extrusion products and is being used for the alloys that are currently in commercial production. However, powder metallurgy methods, including mechanical alloying, may offer advantages for certain product forms such as forgings.

Processing begins with homogenization to reduce segregation, remove the low-melting nonequilibrium phases, and thus improve workability. This thermal treatment also serves to precipitate the dispersoid-forming elements, such as those containing zirconium, so that they may perform their role of grain control during subsequent processing. One must be very careful in going to the final homogenization temperature to ensure that the low-melting phases are dissolved before their melting temperatures are reached. The atmosphere used in the homogenization treatment should be relatively dry in order to minimize oxidation and hydrogen pickup. One also needs to be concerned about lithium loss from the surface (46). The homogenization treatment is followed by hot working for ingot breakdown and shape change to the appropriate product form. The wrought product is then

solution heat treated, quenched, possibly worked, and aged to develop the desired microstructure. The temperature, amount of deformation prior to aging, etc., depend on the alloy composition and the final microstructure and properties that are desired.

Density and Elastic Modulus:

Lithium is the lightest metallic element and, with the exception of beryllium, is the only metal that both increases the modulus and reduces the density when alloyed with aluminum. Although the presence of heavier elements such as copper will somewhat offset the density advantage afforded by lithium, the overall reduction in density achieved will still be dominated by the amount of lithium added (47), Figure 12. Several investigators have developed empirical equations to predict alloy densities from known composition. One such formula by Peel et al. (41) is as follows:

$$\text{Density (g/cc)} = 2.71 + 0.024\%Cu + 0.018\%Zn + 0.022\%Mn - 0.079\%Li - 0.01\%Mg - 0.004\%Si.$$

In this equation the elemental concentrations are expressed in weight percent.

The modulus enhancement of aluminum by lithium additions is due to both solid solution effects as well as to the precipitation of lithium bearing compounds, and will change relative to both the amount of lithium added and the prior thermal treatment (48,49). Copper has a slight beneficial effect and magnesium a slightly negative effect on the modulus of aluminum (50,51). Recent studies by O'Dowd et al. (52) for 2090-type alloys and Broussaud and Thomas (53) for Al-Li binary alloys have shown that a maximum in modulus occurs just prior to the peak strength condition, Figure 13. Using the law of mixtures and a modulus for aluminum of 80.7 GPa O'Dowd et al. calculated a modulus for δ' of 97 GPa and a modulus for T_1 of approximately 350 GPa. They observed a sharp drop in modulus with the precipitation of the icosahedral T_2 phase. Their data suggested that T_2 has an extremely low intrinsic modulus and is very detrimental to the elastic properties of Al-Li-Cu alloys. Figure 14 shows a comparison of the modulus of elasticity of several Al-Li-X and baseline aluminum alloys (54).

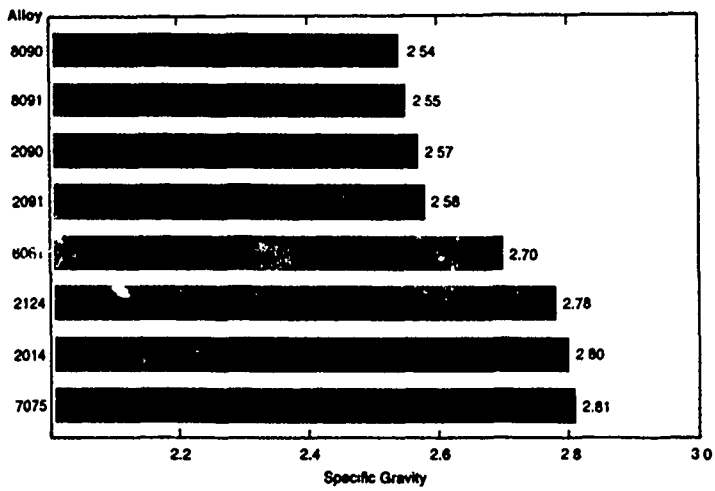

Figure 12. A comparison of densities for several Al-Li and conventional alloys (From Wakeling, reference 54).

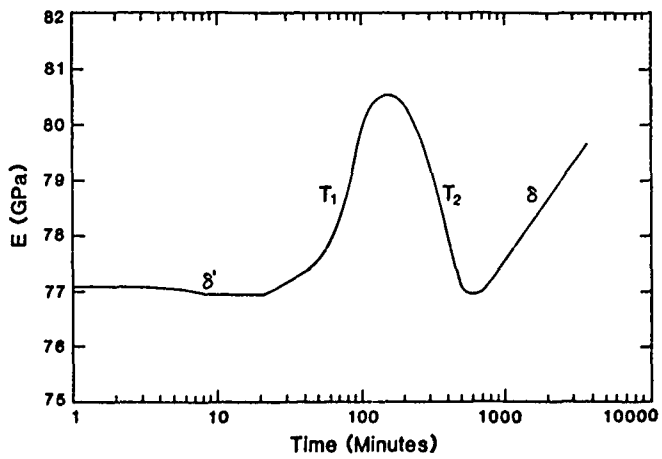

Figure 13. Young's modulus versus aging time at 190°C for an Al-2.31Li-2.24Cu-0.16Zr alloy. Precipitation occurs as indicated on the figure (From O'Dowd et al., reference 52).

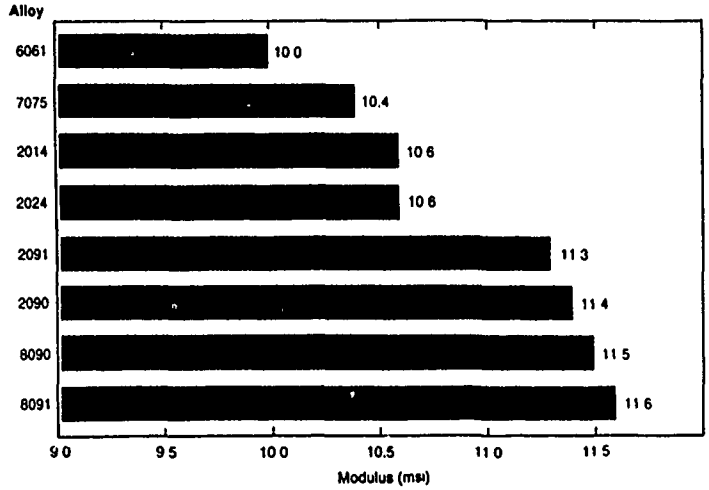

Figure 14. A comparison of Young's modulus for several Al-Li and conventional alloys (From Wakeling, reference 54).

Grain Structure and Crystallographic Texture:

Starke and Lin (33) showed that grain structure and texture can have a significant effect on the ductility of aluminum-lithium alloys. They related the poor ductility and fracture toughness of a 2020 alloy plate product to a partially recrystallized structure, very large recrystallized grains, and a high volume fraction of large inclusions. They were able to significantly improve the ductility of 2020 by thermomechanical treatments that produced either a completely recrystallized structure with small recrystallized grains or a completely unrecrystallized structure with a sharp deformation texture. Subsequently, Lin (55) showed that when PFZ's are present the grain aspect ratio of the recrystallized grains also has a major effect on the deformation behavior and fracture mode.

For alloys that deform by planar slip and/or have soft PFZ's, e.g., 2020, large recrystallized grains result in long slip lengths which produce large stress concentrations at grain boundaries and enhance low-energy intergranular fracture. Deformation is localized within the PFZ only when this region is favorably oriented for slip. This is always the case for equiaxed grains but occurs with less frequency for elongated grains when the stress axis is parallel to the long grain dimension. Grain boundary misorientation, i.e., texture, also plays a role in determining slip length and type of fracture. Grain boundaries can be a major barrier to slip if the misorientation is large, which is the usual case for recrystallized aluminum alloys. However, grain boundaries may not inhibit slip if the misorientation is small, e.g., for unrecrystallized materials with sharp deformation textures (56) (this is the situation for most Al-Li alloy products). The deformation process, i.e., the operative slip system(s), strongly depends on the crystal orientation. Shape accommodation, due to the constraint of material flow, varies with the crystal orientation and the misorientation between adjacent grains.

Small grains and large misorientations enhance multiple slip due to von Mises criterion, which may reduce stress concentrations at grain boundaries and the incidence of intergranular fracture. However, when the grain size is larger than some critical value, (which depends on the strength of the boundary, the degree of slip planarity, etc.) a large misorientation produces an effective barrier to slip, resulting in a stress concentration which may increase the incidence of intergranular fracture. A sharp deformation texture enhances slip continuity across grain boundaries and increases the probability of higher energy transgranular fracture. However, if slip is coarse-planar and strain localization extensive, the fracture toughness may be low even though the fracture mode is transgranular (27).

The desired grain structure may depend on the stress condition (57). Plane stress fracture toughness is believed to be controlled by the amount of plastic deformation occurring in a large plastic zone and a fine recrystallized grain structure aids in producing a maximum amount of plastic deformation. On the other hand, plane strain fracture toughness may be more influenced by grain boundary particles and increased toughness may result from a large grain boundary spacing. In Al-Li alloys these effects are particularly important, and it is found that sheet material with a recrystallized fine grain size often produces the highest plane stress toughness whereas unrecrystallized coarse grained thick section material is best for high plane strain fracture toughness (57).

Texture may have a significant effect on strength as predicted by the Taylor relationship: $\sigma = M\gamma$, where σ is the yield strength, γ the critical resolved shear strength on (111) planes and M an orientation factor which averages the distribution of grain orientations. When this distribution is isotropic, M = 3. The textures produced in aluminum alloys depend on a variety of parameters which include alloy content, precipitate structure and deformation mode, grain size and shape, starting texture, degree of recrystallization, directionality of deformation, and temperature of deformation. The crystallographic texture usually cannot be simply described since it may consist of a number of deformation and recrystallization components.

Commercial aluminum-lithium alloys normally have very strongly developed textures with resultant anisotropic properties (58-67). Both Al-Li-Cu-Zr and Al-Li-Cu-Mg-Zr alloys exhibit pronounced yield stress and ductility anisotropy in sheet, plate, and extruded products. In sheet products, mechanical properties vary with angle of the stress axis to the rolling direction (67), Figure 15. In thicker products, e.g., plate and extrusions, the texture may vary throughout the thickness resulting in an additional anisotropy, Figure 16 (65). Some of the through-thickness texture variation is usually associated with a limited amount of recrystallization that normally occurs near the surface. In addition to anisotropic effects due to crystallographic texture, variation in properties throughout a product may be due to variations in volume fraction and distribution of the strengthening and grain boundary precipitates (14). Rapid heat-up rates during solution heat treatment, e.g., associated with salt baths, may decrease the degree of anisotropy, Figure 15 (67).

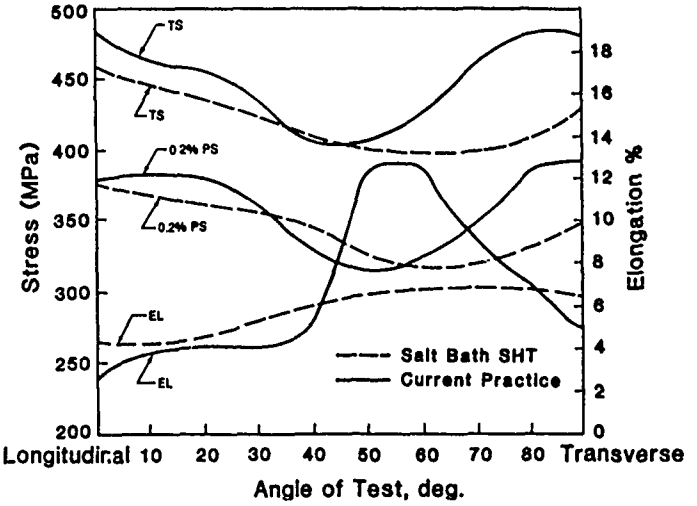

Figure 15. The mechanical properties of Al-Li alloy 8090 as a function of solution heat treatment practice and angle to the rolling direction (From Reynolds et al., reference 67).

The texture may also influence delamination cracks that are often observed in Al-Li alloys. Rolled plate and extrusions of 2090- and 8090-type Al-Li alloys may have a tendency to form delamination cracks extending in the processing direction during fracture (68-72). Some authors have suggested that the delamination phenomena increases the conventional fracture toughness due to "delamination toughening" (72), i.e., the L-T, L-S and T-S oriented specimens show higher fracture toughness than S-L and S-T specimens. Moreover, recent research indicates that the cryogenic fracture toughness in the L-T orientation is higher than at room temperature (68-71) and is accompanied by an increase in the yield strength, UTS, strain to fracture and the strain hardening exponent (68-70). Roven et al. (73) recently examined the influence of PFZ's and variations in the relative misorientations between grains in the S-direction on the delamination behavior of an 8090-type alloy at cryogenic and room temperature. Two conditions are investigated, i.e., one condition having a wide PFZ and the other condition with no PFZ. The recently developed (74) and modified EBSP technique in the SEM (75) was employed for micro-texture measurements. This technique is unique since it makes direct correlations between the microstructure and the crystallographic orientation possible on a macroscopic specimen (75).

Roven et al. (73) found that the delamination behavior could be characterized by (i) a "fine delamination" whose spacing was independent of both aging condition and test temperature, i.e., 77K and room temperature, and (ii) a "coarse delamination" whose spacing varied both with aging condition and test temperature (RT and 77 K). However, the coarse spacing was roughly equal for the two conditions at 77 K. The spacing of the "fine delaminations" correlated very closely to periodical events of high to low relative misorientations of grains in the S direction. The fracture processes of the PFZ-containing condition included slip localization both in slip bands and in the PFZs giving intergranular failure. In the PFZ-free condition the fracture process was dominated by slip localization in slip bands giving slip band decohesion. The latter condition had better cryogenic properties than the PFZ-containing microstructure.

The sharp textures that occur in Al-Li-X-Zr alloys are strongly associated with the use of zirconium as a grain refiner and recrystallization inhibitor. In addition, lithium probably has a contributory effect (76). Unless special procedures are applied no significant amount of recrystallization occurs in Al-Li-X-Zr alloys during ingot breakdown or subsequent thermomechanical processing, including intermediate anneals and solution heat treatments. This results in a very well defined deformation texture and the consequential effects mentioned previously. Cross rolling may spread the predominant poles and decrease the degree of anisotropy (13,61). As noted earlier, recrystallization textures normally lead to more isotropic properties and a very fine recrystallized grain size offers advantages under plane stress conditions (assuming grain boundary effects do not dominate). Sheet products of two alloys, 2091 and 8090, are being marketed in the recrystallized condition to optimize their plane stress fracture toughness.

Alloying additions and/or microstructural features that homogenize deformation normally reduce the effect that a sharp texture has on property variations. Although

Hirsch et al. (63) have shown that some control over texture may be obtained by controlling the initial texture, grain shape and aging, the anisotropy of properties associated with the texture of commercial Al-Li-X alloys is still a major problem and production methods need to be developed to produce the desired texture in all product forms.

Quench Sensitivity and Grain Boundary Precipitates:

The primary purpose of quenching age-hardenable aluminum alloys is to maintain a large degree of supersaturation of solute atoms homogeneously distributed in solid solution. This permits precipitation of an optimum concentration and distribution of hardening particles during the aging treatment. As quench rates decrease, more time is allowed for solute atoms to migrate to grain boundaries or precipitate as matrix phases. Grain boundaries act as heterogeneous nucleation sites by reducing the free energy barrier to nucleation (77). When thermodynamic and kinetic demands are satisfied, precipitation can occur along the grain boundary and enhance intergranular cracking, grain boundary decohesion and premature material failure (46).

Slow quench rates are unavoidable in very thick plate or heavy section forgings and under such conditions precipitation of grain boundary phases may occur. Lewis et al. (14) have shown that when 8090 is quenched from the solution treatment temperature at rates slower than 10°C/sec, precipitation of the icosahedral T_2 phase occurs at high angle grain boundaries. These brittle precipitates can lead to low fracture toughness by acting as stress risers and preferential sites for microvoid nucleation and growth (78).

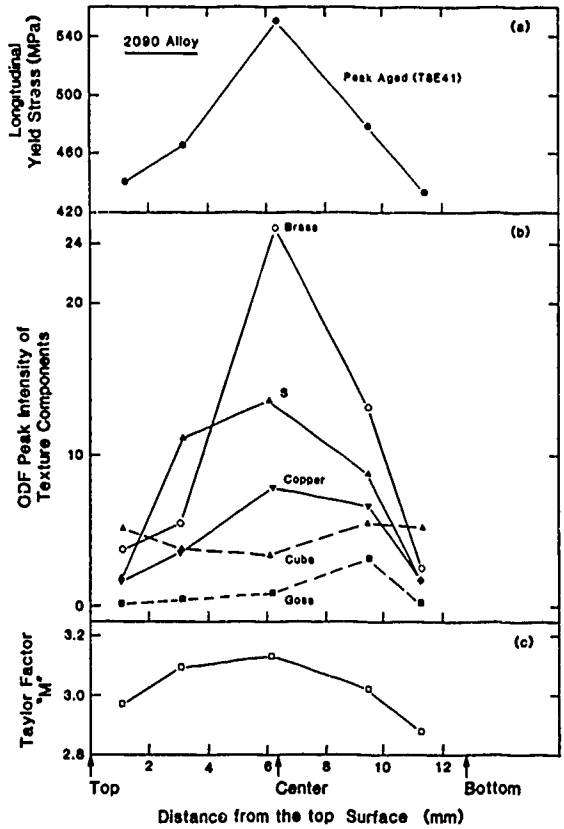

Figure 16. (a) Through thickness variation in longitudinal yield stress, (b) Through thickness variation in intensity of texture components, (c) Variation in the calculated Taylor factor (M) through the thickness (From Vasudevan et al., reference 65).

Colvin and Starke (79) have determined time-temperature-transformation diagrams for the precipitation of both the T_2 and S phases for two compositional variants of 8090, Figure 17. A solute-rich Al-2.58Li-1.36Cu-0.9Mg-0.13Zr alloy exhibited a greater sensitivity to quenching rates than did a solute-lean Al-2.28Li-0.86Cu-0.9Mg-0.13Zr alloy. Colvin and Starke related the precipitation of the T_2 and S phases with the fracture toughness of the alloy, Figure 18, and concluded that T_2 was the principal cause for the loss of mechanical properties in poorly quenched 8090. Staley (80) has recently determined TTT diagrams and related mechanical properties for 2090 and has found results similar to those obtained for 8090.

Strengthening Precipitates:

Engineering properties important in the design of Al-Li alloys for aerospace applications include a proper balance between strength, ductility, fracture toughness, fatigue resistance, formability, and corrosion resistance. The volume fraction, size, spacing, and distribution of the strengthening precipitates are important microstructural features that impact all of these properties. Processing of the wrought product to optimize the microstructure and properties begins with the proper selection of the solution heat-treatment temperature. This treatment should ensure that the maximum amount of solute

has been put in solid solution and that the rate of heat-up and maximum temperature does not result in nonequilibrium eutectic melting (81). The solution heat treatment is followed by a quench which should be sufficiently rapid to prevent deleterious precipitation of grain boundary phases, as discussed previously, without causing quench residual stresses that will produce warping. The warping issue is more serious than with normal aluminum alloys due to the relatively high solution treatment temperatures and low thermal conductivity associated with Al-Li alloys.

Quenching is often followed by some type of cold work in order to redistribute the quenched in residual stresses. However, for Al-Li-Cu and Al-Li-Cu-Mg alloys that contain θ, T_1, and S' strengthening precipitates, cold work prior to aging is used in conjunction with the aging temperature to control the distribution of the precipitates. Deformation prior to aging increases the dislocation density and thereby the number of nucleating sites for heterogeneous precipitation. Since the dislocations would also be in the vicinity of the grain boundary, precipitation of the strengthening precipitates would be encouraged in this region, thus minimizing the probability of PFZ formation. Dislocations are most effective as nucleation sites for those precipitates that have large interfacial energies and/or strains, e.g., θ', T_1 and S', but have no significant effect on the nucleation of δ'.

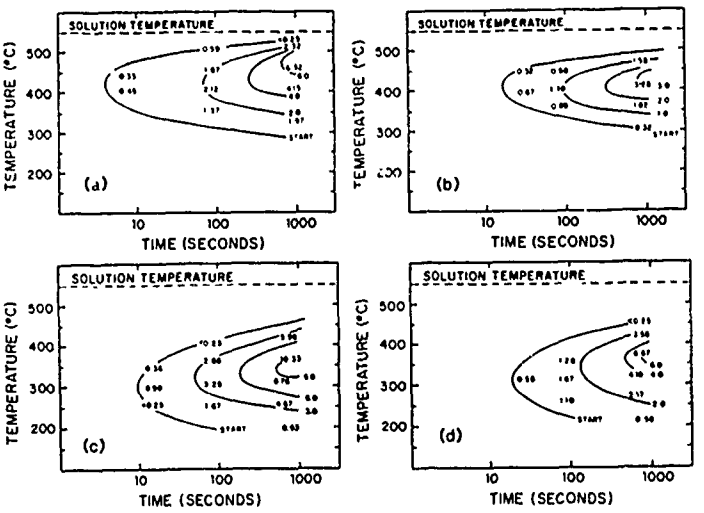

Figure 17. Time-temperature-transformation curves showing volume percents of T_2 and S phases. (a) T_2 for Al-2.58Li-1.36Cu-0.9Mg-0.13Zr (rich) alloy; (b) T_2 for Al-2.28Li-0.86Cu-0.9Mg-0.13Zr (lean) alloy; (c) S for the rich alloy and (d) S for the lean alloy (From Colvin and Starke, reference 79).

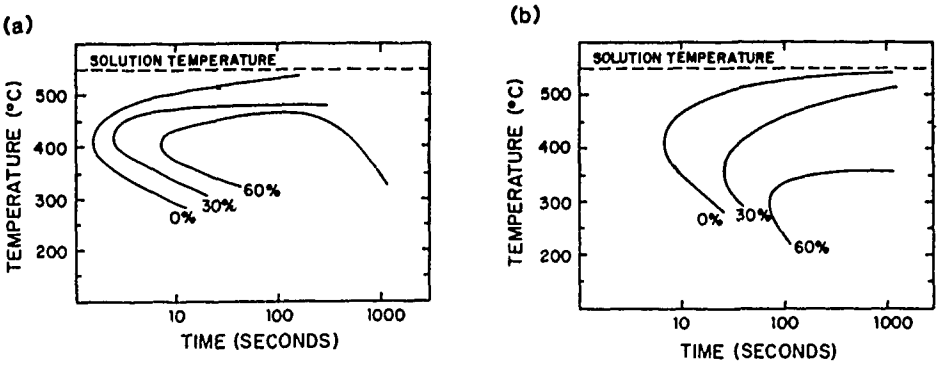

Figure 18. Iso mechanical lines showing the percent loss of Charpy energy values as a function of time at various temperatures (a) rich 8090 alloy and (b) lean 8090 alloy (From Colvin and Starke, reference 79).

Figure 19 shows the effects of different amounts of deformation prior to aging on the number density of the T_1 precipitates formed during aging for various times at 190°C (82). Since strength is related to the precipitate structure, there is a corresponding effect on strength, as shown in Figure 19(b). The significance of this data relates to commercial processing and different product forms, since a nonuniform distribution of deformation prior to aging can result to wide variances in strength within a product. Some product forms, such as complex forgings and those formed by superplastic deformation, are

not easily conducive to cold deformation prior to aging. Consequently, there is interest in examining heat treatment procedures and/or alloying additions that may aid in the nucleation of the strengthening precipitates in a way that is similar to the effect of dislocations.

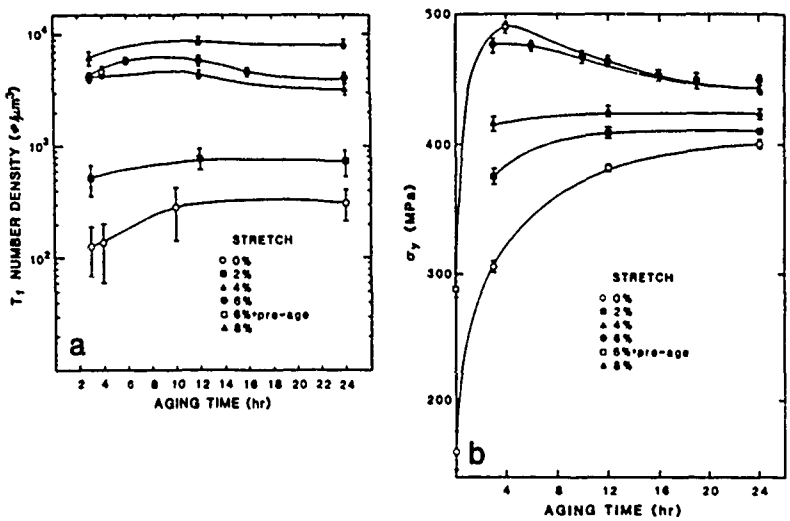

Figure 19. Effect of stretch on the precipitation and strength of an Al-2.4Li-2.4Cu-0.18Zr alloy. (a) Number density of T_1 as a function of aging time at 463K for various degrees of stretch prior to aging and (b) corresponding yield strength vs. aging time (From Cassada, Shiflet and Starke, reference 82).

Lewis et al. (14) have improved the fracture toughness and stress corrosion resistance of 8090 by aging at 150°C instead of the commonly used 190°C. Pitcher (83) has recently shown that a slow heat-up rate to the aging temperature can lead to a better balance of tensile strength and toughness in 8091 than a rapid heat-up rate when deformation prior to aging is impossible. He relates the enhanced precipitation of S' to the release of vacancies, as the δ' precipitates grow during the slow heat up. These vacancies assist the formation of homogeneous S'. A slow heat-up rate has the same effect as a duplex age, i.e., at a low temperature followed by aging at a high temperature. Both a slow heat-up rate to the aging temperature and a low → high temperature duplex age are common practices for 7XXX alloys. Recent studies by Blackburn et al. (84) have demonstrated that small additions of indium to 2090 can aid in the nucleation of both T_1 and θ'. This has an effect similar to a 3 to 4% stretch, when compared with an indium-free alloy.

Ashton et al. (47) have established that a combination of cold work (up to 7%) prior to aging and a low aging temperature can significantly improve the strength-toughness relationship in both 2090 and 8091. As mentioned, deformation increases the number of nucleation sites for θ', T_1 and S'. Lowering the aging temperature increases the degree of supersaturation and the driving force for nucleation of the strengthening precipitates. Consequently, higher strengths than realized at higher aging temperatures may be obtained. In addition, since diffusion rates are decreased, the size and volume fraction of the grain boundary precipitates are also decreased, which produces an improvement in the fracture toughness.

In general, for alloys that contain a low volume fraction of constituent phases and grain boundary precipitates, the fracture toughness is controlled by the deformation behavior, being maximized when deformation is homogeneous (36). Jata and Starke (36) showed that the fracture toughness variation with aging time can be quantitatively related to the changes in slip planarity, i.e., the fracture toughness decreases as the slip band width decreases and the slip band spacing increases. They also determined (85) that slip localization decreases with decreasing temperature, thus explaining the major reason for the large improvement in fracture toughness with decreasing temperature. The higher fracture toughness at cryogenic temperatures has also been attributed to: (a) low melting point grain boundary phases which solidify at low temperatures and remain liquid at room temperature (85,86), (b) a larger number of crack delaminations perpendicular to the short transverse direction or perpendicular to the fracture surface in an L-T oriented specimen (71,87) and in plane crack deflections (71) and (c) higher strain hardening capacity at low temperatures (88). The Jata and Starke model is consistent with the increase in strain hardening capacity at low temperatures.

The optimum microstructure for fatigue crack initiation resistance is consistent with that required for high fracture toughness (89). However, the situation is somewhat different for fatigue crack growth resistance (90). Lin and Starke (91) have shown that a tortuous crack path and crack branching, both of which are enhanced by coarse planar slip, are desirable for a high fatigue crack growth resistance in aluminum alloys. The torturous crack path reduces the "crack driving force" due to extrinsic effects which include roughness-induced crack closure (92-94), Figure 20. The propensity of Al-Li

alloys to deform by coarse planar slip results in a significant improvement in fatigue crack growth resistance under both constant amplitude (57,94-96) and variable amplitude loading (97) when compared with conventional high strength aluminum alloys. Figure 21, taken from the work of Ritchie and co-workers (98), compares the crack growth behavior of 2090-T8E41 (T-L orientation) with that for two different tempers of 2124 and 7150.

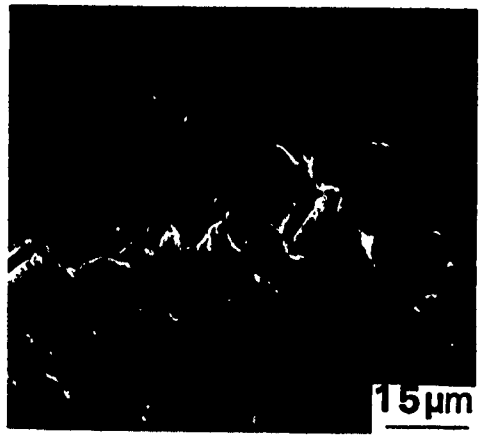

Figure 20. Scanning electron micrcgraph showing the fatigue crack profile and the presence of "roughness induced closure" in an Al-Li-Mg alloy.

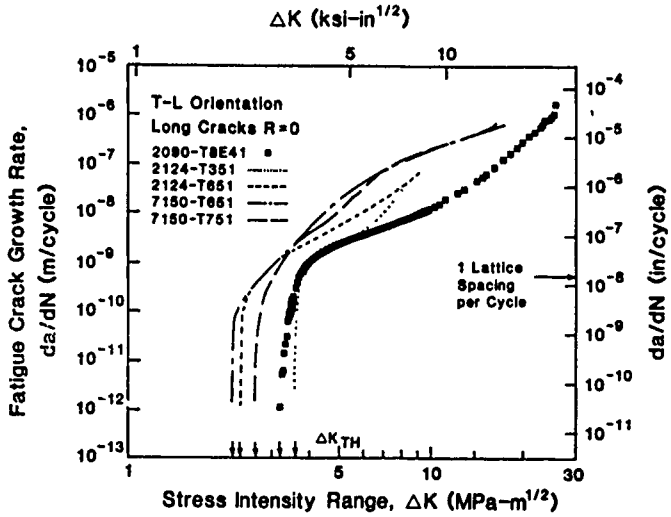

Figure 21. Crack propagation behavior of long fatigue cracks in 2090-T8E41 (T-L orientation), as a function of the nominal stress intensity range, compared to corresponding results in 2124 and 7150 alloys. Data for tests in moist air at R = 0.1 (From Ritchie and coworkers, reference 98).

Aluminum-lithium alloys have not demonstrated the same significant advantages over baseline alloys for short crack growth resistance (99). This is partially the result of reduced crack tip shielding effects (94,100). However, even in this regime Al-Li should show some improvement considering that they normally have a modulus of between 10 to 15 percent larger than conventional aluminum alloys. Although the fatigue crack initiation resistance of Al-Li alloys may be somewhat poorer than that of conventional alloys (101,102) (most likely due to the extensive strain localization and sharp texture normally present) their overall fatigue performance under S-N type test conditions is generally equivalent to, or better than, that of standard aluminum alloys.

The precipitate structure also has a significant effect on the stress corrosion cracking behavior of Al-Li alloys (103). While Al-Li, Al-Li-Zr, and Al-Mg-Li-Zr alloy systems exhibit a high resistance to stress corrosion crack initiation (104,105) the Al-Li-Cu-Zr and Al-Li-Cu-Mg-Zr systems do not (104,106-110). This suggests that the presence of one of the copper containing precipitate phases, e.g., T_1, S', T_2 or $Al_6Cu(MgLi)_3$ may be responsible for promoting crack initiation rather than AlLi or Al_2MgLi (103). Underaged tempers have been shown to be less susceptible than peak or overaged tempers to

SCC initiation for Al-Cu-Li-Zr alloys (103) but overaging has been shown to decrease the susceptibility of Al-Li-Cu-Mg-Zr alloys, Figure 22. Although underaged tempers appear to offer the highest resistance to SCC propagation for both alloy systems, Figure 23, the propagation behavior is relatively insensitive to temper as well as being insensitive to alloy chemistry and test environment (103).

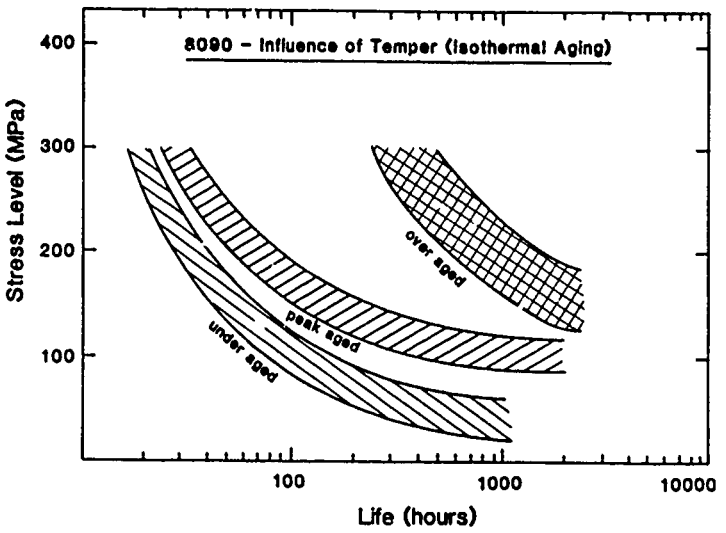

Figure 22. The influence of temper on the stress-life curve of 8090 plate (ST orientation). (From Gray et al., reference 103).

Aluminum-lithium alloys, particularly 2090, have surprisingly different forming characteristics than the industry standard aircraft aluminum alloys such as 2024 and 7075 (111). These differences in formability reflect the unique deformation behavior and grain structure exhibited by Al-Li alloys, in particular, their propensity for localized planar slip. The formability of Al-Li alloys has also been shown to be more sensitive to grain direction and prior cold work than the standard aircraft aluminum alloys. Maximum formability has been observed when Al-Li alloys are in the "as-quenched" condition and the bend axis is parallel to the long grain direction (111). It was previously shown that cold work prior to aging is necessary to develop the optimum strength-fracture toughness in Al-Li-Cu-X alloys. However, this step often reduces formability, forcing a compromise between the most desirable part shape and the resulting properties. This has necessitated the development of procedures which utilize the cold work imparted during forming to bring the final product to the required strength level.

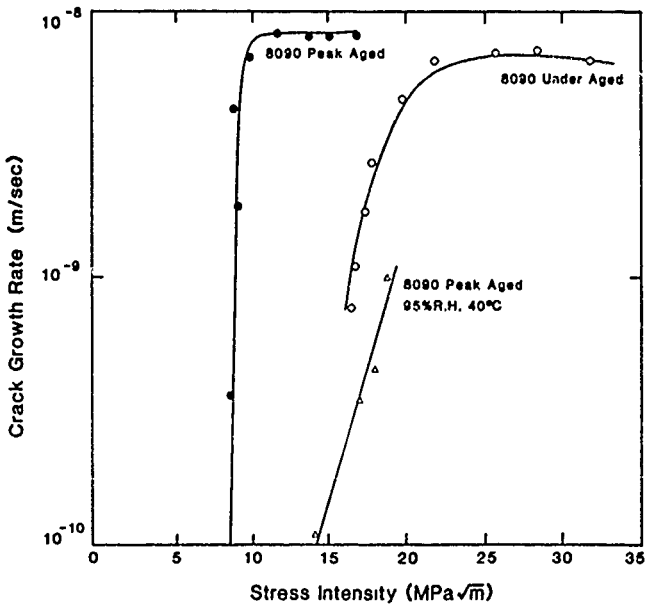

Figure 23. Crack growth velocity versus stress intensity curves for under- and peak-aged 8090 in artificial sea water and peak-aged 8090 in a 95 percent relative humidity atmosphere at 40°C (From Gray et al., reference 103).

OTHER ENGINEERING PROPERTIES

In addition to those properties discussed above, there are certain other engineering properties of Al-Li alloys that are attractive in comparison to conventional baseline aluminum alloys. For example, most Al-Li alloys are amenable to superplastic forming (112,113), display moderate to good weldability (114,115), can be chemically milled, bonded, anodized, alclad, and painted. On the debit side, as noted previously, Al-Li alloys often display considerable anisotropy in strength and ductility. They are somewhat more susceptible to surface oxidation at moderate temperatures, and are prone to warping during quenching (mostly attributable to the relatively high quenching temperature). Diffusion of lithium can occur out to the surface during high temperature heat treatments which may lead to a lithium-depleted layer, and for sheet products a reduction in strength (116). In addition, all Al-Li-X alloys suffer from low ductility and fracture toughness in the short transverse direction. These problems are due to a combination of grain structure and segregation effects and should be minimized by improved processing. Most problems associated with Al-Li-X alloys appear to be solvable by the development of intelligent processing methods and the advantages in density and modulus that they offer over conventional aluminum alloys have already led to their usage in a number of aerospace systems.

ACKNOWLEDGEMENTS

One author, Edgar A. Starke, Jr., would like to gratefully acknowledge support from the following: U.S. Army Research Office, under grant #DAAL03-86-K0128, Dr. Andrew Crowson, Program Monitor; U.S. Air Force Office of Scientific Research, under grant #AFOSR-87-0082, Dr. Alan Rosenstein, Program Monitor; and U.S. Office of Naval Research, under grant #N00014-85-0526, Dr. George Yoder, Program Monitor.

REFERENCES

1. Reuleaux, O., J. Inst. Met., 33, 1925, p. 346.

2. Scheuer, E., Z. Metallunkunde, 19, p. 16.
3. LeBaron, I. M., U.S. Patent No. 2,381,219, Application date 1942, Granted 1945.

4. Hardy, H.K. and J.M. Silcock, J. Inst. Met., 84, 1955-56, p. 423.

5. Silcock, J.M., J. Inst. Met., 88, 1959-60, p. 357.

6. Fridlyander, I.N., V.F. Shamray and N.V. Shiryayera, Russian Metallurgy, No. 2, 1965, p. 83, Translated from Izvestiya Akademii nauk SSSR Metally, No. 2, p. 153.

7. Ekvall, J.S., J.E. Rhodes and G.G. Wald in Design of Fatigue and Fracture Resistant Structures, ASTM STP 671, 1982, p. 328.

8. Sankaran, K.K. and J.J. Grant, Aluminum-Lithium Alloys, ed. T.H. Sanders, Jr. and E.A. Starke, Jr., The Metall. Soc. AIME, 1981, p. 205.

9. Pickens, J.R., Heubaum, F.H., Langan, T.J., and Kramer, L.S., in Aluminum-Lithium Alloys V, ed. T.H. Sanders, Jr., and E.A. Starke, Jr., MCE Publications Ltd., Birmingham, U.K., 1989, Vol. III, p. 1397.

10. Bretz, P.E., Aluminum-Lithium Alloys; Design, Development and Application Update, ed. Ramesh J. Kar, Suphal P. Agrawal and William E. Quist, ASM International, 1988, p. 1.

11. Labarre, L.C., R.S. James, J.J. Witters, R.J. O'Malley and M.R. Emptage, 4th International Aluminum Lithium Conference, ed. by G. Champier, B. Dubost, D. Miannay and L. Sabetay, J. de Physique, Colloque C3, 1987, p. C3-93.

12. Last, H.R., T.H. Sanders, Jr. and J. G. Gonsalves, "Stability of Twinned Columnar Grain Structures in Aluminum Alloy Castings," submitted to Metall. Trans. A.

13. Ashton, R.F., D. S. Thompson and F.W. Gayle, Aluminum Alloys - Physical and Mechanical Properties, ed. E.A. Starke, Jr. and T.H. Sanders, Jr., EMAS, Warley, West Midlands, U.K., 1986, p. 403.

14. Lewis, R.E., E.A. Starke, Jr., W.C. Coons, G.J. Shiflet, E. Willner, J.G. Bjeletich, C.H. Mills, R.M. Harrington, and D.N. Petrakis, 4th International Aluminum Lithium Conference, ed. by G. Champier, B. Dubost, D. Miannay, and L. Sabetay, J. de Physique, Colloque C3, 1987, p. C3-643.

15. Sanders, T.H., Jr., and E.A. Starke, Jr., Acta Met., 36, 1982, p. 927.

16. Noble, B., and G.E. Thompson, Met. Sci. J., 5, 1971, p. 114.

17. Williams, D.B., and J.W. Edington, Met. Sci., 9, 1975, p. 529.

18. Cassada, W.A., G.J. Shiflet and E.A. Starke, Jr., Acta Met., 34, 1986, p. 367.

19. Sanders, T.H., Jr., "Development of an Al-Mg-Li Alloy", Final Report, Naval Air Developmental Center Contract No. N622269-74-C-0328, 1976.

20. Thompson, G.E., and B. Noble, J. Inst. of Met., 101, 1973, p. 111.

21. Mondolfo, L.F., "Aluminum Alloys - Structure and Properties", Butterworths, London, 1976, p. 554.

22. Sanders, T.H., Jr., H.R. Last and S.C. Jha, "Microstructure and Properties of Al-Li-Mg Alloys," Proceedings of the International SAMPE Metals Conference, Cherry Hill, N.J., August 18-20, 1987, in press.

23. Bauman, S.F., and D.B. Williams, in Aluminum-Lithium Alloys II, ed. E.A. Starke, Jr. and T.H. Sanders, Jr., The Metallurgical Society of AIME, Warrendale, PA., 1983, p. 17.

24. Nobel, B., and G.E. Thompson, Met. Sci. J., 6, 1972, p. 167.

25. Rioja, R.J., and E.A. Ludwiczak, in Aluminum-Lithium Alloys III, ed. C. Baker, P.J. Gregson, S.J. Harris, and C.J. Peel, The Institute of Metals, London, 1985, p. 471.

26. Gregson, P.J. and H. M. Flower, Acta Met., 33, 1985, p. 527.

27. Sanders, T.H., Jr., Unpublished Research Presented at "Aluminum-Lithium II", Monterey, CA, April 12-14, 1983.

28. Cassada, W.A., G.J. Shiflet, and E.A. Starke, Jr., Scripta Met., 20, 1986, p. 751.

29. Cassada, W.A., G.J. Shiflet, and S.J. Poon, Phys. Rev. Let., 56, 1986, p. 2276.

30. Cassada, W.A., G.J. Shiflet and E.A. Starke, Jr., in Aluminum Alloys, Their Physical and Mechanical Properties, Vol. II., ed. E. A. Starke, Jr. and T.H. Sanders, Jr., EMAS, 1986, p. 695.

31. Barges, C., M.H. Tosten, P.R. Howell and E.R. Ryba, J. Mat. Sci., 22, 1987, p. 1663.

32. Price, R.J., and A. Kelly, Acta Met., 12, 1964, p. 159.

33. Starke, E.A., Jr., and F.S. Lin, Metall. Trans. A., 13A, 1982, p. 2259.

34. Huang, J.C., and A.J. Ardell, 4th International Aluminum Lithium Conference, ed. G. Champier, B. Dubost, D. Miannay, and L. Sabetay, J. de. Physique, Colloque C3, 1987, p. C3-373.

35. Sainfort, P. and P. Guyot, in Aluminum-Lithium Alloys III, ed. by C. Baker, P.J. Gregson, S. J. Harris and C.J. Peel, Inst. of Metals, London, 1986, p. 420.

36. Jata, K.V., and E. A. Starke, Jr., Metall. Trans. A., 17A, 1986, p. 1011.

37. Howe, J.M., Lee, J. and Vasudevan, A.K., Metall. Trans. A, 19A, 1988, p. 2911.

38. Tomura, M., T. Mori and T. Nakam ra, J. Japan Inst. Metals, 34, 1970, p. 919.

39. Blankenship, C.P., Jr., and Starke, E.A., Jr., "The Fatigue Crack Growth Behavior of the Al-Cu-Li Alloy Weldalite 049," submitted to the Journal of Engineering Materials and Structures.

40. Crooks, R.E., and E.A. Starke, Jr., Metall. Trans. A., 15A, 1984, p. 1367.

41. Peel, C.J., B. Evans, C.A. Baker, D.A. Bennett, P.J. Gregson and H.M. Flower, in Aluminum-Lithium II, ed. E.A. Starke, Jr. and T.H. Sanders, Jr., The Metall. Society AIME, Warrendale, PA, 1984, p. 363.

42. Sainfort, P., and B. Dubost, in 4th International Aluminum-Lithium Conference, ed. G. Champier, B. Dubost, D. Mainnay, L. Sabetay, Journal De Physique, Colloque C3, 1987, p. 407.

43. Hautefeuille, I., R. Rahouadj, Y. Barbaux and M. Clavel, ibid, p. 669.

44. Narayanan, G.H., B.L. Wilson, W.E. Quist, and A.L. Wingert, "Low Density Aluminum Alloy Development", Third Interim Technical Report; 1983, AFWAL Contract No. F33615-81-5053.

45. Crooks, R.E., E.A. Kenik and E.A. Starke, Jr., Scripta Met., 17, 1983, p. 643.

46. Ashton, R.F., D.S. Thompson, E.A. Starke, Jr., and F.S. Lin, in Aluminum-Lithium Alloys III, ed. by. C. Baker, P.J. Gregson, S.J. Harris and C.J. Peel, The Institute of Metals, London, 1986, p. 66.

47. Dean, W.A., in Aluminum-Properties and Physical Metallurgy, ed. J.L. Hatach, ASM, Metals Park, OH, 1984, p. 200.

48. Muller, W., E. Bubeck and V. Gerold, in Aluminum-Lithium Alloys, III, ed. by C. Baker, P.J. Gregson, S.J. Harris, and C. Peel, The Institute of Metals, London, 1986, p. 435.

49. Agyekum, E., W. Ruch, E.A. Starke, Jr., S.C. Jha, and T.H. Sanders, Jr., ibid, p. 448.

50. Narayanan, G.H., W.E. Quist, B.L. Wilson, and A.L. Wingert, "Low Density Aluminum Alloy Development", First Interim Tech. Report, 1982, AFWAL Contract No. F33615-81-C-5053, p. 95.

51. Dudzinski, N., J. Inst Met., 81, 1952-53, p. 49.

52. O'Dowd, M.E., W. Ruch and E.A. Starke, Jr., in 4th International Aluminum-Lithium Conference, ed. G. Champier, B. Dubost, D. Miannay, L. Sabetay, J. de Physique, Colloque C3, 1987, p. 565.

53. Broussaud, F., and M. Thomas, in Aluminum-Lithium Alloys, III, C. Baker, P.J. Gregson, S.J. Harris, and C.J. Peel, The Institute of Metals, London, 1986, p. 442.

54. Wakeling, P.O., "ALCAN Developments in Al-Li Technology," NASA Workshop, Langley, VA, 1987.

55. Lin, F.S., Scripta Met., 16, 1982, p. 1295.

56. Kuo, Victor W.C., and E.A. Starke, Jr., Metall. Trans. A. 16A, 1985, p. 1089.

57. Peel, C.J., D. McDarmaid, and B. Evans, "Considerations of Critical Factors for the Design of Aerospace Structur- : Using Current and Future Aluminum-Lithium Alloys", in Aluminum-Lithium Alloys: Design, Development and Application Update, ed. R.J. Kar, S.P. Agrawal, and W.E. Quist, ASM International, Metals Park, Ohio, 1987, p. 315.

58. Peters, M., K. Welpmann, and T.H. Sanders, Jr., Advanced Materials Research and Developments for Transport Light Metals, RVII, Les Editions, Les Ulis, France, 1985, p. 63.

59. Peters, M., J. Eschweiler and K. Welpmann, Scripta Met., 20, 1986, p. 259.

60. Fox, S., H.M. Flower and D.S. McDarmaid, Aluminum Alloys - Physical and Mechanical Properties, ed. E.A. Starke, Jr., and T.H. Sanders, EMAS, West Midlands, United Kingdom, 1986, p. 939.

61. Bull, M.J. and D.J. Lloyd, Aluminum Lithium Alloys III, ed. C. Baker, P.J. Gregson, S.J. Harris and C.J. Peel, The Institute of Metals, London, 1986, p. 402.

62. Eroussaud F. and C. Diot, 4th International Aluminum Lithium Conference, ed. G. Champier, B. Dubost, D. Miannay and L. Sabetay, J. de Physique, Colloque C3, 48, 1987, p. C3-597.

63. Hirsch, J., O. Engler, K. Lucke, M. Peters and K. Welpmann, 4th International Aluminum Lithium Conference, ed. G. Champier, B. Dubost, D. Miannay and L. Sabetay, J. de Physique, Colloque C3, 48, 1987, p. C3-605.

64. Lipinski, P., M. Berveiller, A. Hihi, P. Sainfort and P. Meyer, 4th International Aluminum Lithium Conference, ed. G. Champier, B. Dubost, D. Miannay and L. Sabetay, J. de Physique, Colloque C3, 48, 1987, p. C3-613.

65. Vasudevan, A.K., W.G. Fricke, Jr., R.C. Malcolm, R.J. Bucci, M.A. Przystupa and F. Barlat, Metall. Trans. A, 19A, 1988, p. 731.

66. Sadananda, K., and K.V. Jata, Metall. Trans. A, 19A, 1988, p. 847.

67. Reynolds, M.A., A. Gray, E. Creed, R.M. Jordan and A.P. Titchener, in Aluminum-Lithium Alloys III, ed. by C. Baker, P.J. Gregson, S.J. Harris and C.J. Peel, The Institute of Metals, London, 1986, p. 57.

68. Jata, K.V., and Starke, E.A., Jr., Scripta Met., 22, 1988, p. 1553.

69. Morris, J.W., Jr., and J. Glazer, Lecture at the 1988 Int. Cryogenic Mater. Conf., Shenyang, China (1988).

70. Glazer, J., Ph.D. Thesis, Lawrence Berkeley Lab., Univ. of California, July 1989.

71. Rao, K.T.V., H.F. Hayashigatani, W. Yu and R.O. Ritchie, Scripta Met., 22, 1988, p. 93.

72. Rao, K.T.V., W. Yu, and R.O. Ritchie, Metall. Trans. A, 20A, 1989, p. 485.

73. Roven, H.J., E.A. Starke, Jr., O. Sodahl, and J. Hjelen, Scripta Met., 1990, in press.

74. Dingley, D.J., Scanning El. Micro. 2, 1984, p. 569.

75. Hjelen, J., and Nes, E., Proc. 8th Int. Conf. on Textures of Materials, AIME, Warrendale, PA, 1988, p. 597.

76. Makin, P.L. and W.M. Stobbs, ibid, 1986, p. 392.

77. Christian, J.W., The Theory of Transformations in Metals and Alloys, First Edition, Pergamon Press, Oxford, England (1965).

78. Starke, E.A., Jr., in Strength of Metals and Alloys, ICSMA 6, ed. by R.C. Gifkins, Vol. 3, Pergamon Press, 1982, p. 1025.

79. Colvin, G.N., and E.A. Starke, Jr., SAMPE Quarterly, 19, 1988, p. 10.

80. Staley, J.T., Alcoa Research Laboratory, Alcoa Center, PA, unpublished research, 1988.

81. Bourgasser, P., J.A. Wert and E.A. Starke, Jr., "Intergranular Fracture of an Al-Li-Cu-Mg Alloy as a Result of Non-equilibrium Eutectic Melting During Solution Treatment", Materials Science and Technology, in press.

82. Cassada, W.A., G.J. Shiflet and E.A. Starke, Jr., in 4th International Aluminum Lithium Conference, ed. by G. Champier, B. Dubost, D. Miannay, and L. Sabetay, J. de Physique, Colloque C3, 1987, p. C3-397.

83. Pitcher, P.D., "Ageing of Forged Aluminum-Lithium 8091 Alloy", Scripta Met., in press.

84. Blackburn, L., W. Casada, G. Colvin, G. Shiflet, and E.A. Starke, Jr., Aluminum-Lithium Alloys: Design, Development and Application Update, ed. Ramesh J. Kar, Suphal P. Agrawal, and William E. Quist, ASM International, Metals Park, Ohio, 1987, p. 187.

85. Webster, D., Aluminum Lithium Alloys III, ed. by C. Baker, P.J. Gregson, S.J. Harris and C.J. Peel, Institute of Metals, London, 1986, p. 602.

86. Webster, D., Met. Trans. A, 18A, 1987, p. 2181.

87. Dorward, R.C., Scripta Met., 20, 1986, p. 1379.

88. Glazer, J., S.L. Verzasconi, R.R. Sawtell and J.W. Morris, Met. Trans. A, 18A, 1987, p. 1695.

89. Starke, Edgar A., Jr., and Gerd Luetjering, "Cyclic Plastic Deformation and Microstructure", in Fatigue and Microstructure, ed. M. Meshii, ASM, Metals Park, Ohio, 1979, p. 205.

90. Starke, E.A., Jr., and J. C. Williams, "Microstructure and the Fracture Mechanics of Fatigue Crack Propagation", Fracture Mechanics: Perspectives and Directions, STP 1020, ed. R.P. Wei and R.P. Gangloff, ASTM, Philadelphia, PA, 1989, p. 184.

91. Lin, F.S., and E.A. Starke, Jr., Mater. Sci. and Engr., 43, 1980, p. 65.

92. Jata, K.V., and E.A. Starke, Jr., in Aluminum-Lithium Alloys III, ed. by C. Baker, P.J. Gregson, S.J. Harris and C.J. Peel, The Institute of Metals, London, 1986, p. 247.

93. Petit, J., S. Suresh, A.K. Vasudevan and R.C. Malcolm, ibid, 1986, p. 257.

94. Venkateswara Rao, K.T., W. Yu and R.O. Ritchie, Scripta Met., 20, 1986, p. 1459.

95. Coyne, E.J., Jr., T.H. Sanders, Jr., and E.A. Starke, Jr., in Aluminum-Lithium Alloys, ed. T.H. Sanders, Jr., and E.A. Starke, Jr., AIME, Warrendale, PA, 1981, p. 293.

96. Vasudevan, A.K., P.E. Bretz, A.C. Miller and S. Suresh, Mat. Sci. and Engr., 64, 1984, p. 113.

97. Scarich, G.V., K.M. Bresnahan, and P.E. Bretz, in "Fatigue Crack Growth Resistance of Aluminum Alloys Under Spectrum Loading", Vol. II, Aluminum-Lithium Alloys, Tech. Rep. No. NOR-85-141, NASC, Northrop Corporation, Hawthorne, CA.

98. Venkateswara Rao, K.T., W. Yu and R.O. Ritchie, Met. Trans. A, 19A, 1988, p. 549.

99. Venkateswara Rao, K.T., W. Yu and R.O. Ritchie, ibid, 1988, p. 563.

100. James, M.R., Scripta Met., 21, 1987, p. 783.

101. Peters, M., K. Welpmann, W. Zink and T.H. Sanders, Jr., in Aluminum-Lithium Alloys III, ed. C. Baker, P.J. Gregson, S.J. Harris and C.J. Peel, The Institute of Metals, London, 1986, p. 239.

102. Farcy, L., C. Carre, M. Clavel, Y. Barbaux and D. Aliaga, in 4th International Aluminum-Lithium Conference, ed. by G. Champier, B. Dubost, D. Miannay and L. Sabetay, J. de Physique, Colloque C3, 1987, p. 565.

103. Gray, A., N.J.H. Holroyd and W.S. Miller, "The Environmental Cracking Behaviour of Aluminum-Lithium Based Alloys", Proceedings of the International SAMPE Metals Conference, Cherry Hill, N.J., August 18-20, 1987, in press.

104. Holroyd, N.J.H., A. Gray, G.M. Scamans and R. Hermann, in Aluminum-Lithium Alloys III, ed. C. Baker, P.J. Gregson, S.J. Harris and C.J. Peel, Institute of Metals, London, 1986, p. 310.

105. Christodoulou, L., L. Struble and J.R. Pickens, in Aluminum-Lithium Alloys II, ed. by E.A. Starke, Jr., and T.H. Sanders, Jr., The Met. Soc. AIME, 1984, p. 561.

106. Meletis, E.I., "Stress Corrosion Cracking Properties of 2090 Al-Li Alloy", Proceedings International Conference on Fatigue Corrosion Cracking, Salt Lake City, UT, 1985.

107. Rinker, J.G., M. Marek and T.H. Sanders, Jr., Mat. Sci. Eng., 64, 1984, p. 203.

108. Vasudevan, A.K., P.R. Ziman, S.C. Jha and T.H. Sanders, Jr., in Aluminum-Lithium Alloys III, ed. by. C. Baker, P.J. Gregson, S.J. Harris and C.J. Peel, Institute of Metals, London, 1986, p. 303.

109. Colvin, E.L., S.J. Murtha and R.K. Wyss, in Aluminum Alloys: Physical and Mechanical Properties, ed. by E.A. Starke, Jr., and T.H. Sanders, Jr., EMAS, 1986, p. 1853.

110. Meletis, E.I., J.M. Sater and T.H. Sanders, Jr., ibid, 1986, p. 1157.

111. Yavari, P., D. Ward and J.J. Christiana, "Forming and Post-Formed Properties of 2090", presented at the Al-Li Conference, WESTEC, Los Angeles, CA, March, 1988, to be published in the Proceedings.

112. Agrawal, S.P. and R.J. Kar, eds., "Aluminum-Lithium Development, Application and Superplastic Forming", Proceedings, WESTEC '86, ASM, Metals Park, Ohio, 1986.

113. Wadsworth, J., C.A. Hensahall and T.E. Nieh, in Aluminum-Lithium III, ed. by C. Baker, P.J. Gregson, S.J. Harris and C.J. Peel, The Institute of Metals, London, 1986, p. 199.

114. Pickens, J.R., "A Review of the Weldability of Lithium-Containing Aluminum Alloys", Martin-Marietta Report MML TR 84-22.

115. Edwards, M.R. and V.E. Stoneham, in 4th International Aluminum-Lithium Conference, ed. G. Champier, B. Dubost, D. Miannay and L. Sabetay, J. de Physique, Colloque C3, 1987, p. C3-293.

116. Papazian, J.M., G.G. Bott, and P. Shaw, in Proceedings of the 17th National SAMPE Conference, 1985, p. 688.

NEW LOW DENSITY AND HIGH TEMPERATURE ALUMINUM ALLOYS

E.A. Starke, Jr., and H.G.F. Wilsdorf
Department of Materials Science
University of Virginia
Charlottesville, VA 22901

Although aluminum alloys have been the materials of choice for aerospace structures, the demands for higher performance and supersonic flight has placed severe limitations on their use in advanced systems. This has led to an increased use of titanium alloys and fiber reinforced non-metallic composites when high temperature stability and high specific strength are design requirements. These higher cost materials are often not readily available and can be difficult to fabricate. Aluminum's low cost, low density, and ease of fabrication has encouraged the development of two new families of aluminum alloys: one having reduced density and greater stiffness and one having improved thermal stability. This paper will describe these two new aluminum alloy systems.

INTRODUCTION

High-strength aluminum alloys have historically been the primary materials choice for aerospace systems; however, new and future high performance military aircraft, high speed civil aircraft and space systems will require materials properties unattainable with conventional aluminum alloys. As with most aerospace systems, designers are primarily concerned with strength to weight ratio, durability, which includes corrosion resistance, damage tolerance, and the stability of properties in the operating

environment. Economic considerations, which include materials costs and their availability, producibility and maintainability, as well as the fly to buy ratio are also of major concern. Although titanium alloys offer superior high temperature performance and nonmetallic composites have higher specific strength, when compared with conventional aluminum alloys, their high cost and manufacturing requirements have encouraged the development of new aluminum alloys which may be competitive in certain operating environments.

LOW DENSITY ALUMINUM ALLOYS

Although carbon fiber and boron fiber non-metallic composites offer a considerable density and stiffness advantage over all other structural materials used in aerospace systems, reducing the density and increasing the stiffness of aluminum alloys is desirable due to their low acquisition cost and the aerospace community's extensive design and manufacturing experience with these materials. Since lithium is the lightest metallic element, alloying it with aluminum will significantly reduce the density of aluminum alloys and early work at Alcoa (1) showed that lithium also increases aluminum's elastic modulus. Lithium can reduce the density of aluminum by three percent and increase the elastic modulus by six percent for every weight percent added, at least up to additions of three weight percent lithium (2). During the 1970-80's extensive research and development focused on producing a new class of medium and high strength aluminum-lithium alloys

having lower density and higher stiffness than conventional 2xxx and 7xxx alloys.

Alloy designations and compositions of the new lithium-containing aluminum alloys are listed in Table 1. The improvements in density and stiffness of these alloys offer the opportunity of achieving weight reductions in conventional aluminum aerospace systems of up to 15%. Many of these materials possess good combinations of strength, damage tolerance and durability, in general are quite weldable, and several have demonstrated excellent cryogenic and moderate temperature properties. The properties of most of the new aluminum-lithium alloys appear particularly sensitive to small variations in composition and processing. This sensitivity seems to be associated with the difficulty in maintaining metal quality during casting, the presence of recrystallization inhibiting elements, and the complexity of the microstructure after primary processing and heat treatment.

As with most aluminum alloys, microstructural features of importance for property control of Al-Li alloys include: (a) cast structure, (b) grain structure and crystallographic texture, (c) volume fraction, size and distribution of insoluble intermetallic particles and grain boundary precipitates, and (d) coherency, volume fraction and distribution of strengthening precipitates. Since one of the goals of this conference is to identify promising technology for application to the interdisciplinary design and development of thermal structures we will focus on the effect of processing of new aluminum alloys and their use as a structural

material.

Processing begins with homogenization to reduce segregation, remove the low-melting nonequilibrium phases, and thus improve workability. This thermal treatment also serves to precipitate the dispersoid-forming elements, such as those containing zirconium, so that they may perform their role of grain control during subsequent processing. One must be very careful in going to the final homogenization temperature to ensure that the low-melting phases are dissolved before their melting temperatures are reached. The atmosphere used in the homogenization treatment should be relatively dry in order to minimize oxidation and hydrogen pickup. One also needs to be concerned about lithium loss from the surface (3,4). The homogenization treatment is followed by hot working for ingot breakdown and shape change to the appropriate product form. The bulk of aluminum used in airframe manufacture consists of sheet, plate, and extruded bar. The wrought product is usually solution heat treated, quenched, possibly worked, and aged to develop the desired microstructure. The heat treatment temperature, amount of deformation prior to aging, etc., depend on the alloy composition and the final microstructure and properties that are desired.

Recrystallization and Texture

All of the currently available Al-Li-X alloys contain zirconium as the dispersoid forming element and the Al_3Zr dispersoid is very effective in inhibiting recrystallization (5,6),

especially in the presence of lithium (7). During normal processing no recrystallization occurs from the casting stage to the final wrought product. Consequently, the wrought product is highly textured which results in a significant effect on forming operations and the anisotropy of properties, Figure 1. This figure also shows that recrystallization reduces anisotropy (9). The tensile properties obtained in recrystallized material are normally lower that those obtained for unrecrystallized material, although the fracture toughness is higher (10).

The deformation texture has an additional secondary effect on anisotropy for T8 tempers. In order to obtain the most favorable combination of strength and fracture toughness most Al-Li-Cu-X alloys are stretched from three to six percent prior to artificial aging. In highly textured materials, some slip planes will be more favorably oriented for slip than others and dislocation density resulting from the cold work will not be the same on all (111) planes. The (111) plane is the habit plane for T_1 precipitates and the dislocations aid in their nucleation (11). Consequently, T_1 precipitation will be non-uniform adding to the anisotropy of the final product (12). In the late stages of aging, T_1 will precipitate on all (111) planes, so the degree of anisotropy may be reduced by overaging, Figure 2 (13).

Rapid heat up rates during solution heat treatment, e.g. associated with salt baths, may also decrease the degree of anisotropy (14) as shown in Figure 3. However, depending on alloy composition, the rapid heat up rates may have a deleterious effect

on ductility. Bourgasser et al. (15) have shown that heating an Al-Li-Cu-Mg alloy to a solution treatment temperature greater than 543°C (which is desired for maximum solubility) at a rate greater than 50K/h can cause intergranular cracking, without application of an external stress. This can occur even after proper ingot preheat and homogenization treatments. The phenomenon is associated with non-equilibrium eutectic melting of a grain boundary precipitate phase and the liquid spreading along grain boundaries as a thin film. On quenching, intergranular cracks occur at grain boundaries into which the liquid film has penetrated during the solution heat treatment. No evidence of non-equilibrium melting has been observed in Al-Li-Cu alloys irrespective of the rate of heating to the solution heat treatment temperature. The melting that occurs in Al-Li-Cu-Mg alloys is associated with a soluble precipitate phase which forms in the solid state and not with a low melting eutectic formed during solidification. Caution should be exercised when solution heat treating small parts or thin gage 8091-type alloys if heat up rates exceed 50K/h.

Thick products, e.g., plate and extrusions, may exhibit variations in texture in the short transverse direction resulting in an additional anisotropy, Figure 4, (16). Some of the through-thickness texture variation may be associated with a limited amount of recrystallization that normally occurs near the surface.

The degree of recrystallization near the surface may be increased by the loss of lithium during heat treatments. Alloy

losses through heat treatment are caused by the relatively high diffusion coefficients of the Li and Mg atoms in the Al-matrix and, more importantly, by the extreme affinity of these alloying elements for oxygen (17). Unlike conventional non-Li containing aluminum alloys, the oxidation products found on Al-Li alloys are permeable to lithium, and, when heat treated in air, oxidation is continuous. With the loss in Li there is a concomitant growth of the recrystallization layer at the surface (3) and a decrease in strength of the surface layer. Consequently, heat treatment procedures which minimize lithium loss should be employed, especially for sheet products since surface affects can significantly effect bulk properties.

Precipitation

The commercial Al-Li-Cu-X alloys have a very complex precipitate structure and a number of phases co-precipitate during aging. A schematic illustration of the precipitate phases that form in the Al-Li-X systems is shown in Figure 5 (18).

A transmission electron micrograph showing the presence of a number of the precipitates in an aged 2090 alloys is given in Figure 6. The major strengthening precipitates are: Al_3Li, δ', which is a metastable ordered phase that is spherical and coherent with the aluminum matrix; Al_2CuLi, T1, which precipitates as platelets on (111) matrix planes; Al_2Cu, Θ', which precipitates as platelets on (100) matrix planes. In alloys containing Mg, Al_2CuMg, S', which forms initially as rods or needles aligned along the

(100) directions in the matrix may be present. The T_1, θ', and S' precipitates are partially coherent with the matrix and show a strong tendency for heterogeneous nucleation on matrix dislocations and low angle grain boundaries. Consequently, the nucleation frequency and aging kinetics of these partially coherent precipitates are greatly affected by cold work, which increases the dislocation density, prior to artificial aging.

Figure 7 (a) shows the effects of different amounts of deformation prior to aging on the number density of the T_1 precipitates formed during aging for various times at 190°C (11). Since strength is related to the precipitate structure, there is a corresponding effect on strength, as shown in Figure 7 (b). The significance of this data relates to commercial processing and different product forms, since a nonuniform distribution of deformation prior to aging can result to wide variances in strength within a product. Some product forms, such as complex forgings and those formed by superplastic deformation, are not easily conducive to cold deformation prior to aging. Consequently, there is interest in examining heat treatment procedures and/or alloying additions that may aid in the nucleation of the strengthening precipitates in a way that is similar to the effect of dislocations. The qualitative effects that some trace additions have on precipitation in a number of alloy systems are given in Table 2.

Lewis et al. (19) have improved the fracture toughness and stress corrosion resistance of 8090 by aging at 150°C instead of

the commonly used 190°C. Pitcher (20) has shown that a slow heat-up rate to the aging temperature can lead to a better balance of tensile strength and toughness in 8091 than a rapid heat-up rate when deformation prior to aging is impossible. He relates the enhanced precipitation of S' to the release of vacancies, as the δ' precipitates grow during the slow heat up. These vacancies assist the formation of homogeneously distributed S'. A slow heat-up rate has the same effect as a duplex age, i.e., at a low temperature age followed by a higher temperature age. Both slow heat-up rates and duplex aging are common practices for 7XXX alloys.

Fracture Toughness, Fatigue, and Stress Corrosion Cracking

One of the major deficiencies of the new Al-Li-X alloys has been poor short transverse fracture toughness. Rolled plate and extrusions of 2090 and 8090 Al-Li alloys also show a tendency to form delamination cracks in the short transverse direction which extend in the processing direction during fracture (21-23). Some authors have suggested that the delamination phenomena increases the conventional fracture toughness in other directions due to "delamination toughening", i.e. the L-T, L-S and T-S oriented specimens show higher fracture toughness than S-T specimens. Moreover, recent research indicates that the cryogenic fracture toughness in the L-T orientation is higher than at room temperature and is accompanied by an increase in the yield strength, UTS, strain to fracture and strain hardening exponent (21-23). Roven et al. (24) recently examined the influence of PFZ's and variations in

the relative misorientations between grains in the S-direction on the delamination behavior of an 8090-type alloy at cryogenic and room temperature. They found that the delamination behavior could be characterized by (i) a "fine delamination" whose spacing was independent of both aging condition and test temperature, i.e. 77K and RT, and (ii) a "coarse delamination" whose spacing varied both with aging condition and test temperature. The spacing of the "fine delaminations" correlated very closely to periodical events of high to low relative misorientations of grains in the S direction, i.e. with the through thickness texture. The "coarse delamination" appeared to be more associated with the presence of PFZ's and deformation behavior, i.e. planar versus homogeneous slip.

Lynch (25) has recently developed a processing procedure that significantly increases the short transverse fracture toughness in 8090-T377 plate. Lynch found that re-aging at temperatures between 200°C-230°C for short aging times (approximately 5 minutes) significantly increased the short transverse fracture toughness with only a small loss in strength, Figure 8. The increase in toughness is most significant when the heat up rate to the aging temperature and the cooling rate from the aging temperature are rapid. Lynch also found that the increase in toughness produced by double-aging is greater for specimens initially underaged than for specimens initially aged near peak strength. Lynch offered the following explanation for his observations: (i) lithium segregation at grain boundaries is mainly responsible for brittle

intergranular fracture and low toughness in single-aged material, (ii) double aging decreases the extent of lithium segregation, and (iii) re-embrittlement is caused by resegregation due to diffusion of lithium from the matrix to the grain boundaries. A more reasonable explanation may be that (i) reversion of some of the δ' occurs at the higher aging temperature (ii) this reduces the degree of strain localization, and (iii) more homogeneous deformation results in a lower stress concentration at grain boundaries and a higher fracture toughness. This explanation is also consistent with the effect of rapid heat up rates, short reversion times (to minimize the effect on S'), and rapid quenching rates (to minimize the reprecipitation of δ').

In general, for alloys that contain a low volume fraction of constituent phases and grain boundary precipitates, the fracture toughness is controlled by the deformation behavior, being maximized when deformation is homogeneous. Jata and Starke (26) showed that the fracture toughness variation with aging time can be quantitatively related to the changes in slip planarity, i.e., the fracture toughness decreases as the slip band width decreases and the slip band spacing increases. They also determined that slip localization decreases with decreasing temperature, thus explaining, in part, the large improvement in fracture toughness with decreasing temperature.

The propensity of Al-Li alloys to deform by coarse planar slip results in a significant improvement in fatigue crack growth resistance under both constant amplitude (27-29) and variable

amplitude loading (30) when compared with conventional high strength aluminum alloys. Figure 9, taken from the work of Ritchie and co-workers (31) compares the crack growth behavior of 2090-T8E41 (T-L orientation) with that for two different tempers of 2124 and 7150. Coarse planar slip, e.g. occurs in 2090-T8E41, leads to a torturous crack path which reduces the "crack driving force" due to extrinsic effects which include roughness-induced crack closure (32), Figure 10.

Aluminum-lithium alloys have not demonstrated the same significant advantages over baseline alloys for short crack growth resistance (33). This is partially the result of reduced crack tip shielding effects (27,34). However, even in this regime Al-Li should show some improvement considering that they normally have a modulus of between 10 to 15 percent larger than conventional aluminum alloys. Although the fatigue crack initiation resistance of Al-Li alloys may be somewhat poorer than that of conventional alloys (35,36) (most likely due to the extensive strain localization and sharp texture normally present) their overall fatigue performance under S-N type test conditions is generally equivalent to, or better than, that of standard aluminum alloys, Figure 11.

The Al-Li, Al-Li-Zr, and Al-Mg-Li-Zr alloy systems exhibit a high resistance to stress corrosion crack initiation (37,38), however, the Al-Li-Cu-Zr and Al-Li-Cu-Mg-Zr systems do not (37,39,40). The susceptibility of these copper containing alloys may be related to the activity of the T_1, S', T_2 phases (41).

Underaged tempers have been shown to be less susceptible than peak or overaged tempers to SCC initiation for Al-Cu-Li-Zr alloys (41) but overaging has been shown to decrease the susceptibility of Al-Li-Cu-Mg-Zr alloys, Figure 11. Although underaged tempers appear to offer the highest resistance to SCC propagation for both alloy systems, Figure 12, the propagation behavior is relatively insensitive to temper as well as being insensitive to alloy chemistry and test environment (41).

Other Engineering Properties

In addition to those properties discussed above, there are certain other engineering properties of Al-Li alloys that are attractive in comparison to conventional baseline aluminum alloys. For example, most Al-Li alloys are amenable to superplastic forming (42,43), display moderate to good weldability (44), can be chemically milled, bonded, anodized, alclad, and painted. On the debit side, Al-Li alloys often display considerable anisotropy in strength and ductility (although special processing procedures may minimize these effects). They are somewhat more susceptible to surface oxidation at moderate temperatures which can lead to lithium loss near the surface. In addition, a commercial practice, similar to that developed by Lynch, must be developed to improve the short transverse fracture toughness. In fact, most problems associated with Al-Li alloys are due to a combination of grain structure, texture, precipitate type and distribution, the adverse effects of which may be minimized by intelligent processing

methods.

HIGH TEMPERATURE ALUMINUM ALLOYS

The tensile strength of commercially cast and wrought aluminum alloys deteriorates quickly at elevated temperatures. As such, these products have not been used for structural applications where the environmental temperature the component must withstand exceeds 200°C for any length of time.

Two approaches in developing dispersion strengthened, elevated temperature aluminum alloys have evolved. The first involves rapid solidification (RS) of aluminum alloys that contain a high percentage of solute elements that form intermetallic dispersoids which have low coarsening rates at moderate to high temperatures. RS aluminum alloys can be produced with compositions that are unattainable through normal ingot casting methods. The severe undercooling during solidification results in a dispersoid size sufficiently small to offer significant strengthening and substructure control when present in quantities of 10 to 25 volume percent. The RS particulate is consolidated using normal powder metallurgy methods. The most advanced of the RS aluminum alloys that have been developed are based on the Al-Fe-V-Si system, described by Gilman in this proceedings (45), and have very good tensile properties in the 200°C-400°C temperature range.

The second approach, mechanical alloying (MA) of elemental or master alloy powder charges, produces a fine grained microstructure containing Al_2O_3 and Al_4C_3 as the primary dispersoid strengthening

phases (46). Other desired precipitate phases can be produced as well, by adding the appropriate combination of elemental or pre-alloyed powders. Mechanically alloyed aluminum alloys are characterized by a very fine grain size (less than 0.5 microns in diameter) which is stable up to temperatures approaching the melting point of aluminum. Other stable inert dispersoids (such as Y203) can be deliberately added during the MA process. This combination of dispersoids assists in maintaining the ultra-fine grain size of the microstructure, and when these factors are taken together, is responsible for the characteristic strength of MA alloys through a wide range of temperature/exposure conditions.

In addition to the grain size and inert dispersoid strengthening mechanisms already mentioned, strengthening--particularly at elevated temperatures--can also be obtained from the presence of aluminum-transition element dispersoids. A large part of the research activity on high temperature aluminum alloys has focused on developing means to incorporate large volume fractions of fine, relatively stable, aluminum-transition metal dispersoids within aluminum alloys. Mechanical alloying offers a particularly attractive technique for preparing such alloys.

A recent Air Force sponsored program (47) explored the high temperature performance limitations of aluminum-base alloys and was successful in developing MA aluminum alloys that have promising properties up to 500°C. A new Al-Nb-Ti alloy has an ultimate tensile strength of 107 MPa (15Ksi) at 500°C and an elongation of 6.1%, exceeding for the first time the 100 MPa limit at 500°C.

Room temperature yield strength is 580 MPa with an elongation of 14%. Creep resistance for a series of MA Al-Ti-X alloys was one order of magnitude better than that reported in the literature for other high temperature aluminum alloys in the 400-500°C temperature range. All of these new MA alloys have superior corrosion resistance when compared to conventional aluminum alloys. However, the fracture toughness of the MA alloys is rather low at room temperature as well as at elevated temperatures and this shortcoming needs to be addressed in future research and development.

The fine grain microstructure of an MA Al-9Ti alloy is shown in Figure 13 and consists of grains of both aluminum and Ti_3Al, and carbide and oxide dispersoids. The dispersoids serve to stabilize the grain structure preventing excessive grain growth during high temperature exposure. Room temperature stress-strain curves after various annealing treatments are shown in Figure 14. There is no precipitant decrease in strength with increasing temperature, Figure 15, indicating that there is no significant change in microstructure with increasing temperature, at least for the times and temperatures of this study. A variety of strengthening mechanisms, i.e. grain structure strengthening, dispersoid strengthening, etc. probably operate over this large temperature range. However, the results indicated that the dispersoid volume fraction was insufficient to aid in the development of an ultra fine grain structure during processing and the resulting large grain size (when compared with other MA alloys) may have allowed

the development of large internal stresses during mechanical testing which limited strength and ductility. Niobium was added to an Al-Ti alloy with the objective of forming small Al_3Nb particles to reduce the grain size and offer an additional component of dispersion strengthening.

The microstructure of an MA Al-9Nb-3Ti alloy is shown in Figure 16. The structure of this alloy is a highly suppressed two-phase aggregate structure when compared to the Al-9Ti alloy. In addition, a volume fraction of 10.5% Al_3Nb particles are present which together with the small grain size provides a large number of very strong obstacles to dislocation motion. The aluminum grains are strengthened by 11 volume percent Al_4C_3 and 1.6 volume percent Al_2O_3. With the very small average grain size of 0.05 microns and an average Al_3Nb spacing of 0.02 microns, the conditions for a very strong alloy have been provided. Figure 17 is the alloy's room temperature stress-strain curve and illustrates the familiar negative work hardening behavior of these fine grained powder metallurgy alloys. Figure 18, which shows the yield strength as a function of temperature, indicates that the yield stress at room temperature increases after creep loading for 100 hours at 446°C. Post-creep transmission electron microstructural studies confirmed that the structure is very stable after long time exposure at temperatures up to 500°C. The 107 MPa ultimate tensile strength at 500°C is the highest ever reported for a monolithic aluminum alloy.

Although much research and development needs to be done on these high temperature aluminum alloys before they are ready for

commercialization, especially on improving the fracture toughness, they do offer the promise of being able to replace the more expensive titanium alloys in structural applications for aircraft whose speeds do not exceed Mach 2.4.

ACKNOWLEDGEMENTS

E.A. Starke, Jr., would like to acknowledge support from the Office of Naval Research under contract number N00014-85-K-0526, Dr. George Yoder, Program Monitor. H.G.F. Wilsdorf would like to acknowledge support for High Temperature Aluminum Alloys research from the Air Force Wright Aeronautical Laboratory, Wright-Patterson AFB, Ohio, contract number F33615-86-C-5074. He also wishes to thank Dr. Jeffrey Hawk and Ms. Julie Briggs-Johnson for their assistance with mechanical measurements and microstructural investigations.

LIST OF FIGURES

9. Crack propagation behavior of long fatigue cracks in 2090-T8E41 (T-L orientation) as a function of the nominal stress intensity range, compared to corresponding results in 2124 and 7150 alloys. Data for tests in moist air at R = 0.1 (After Ritchie et al., Ref. 31).

10. Scanning electron micrograph showing the fatigue crack profile and the presence of "roughness induced closure" in an Al-Li-Mg alloy.

11. The influence of temper on the stress-life curve of 8090 plate (ST orientation) (After Gray et al., Ref. 41).

12. Crack growth velocity versus stress intensity curves for under- and peak-aged 8090 in artificial sea water and peak-aged 8090 in a 95 percent relative humidity atmosphere at 40°C (After Gray et al., Ref. 41).

13. Transmission electron micrograph of MA Al-9Ti alloy showing the grain size and size and distribution of dispersoids.

14. Room temperature stress-strain curves for MA Al-9Ti alloy in the as-received and annealed conditions.

15. The yield strength versus temperature for MA Al-9Ti alloy.

16. Transmission electron micrograph of MA Al-9Nb-3Ti showing the suppression of two-phase aggregate structure and a grain size much smaller than for MA Al-9Ti.

17. Room temperature stress-strain curve for Al-9Nb-3Ti.

18. The yield strength versus temperature for MA Al-9Nb-3Ti.

REFERENCES

1. E.H. Spuhler, A.H. Knoll and J.G. Kaufman, Met. Prog., Vol. 79 (1960), p. 80.
2. K.K. Sankaran and N.J. Grant, Aluminum-Lithium Alloys, ed. T.H. Sanders, Jr. and E.A. Starke, Jr., The Metall. Soc. AIME, 1981, p. 205.
3. P.G. Partridge, "A Review of the Oxidation of Al-Li Alloys in the Solid and Liquid States," Technical Report 89037, Royal Aerospace Establishment, Farnborough, Hampshire (1989).
4. F. Fox, H.M. Flower and D.S. McDarmid, Aluminum-Lithium Alloys III, ed. C. Baker, P.J. Gregson, S.J. Harris and C.J. Peel, The Institute of Metals, 1986, p. 263.
5. E.A. Starke, Jr., T.H. Sanders, Jr. and I.G. Palmer, J. of Metals, Vol. 33, (1981) p. 24.
6. S. Rystad and N. Ryum, Aluminium, Vol. 53, (1977) p. 193.
7. G.P. Gu, G.L Liedl, T.H. Sanders, Jr. and K. Welpmann, Mater. Sci. Engr., Vol. 76 (1985) p. 147.
8. C.J. Peel, D.S. McDarmaid and B. Evans, "Considerations of Critical Factors for the Design of Aerospace Structures Using Current and Future Aluminum-Lithium Alloys," Proc. 1987 Symposium on Aluminum-Lithium Alloys Design, ASM International, 1988, p. 315.
9. K.K. Sankaran, V.M. Vasey-Glandon and E.J. Tuegel, Aluminum-Lithium Alloys V, ed. T.H. Sanders, Jr. and E.A. Starke, Jr., MCEP, Birmingham, England, 1989, p. 1625.

10. W.S. Miller, J. White, M.A. Reynolds, D.S. McDarmaid and G.M. Starr, Aluminum-Lithium IV, ed. G. Champier, B. Dubost, D. Miannay and L. Sabetay, Societe Francaise de Metallurgie, Journal de Physique, 1987, C3, p. 151.

11. W.A. Cassada, G.J. Shiflet and E.A. Starke, Jr., Metall. Trans. A, Vol. 22A, (1991) p. 299.

12. E.W. Lee and M.J. Kim, Aluminum-Lithium V, ed. T.H. Sanders, Jr. and E.A. Starke, Jr., MCEP, Birmingham, England, 1989, p. 809.

13. P.J. Gregson and H.M. Flower, Acta Metall., Vol. 33 (1985) p. 527.

14. M.A. Reynolds, A. Gray, E. Creed, R.M. Jordan and A.P. Titchener, Aluminum-Lithium Alloys III, ed. C. Baker, P.J. Gregson, S.J. Harris and C.J. Peel, The Inst. of Metals, London, 1986, p. 57.

15. P. Bourgasser, J.A. Wert and E.A. Starke, Jr., Mater. Sci. Engr., Vol. 5 (1989) p. 1102.

16. A.K. Vasudevan, W.G. Fricke, Jr., R.C. Malcolm, R.J. Bucci, M.A. Przystupa and F. Barlat, Metall. Trans. A, Vol. 19A (1988) p. 731.

17. H.E. Friedrich, R. Mussak, H.M. Tensi and M. Wittmann, Aluminum-Lithium V, ed. T.H. Sanders, Jr. and E.A. Starke, Jr., MCEP, Birmingham, England, 1989, p. 1615.

18. Edgar A. Starke, Jr. and William E. Quist, "The Microstructure and Properties of Aluminum-Lithium Alloys," in New Light Alloys, AGARD-LS-174, North Atlantic Treaty Organization,

1990, p. 2-1.

19. R.E. Lewis, E.A. Starke, Jr., W.C. Coons, G.J. Shiflet, E. Willner, J.G. Bjeletich, C.H. Mills, R.M. Harrington, and D.N. Petrakis, Aluminum-Lithium Alloys IV, ed. G. Champier, B. Dubost, D. Miannay and L. Sabetay, J. de Physique, Colloque C3, 1987, p. C3-643.

20. P.D. Pitcher, Scripta Metall., Vol. 22, (1988) p. 1301.

21. K. Jata and E.A. Starke, Jr., Scripta Metall., Vol. 22 (1988) p. 1553.

22. J. Glazer, PhD Thesis, Lawrence Berkeley Laboratory, University of California, July, 1989.

23. K.T. Venkateswara Rao, H.F. Hayashigatani, W. Yu and R.O. Ritchie, Metall. Trans. A, Vol. 20A (1989) p. 485.

24. H.J. Roven, E.A. Starke, Jr., O. Sodahl and J. Hjelen, Scripta Metall., Vol. 24, (1990) p. 421.

25. S.J. Lynch, "Sustained Load Cracking in Aluminum-Lithium Alloys," J. Mater. Sci. (in press).

26. K.V. Jata and E.A. Starke, Jr., Metall. Trans. A, Vol. 17A, (1986) p. 1011.

27. K.T. Venkateswara Rao, W. Yu and R.O. Ritchie, Scripta Metall., Vol. 20 (1986) p. 1459.

28. E.J. Coyne, T.H. Sanders, Jr. and E.A. Starke, Jr., Aluminum-Lithium Alloys, ed. T.H. Sanders, Jr. and E.A. Starke, Jr., The Metall. Soc. AIME, Warrendale, PA, 1981, p. 293.

29. A.K. Vasudevan, P.E. Bretz, A.C. Miller and S. Suresh, Mater. Sci. and Engr., Vol. 64, (1984) p. 113.

30. G.V. Scarich, K.M. Bresnahan and P.E. Bretz, in "Fatigue Crack Growth Resistance of Aluminum Alloys Under Spectrum Loading," Vol. II, Aluminum-Lithium Alloys, Tech. Rep. No. NOR-85-141, NASC, Northrop Corporation, Hawthorne, CA.

31. K.T. Venkateswara Rao, W. Yu and R.O. Ritchie, Metall. Trans. A, Vol. 19A (1988) p. 549.

32. E.A. Starke, Jr. and J.C. Williams, in Fracture Mechanics: Perspectives and Directions, STP 1020, eds. R.P. Wei and R.P. Gangloff, ASTM, Philadelphia, PA, 1989, p. 184.

33. K.T. Venkateswara Rao, W. Yu and R.O. Ritchie, Metall. Trans. A, Vol. 19A (1988) p. 563.

34. M.R. James, Scripta Metall., Vol. 21, (1987) p. 783.

35. M. Peters, K. Welpmann, W. Zink and T.H. Sanders, Jr., Aluminum-Lithium Alloys III, ed. C. Baker, P.J. Gregson, S.J. Harris and C.J. Peel, The Institute of Metals, London, 1986, p. 239.

36. L. Farcy, C. Carre, M. Clavel, Y. Barbaux and D. Aliaga, in Aluminum-Lithium Alloys IV, J. de Physique, Colloque C3, 1987, p. C3-565.

37. N.J.H. Holroyd, A. Gray, G.M. Scamans and R. Hermann, Aluminum-Lithium Alloys III, ed. C. Baker, P.J. Gregson, S.J. Harris and C.J. Peel, The Institute of Metals, London, 1986, p. 310.

38. L. Cristodoulou, L. Struble and J.R. Pickens, Aluminum-Lithium Alloys II, ed. E.A. Starke, Jr. and T.H. Sanders, Jr., The Metall. Soc. AIME, 1984, p. 561.

39. J.G. Rinker, M. Marek and T.H. Sanders, Jr., Mater. Sci. Engr., Vol. 64, (1984) p. 203.

40. E.L. Colvin, S.J. Murtha and R.K. Wyss, in Aluminum Alloys: Physical and Mechanical Properties, ed. E.A. Starke, Jr. and T.H. Sanders, Jr., EMAS, 1986, p. 1853.

41. A. Gray, N.J.H. Holroyd and W.S. Miller, "The Environmental Cracking Behavior of Aluminum-Lithium Based Alloys," Proceedings of the International SAMPE Metals Conference, Cherry Hill, N.J., August 18-20, 1987.

42. S.P. Agrawal and R.J. Kar, eds., "Aluminum-Lithium Development, Application and Superplastic Forming," Proceedings, WESTEC '86, ASM, Metals Park, Ohio, 1986.

43. J. Wadsworth, C.A. Hensahall and T.E. Nieh, Aluminum-Lithium Alloys III, ed. C. Baker, P.J. Gregson, S.J. Harris and C.J. Peel, The Institute of Metals, London, 1986, p. 199.

44. M.R. Edwards and V.E. Stoneham, Aluminum-Lithium IV, ed. G. Champier, B. Dubost, D. Miannay and L. Sabetay, J. de Physique, Colloque C3, 1987, p. C3-293.

45. Paul Gilman's paper, this Proceedings.

46. V. Arnhold and J. Baumgarten, Powder Metall. Int., Vol. 17 (1985) p. 168.

47. H.G. Wilsdorf, Principal Investigator, "Very High Temperature Aluminum Base Materials Concepts," Air Force Contract F33615-86-C-5074, University of Virginia, Charlottesville, VA 22901.

Alloy / Element*	2090 Alcoa 8/6/84	2091 C. Pechiney 4/8/85	8090 Alcan and C. Pechiney May '1985	8090A Alcoa Late '1985	8091 Alcan 3/29/85	X8092 Alcoa May '985	X8192 Alcoa Aug '1985
Si	0.10	0.20	0.20	0.10	0.30	0.10	0.10
Fe	0.12	0.30	0.30	0.15	0.50	0.15	0.15
Cu	2.4-3.0	1.8-2.5	1.0-1.6	1.1-1.6	1.8-2.2	0.5-0.8	0.4-0.7
Mn	0.05	0.10	0.10	0.05	0.10	0.05	0.05
Mg	0.25	1.1-1.9	0.6 to 1.3	0.8-1.4	0.5-1.2	0.9-1.4	0.9-1.4
Cr	0.05	0.10	0.10	0.05	0.10	0.05	0.05
Ni	—	—	—	—	—	—	—
Zn	0.10	0.25	0.25	0.10	0.25	0.10	0.10
Ti	0.15	0.10	0.10	0.15	0.10	0.15	0.15
Li	1.9-2.6	1.7-2.3	2.2-2.7	2.1-2.7	2.4-2.8	2.1-2.7	2.3-2.9
Zr	0.08-0.15	0.04-0.16	0.04-0.16	0.08-0.15	0.08-0.16	0.08-1.5	0.08-1.5
Other Each	0.05	0.05	0.05	0.05	0.05	0.05	0.05
Total	0.15	0.15	0.15	0.15	0.15	0.15	0.15

*Numbers Shown Are Either Maximums or Ranges

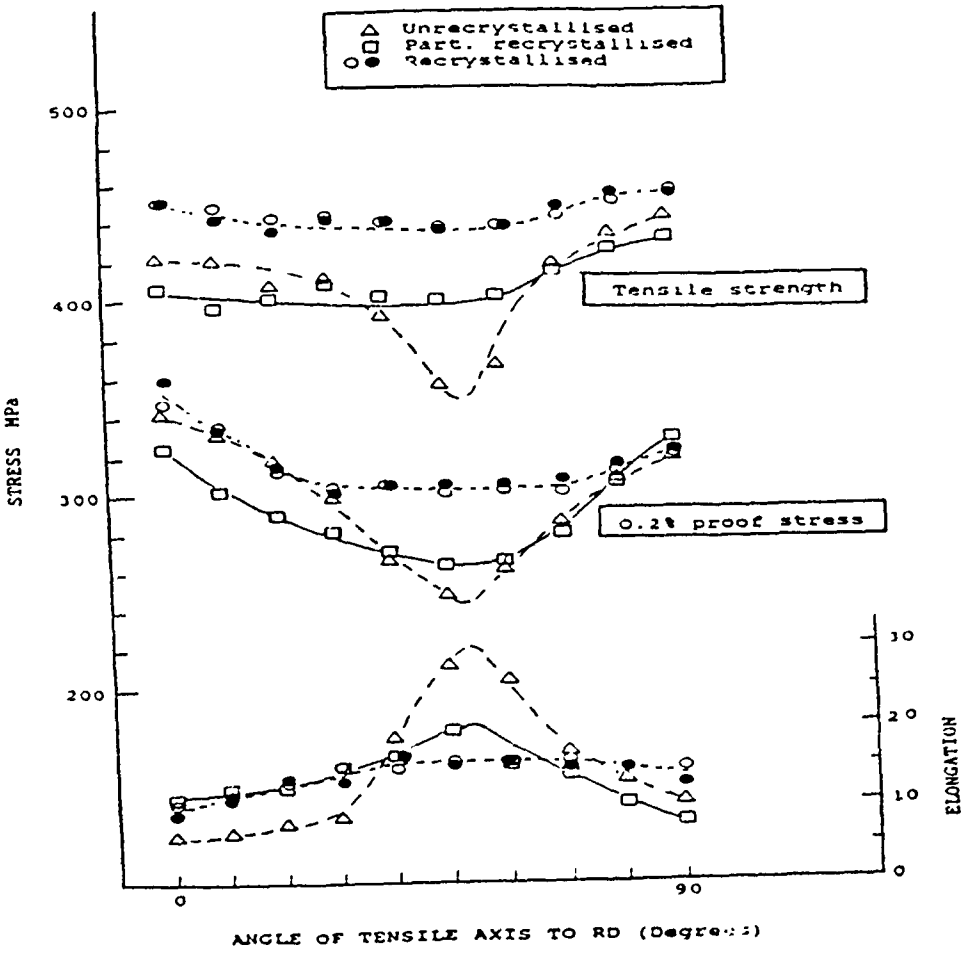

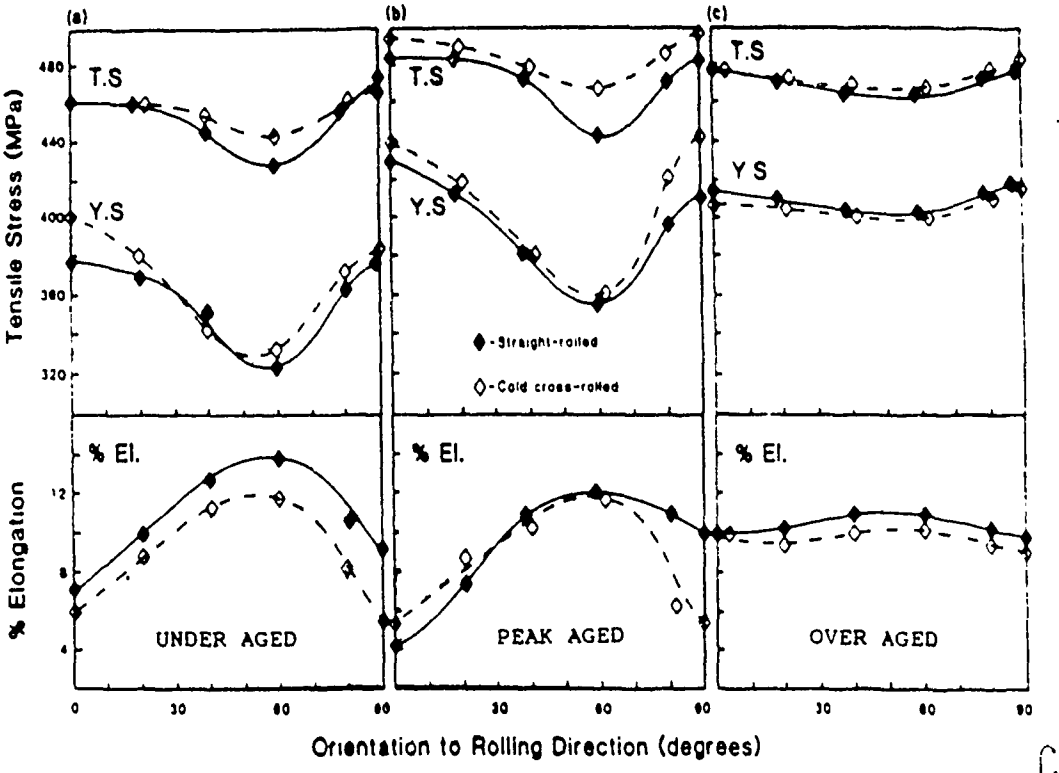
(a)
(b)
(c)
T.S
Y.S
Tensile Stress (MPa)
480
440
400
360
320
◆ - Straight-rolled
◇ - Cold cross-rolled
% El.
% Elongation
12
8
4
UNDER AGED
PEAK AGED
OVER AGED
0
30
60
90
Orientation to Rolling Direction (degrees)

Fig 2

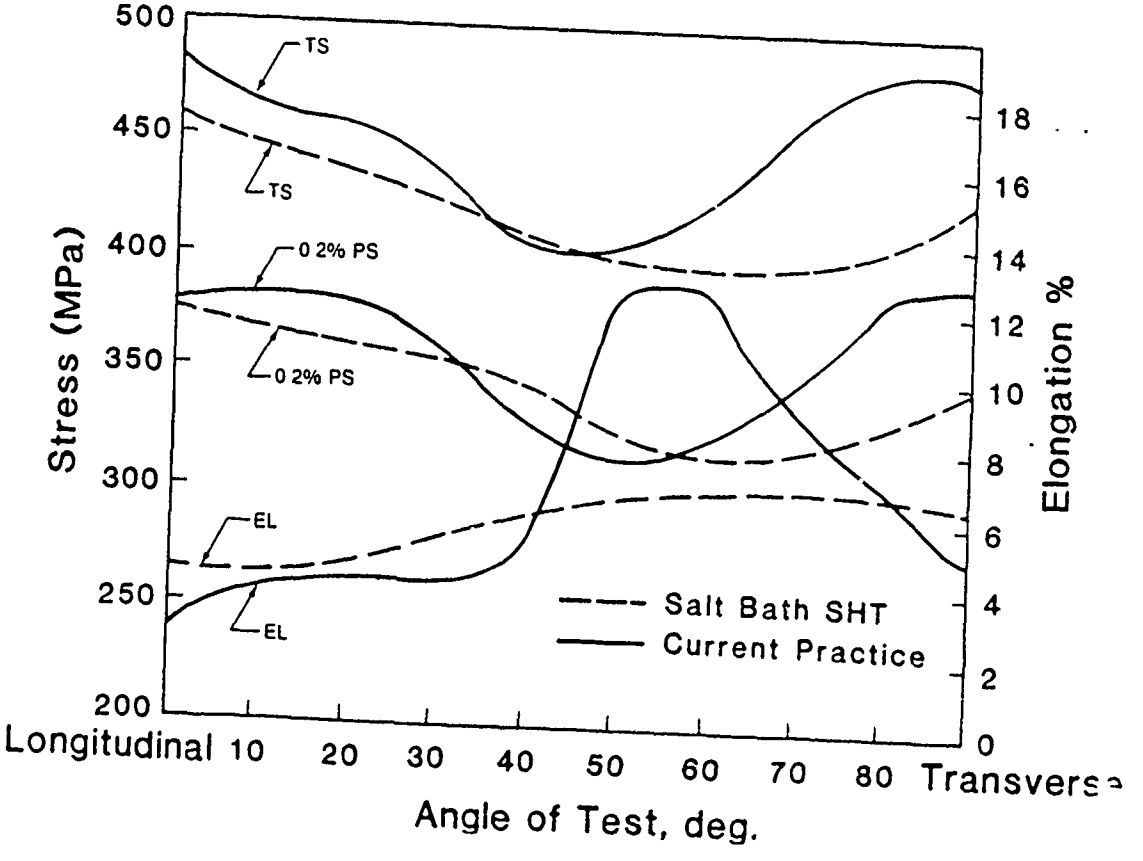
500
450
400
350
300
250
200
TS
0 2% PS
EL
Stress (MPa)
18
16
14
12
10
8
6
4
2
0
Elongation %
Salt Bath SHT
Current Practice
Longitudinal
10
20
30
40
50
60
70
80
Transverse
Angle of Test, deg.

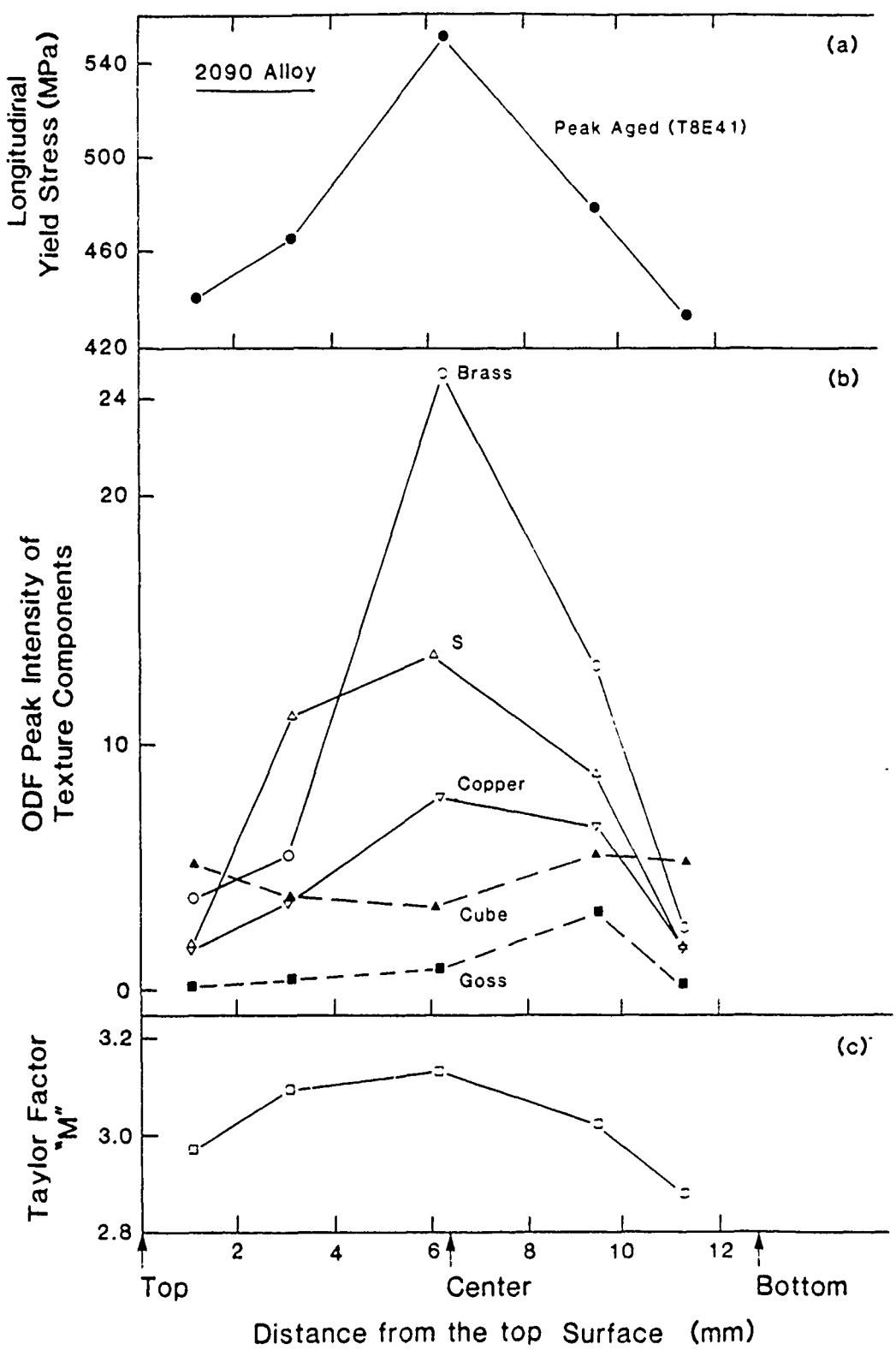
(a)
2090 Alloy
Peak Aged (T8E41)
Longitudinal Yield Stress (MPa)
540
500
460
420
(b)
Brass
S
Copper
Cube
Goss
ODF Peak Intensity of Texture Components
24
20
10
0
(c)
Taylor Factor "M"
3.2
3.0
2.8
2
4
6
8
10
12
Top
Center
Bottom
Distance from the top Surface (mm)

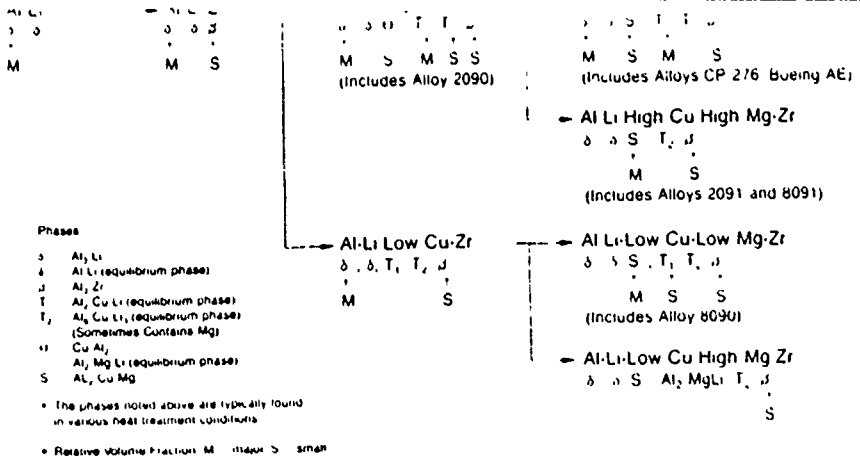
(Includes Alloy 2090)
(Includes Alloys CP 276 Boeing AE)
Al Li High Cu High Mg·Zr
(Includes Alloys 2091 and 8091)
Al·Li Low Cu·Zr
Al Li·Low Cu·Low Mg·Zr
(Includes Alloy 8090)
Al·Li·Low Cu High Mg Zr
Phases
Al3 Li
Al Li (equilibrium phase)
Al3 Zr
Al2 Cu Li (equilibrium phase)
Al6 Cu Li3 (equilibrium phase)
(Sometimes Contains Mg)
Cu Al2
Al2 Mg Li (equilibrium phase)
Al2 Cu Mg
The phases noted above are typically found in various heat treatment conditions
Relative Volume Fraction M major S small

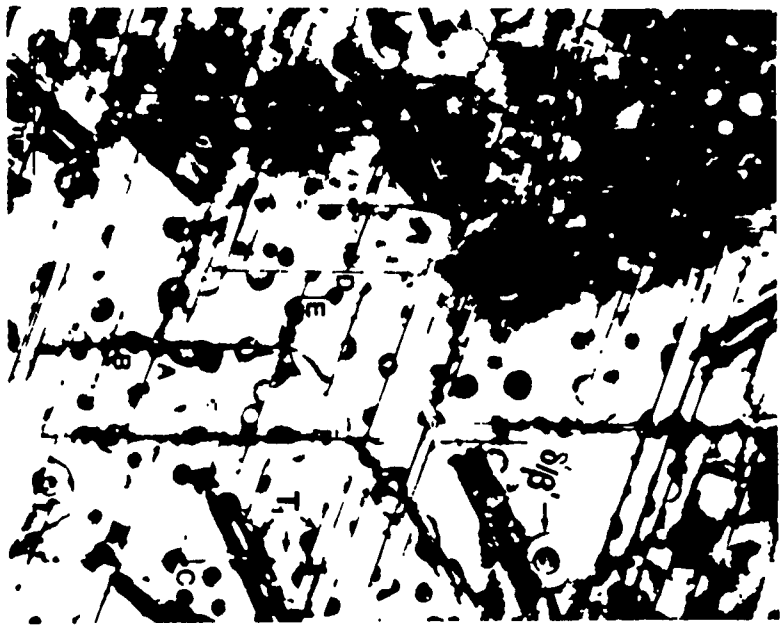

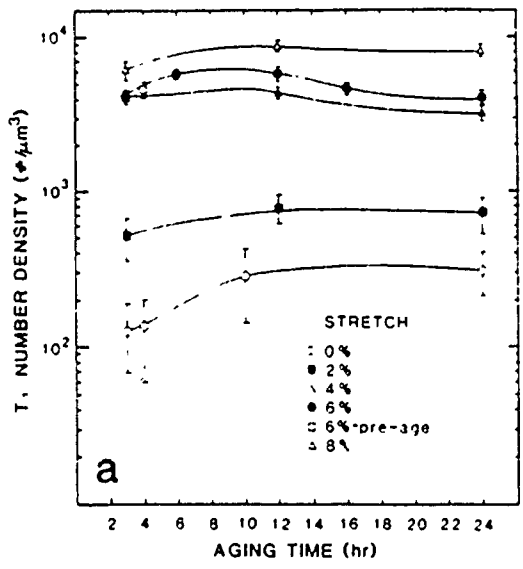
T1 NUMBER DENSITY (#/μm3)
AGING TIME (hr)
STRETCH
0%
2%
4%
6%
6%-pre-age
8%
a

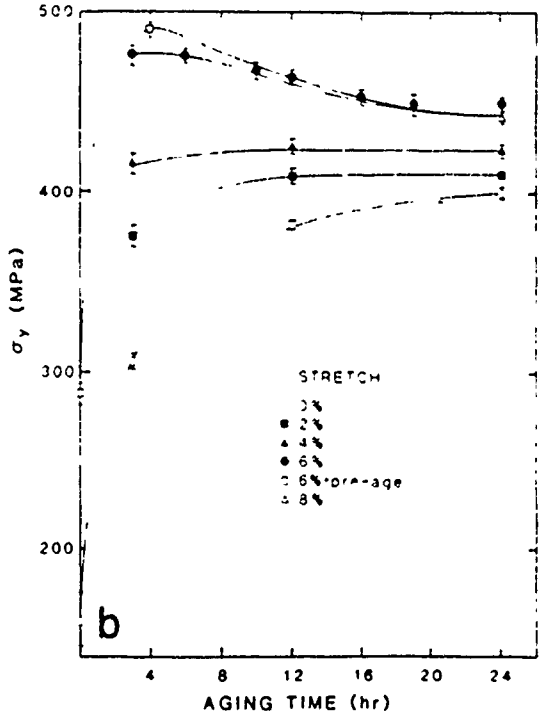
σy (MPa)
AGING TIME (hr)
STRETCH
2%
4%
6%
6%-pre-age
8%
b

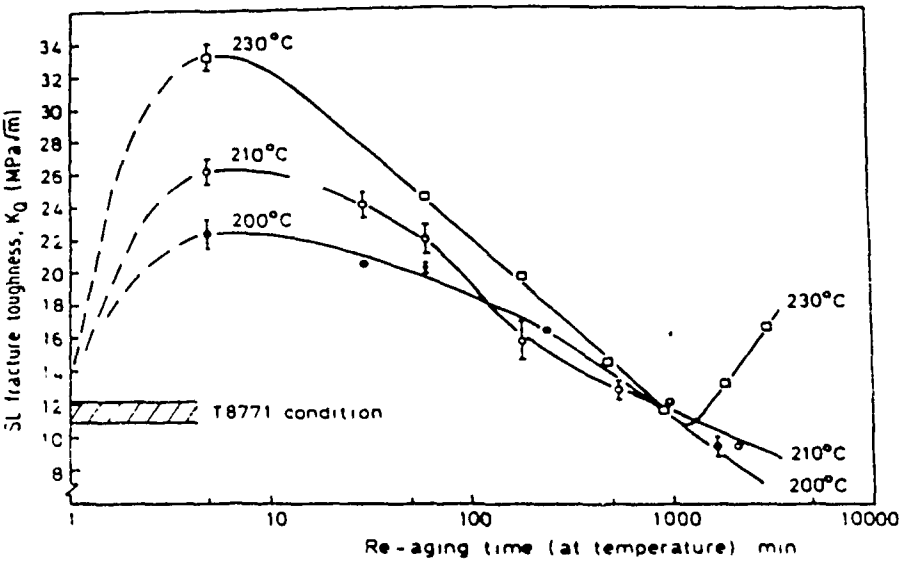
230°C
210°C
200°C
T8771 condition
230°C
210°C
200°C
34
32
30
28
26
24
22
20
18
16
12
10
8
1
10
100
1000
10000
Re-aging time (at temperature) min

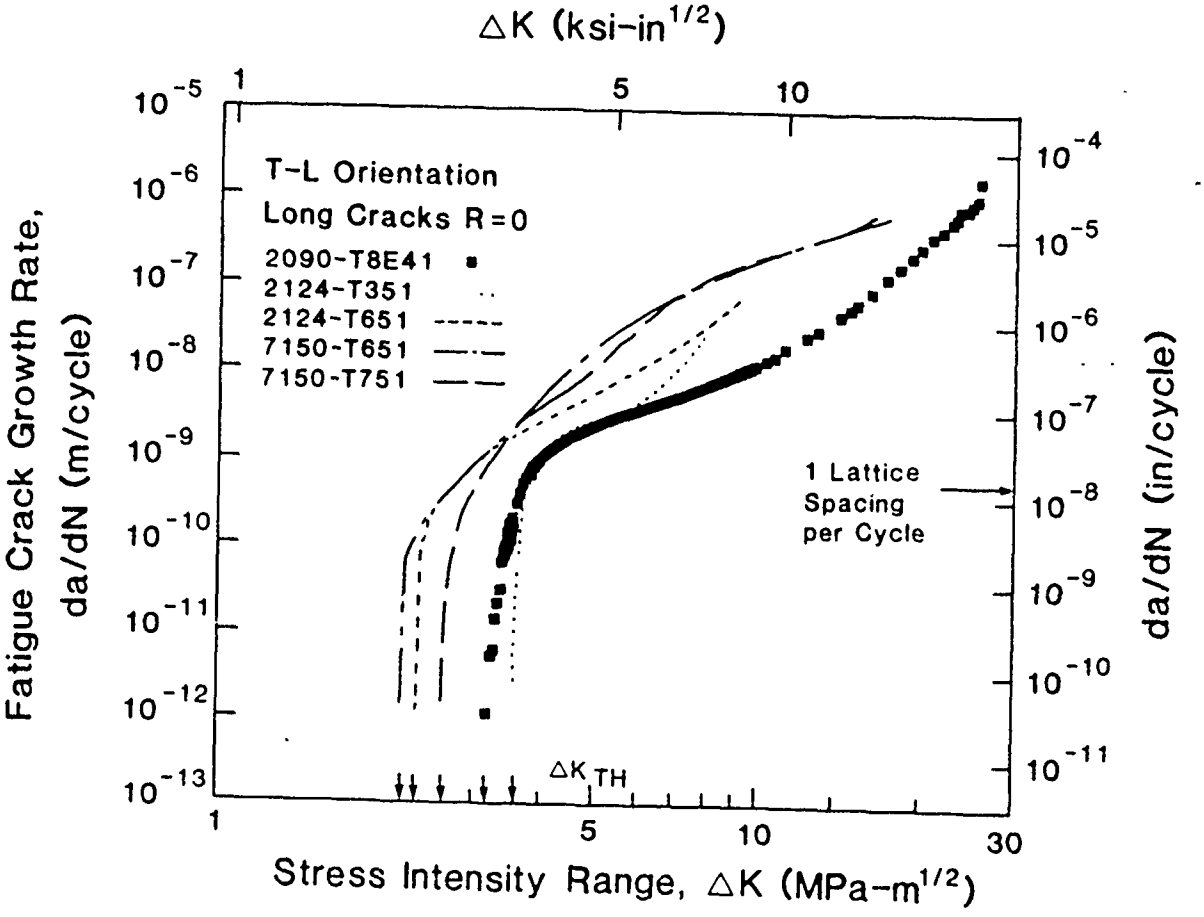
ΔK (ksi-in^1/2)
1
5
10
T-L Orientation
Long Cracks R=0
2090-T8E41
2124-T351
2124-T651
7150-T651
7150-T751
1 Lattice Spacing per Cycle
ΔK TH
Fatigue Crack Growth Rate, da/dN (m/cycle)
da/dN (in/cycle)
Stress Intensity Range, ΔK (MPa-m^1/2)
1
5
10
30

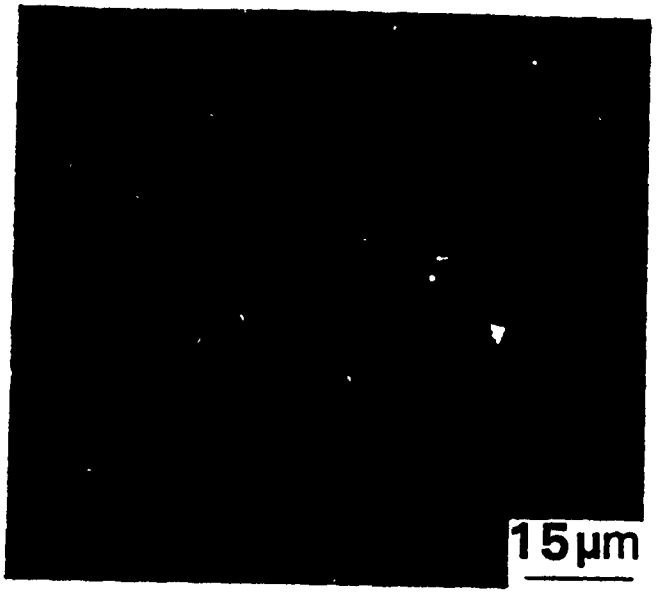
15µm

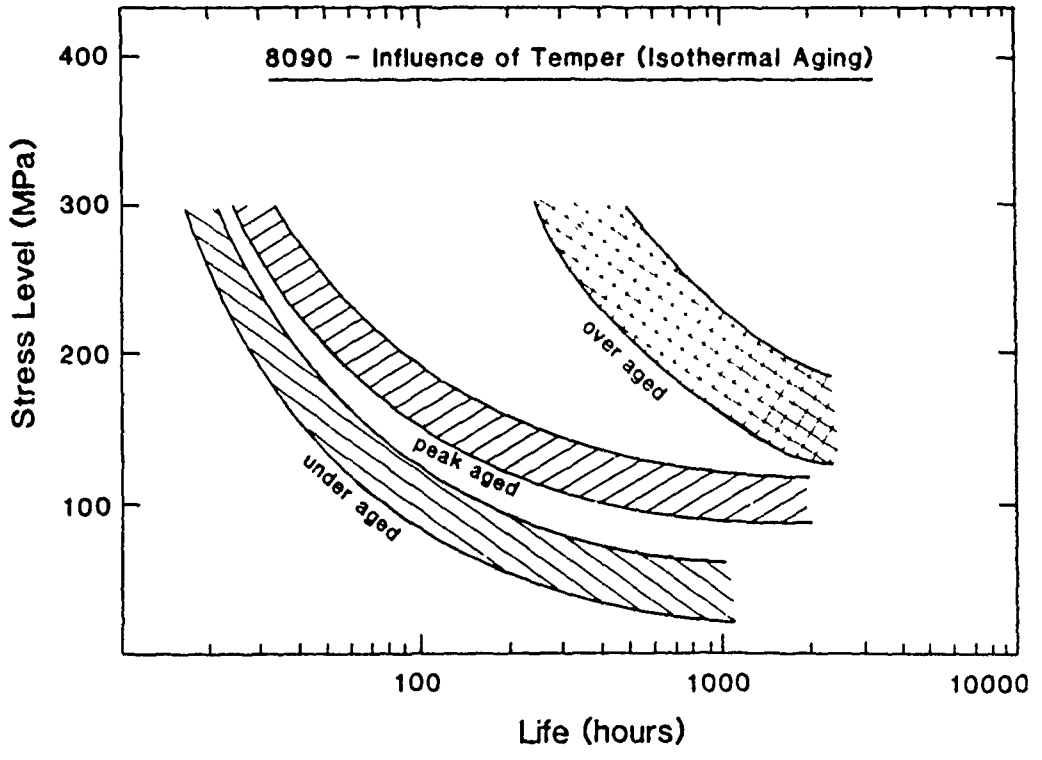
8090 – Influence of Temper (Isothermal Aging)
Stress Level (MPa)
400
300
200
100
over aged
peak aged
under aged
100
1000
10000
Life (hours)

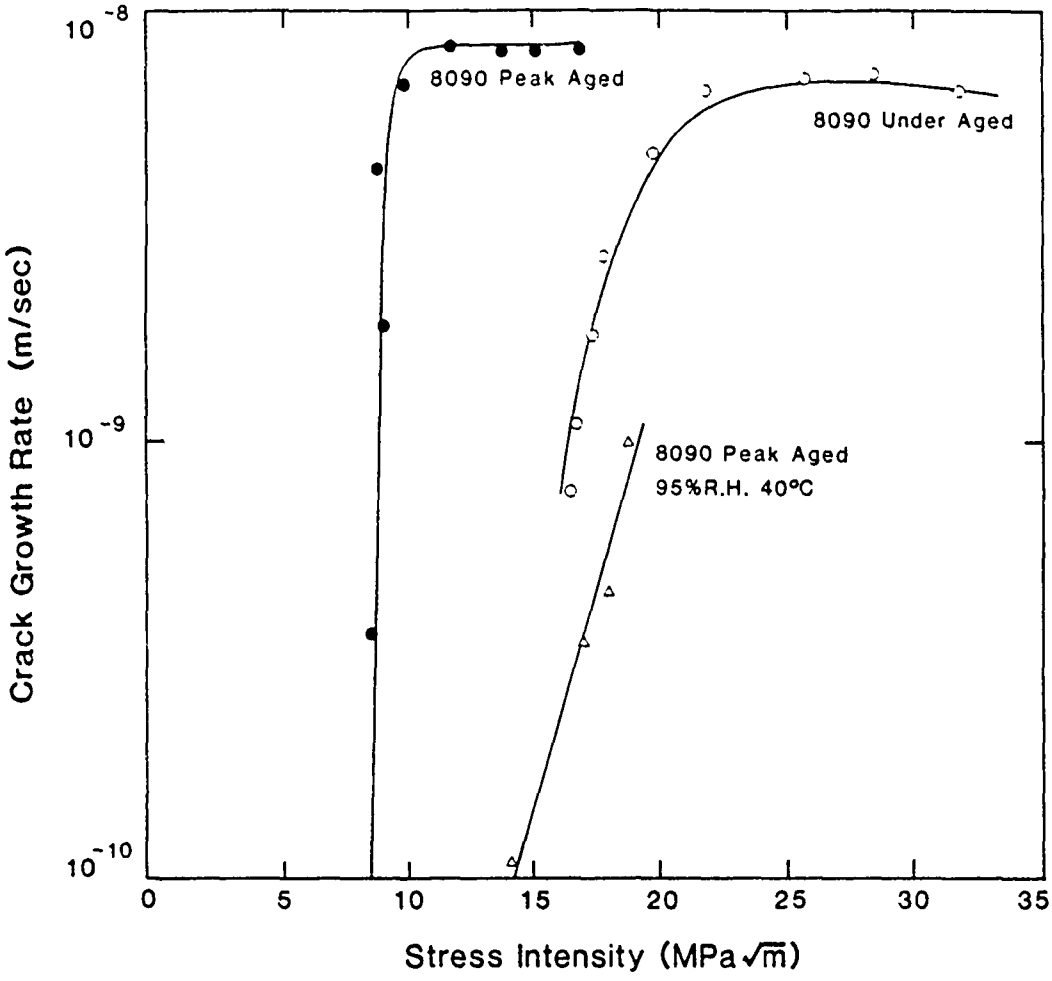
Crack Growth Rate (m/sec)
10 -8
10 -9
10 -10
8090 Peak Aged
8090 Under Aged
8090 Peak Aged
95%R.H. 40°C
0
5
10
15
20
25
30
35
Stress Intensity (MPa√m)


200 nm

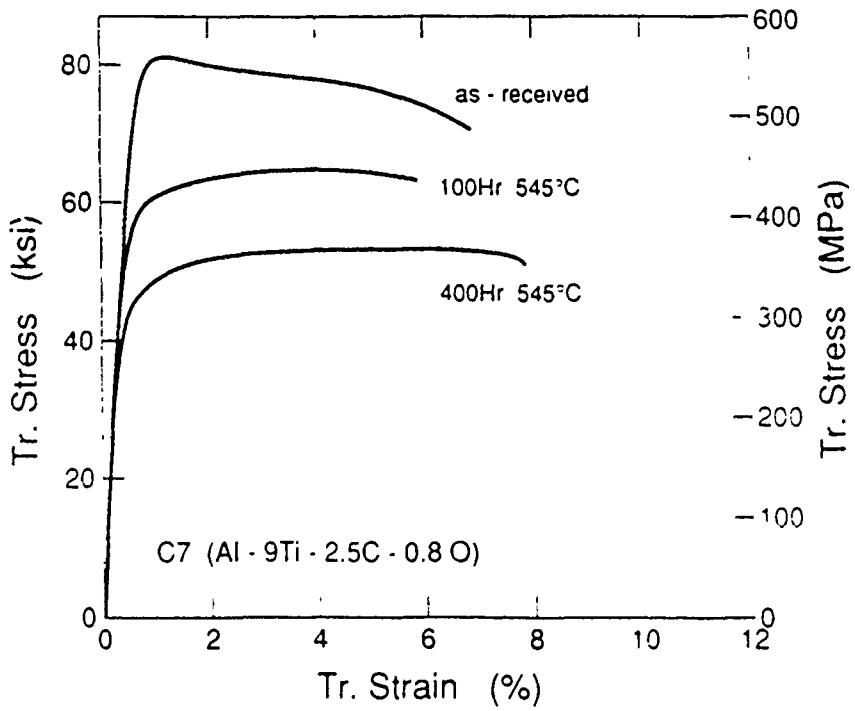
as - received
100Hr 545°C
400Hr 545°C
C7 (Al - 9Ti - 2.5C - 0.8 O)
Tr. Stress (ksi)
Tr. Stress (MPa)
Tr. Strain (%)
0
20
40
60
80
100
200
300
400
500
600
2
4
6
8
10
12

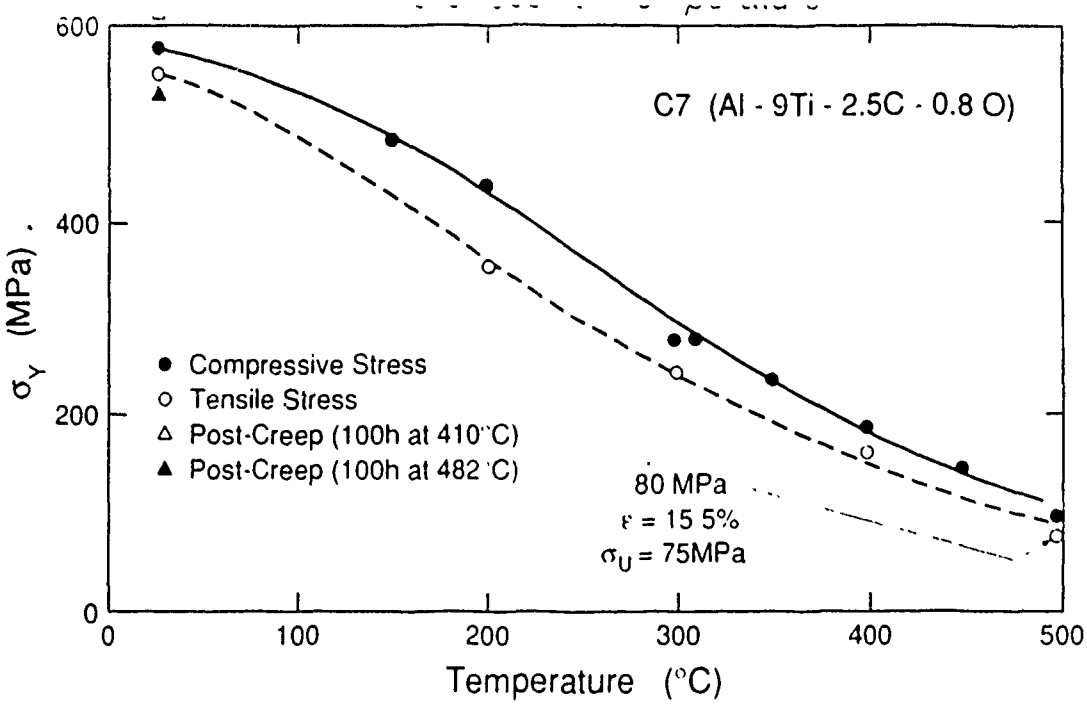
C7 (Al - 9Ti - 2.5C - 0.8 O)
σ_Y (MPa)
600
400
200
0
0
100
200
300
400
500
Temperature (°C)
● Compressive Stress
○ Tensile Stress
△ Post-Creep (100h at 410°C)
▲ Post-Creep (100h at 482°C)
80 MPa
ε = 15.5%
σ_U = 75MPa


100 nm

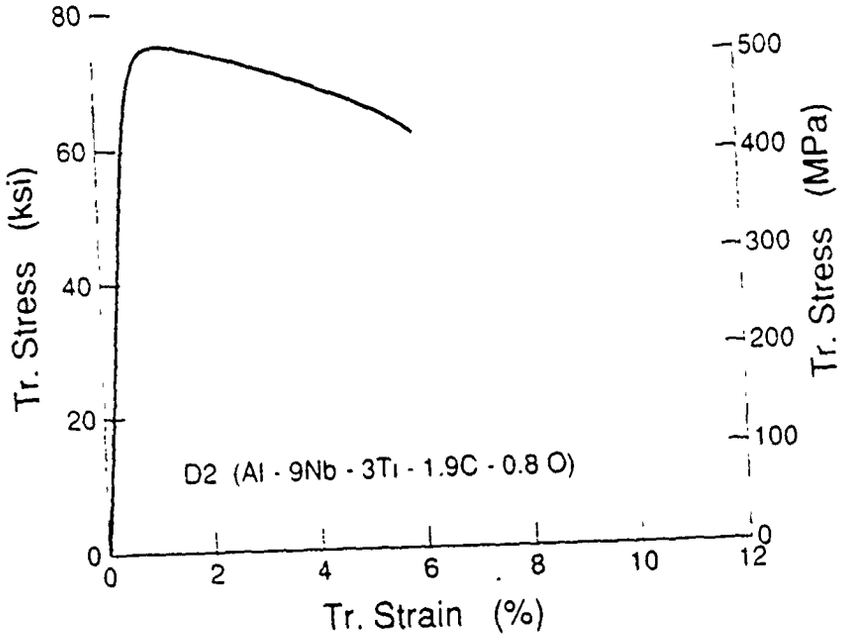
Tr. Stress (ksi)
Tr. Stress (MPa)
D2 (Al - 9Nb - 3Ti - 1.9C - 0.8 O)
Tr. Strain (%)

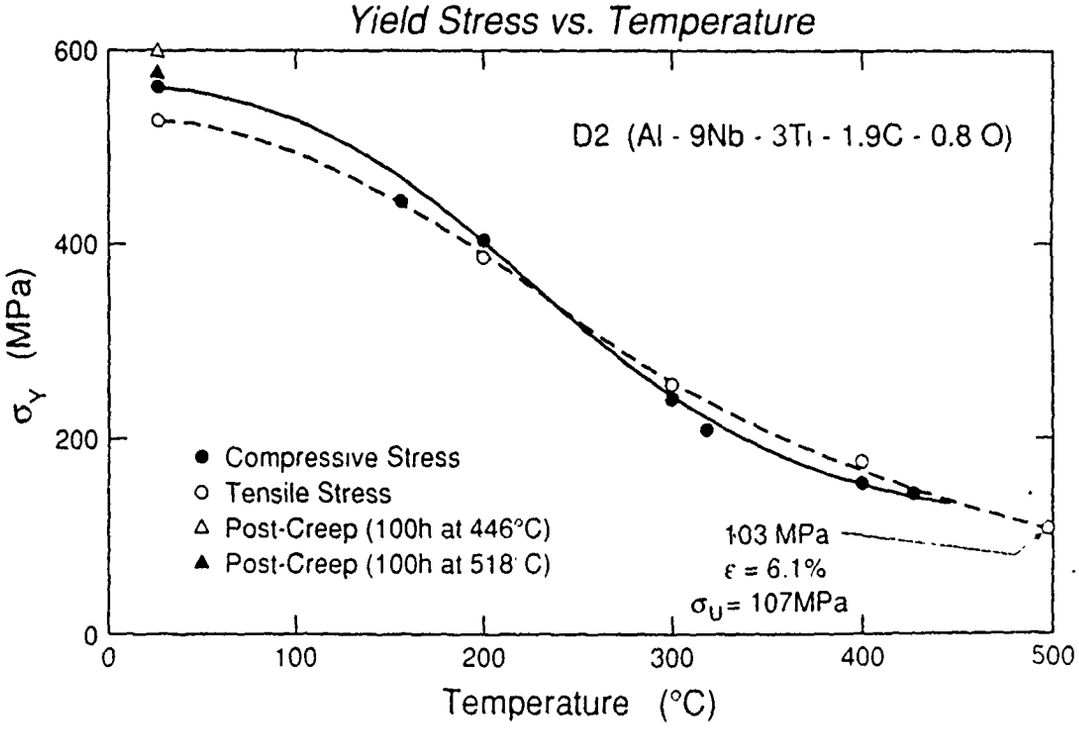
Yield Stress vs. Temperature
D2 (Al - 9Nb - 3Ti - 1.9C - 0.8 O)
σY (MPa)
Compressive Stress
Tensile Stress
Post-Creep (100h at 446°C)
Post-Creep (100h at 518° C)
103 MPa
ε = 6.1%
σU = 107MPa
Temperature (°C)

ALUMINIUM–LITHIUM ALLOYS III

Proceedings of the
Third International
Aluminium-Lithium Conference
sponsored and organized by
The Institute of Metals

University of Oxford
8-11 July 1985

EDITED BY

C Baker
Alcan International Ltd, Banbury, Oxfordshire

P J Gregson
The University of Southampton

S J Harris
The University of Nottingham

C J Peel
Royal Aircraft Establishment, Farnborough, Hampshire

The Institute of Metals
LONDON
1986

Effect of precipitate type on elastic properties of Al–Li–Cu and Al–Li–Cu–Mg alloys

E AGYEKUM, W RUCH, E A STARKE Jr, S C JHA and T H SANDERS Jr

EA and WR are in the Department of Materials Science at the University of Virginia, USA.
EAS is in the School of Engineering and Applied Science at the University of Virginia, USA
SCJ and THS are in the Department of Metallurgy at Purdue University, USA

SYNOPSIS

Lithium additions are known to significantly increase the elastic modulus of aluminum alloys when present in solid solution or as Al_3Li. However, there has been no systematic fundamental study of the effect of lithium on the elastic properties of the complex Al-Li-Cu and Al-Li-Cu-Mg alloys currently being considered for commercial utilization. A series of Al-Li-Cu and Al-Li-Cu-Mg alloys were processed to contain various amounts of lithium-containing precipitates, e.g., Al_3Li, and Al_2CuLi. The elastic moduli were determined by the pulse echo technique. The results were correlated with the type and volume fraction of precipitates. The differences in elastic properties among the various alloys and heat treatments will be described with respect to the individual contributions of the different precipitates.

INTRODUCTION

Binary aluminum-lithium alloys show low density and high stiffness but are not attractive to commercial applications mainly due to strength and ductility problems. Good overall mechanical properties are found in ternary and quaternary Al-Li alloys where copper and/or magnesium are also present and which still show low density and high elastic modulus compared to lithium free aluminum alloys. The elastic modulus of such complex alloys is composed of individual contributions from the matrix and various types of precipitates. In addition to Al_3Li, the other major strengthening precipitates that form in the ternary and quaternary alloys are the Al_2CuLi and Al_2CuMg phases.

The Young's modulus of a multi-phase alloy results from the individual contributions of each phase. In precipitation hardenable Al-Li alloys, the largest phase is the solid solution or matrix phase. The other phases present, such as constituent particles, dispersoids and strengthening precipitates exist very often in relatively low volume fractions. In order to influence the elastic properties of the alloy, the moduli of these phases must be very different from the modulus of the matrix. Some recent work on Al-Li binary and Al-Li-Mg ternary alloys has resulted in estimations of the effect of Li on the modulus of Al when it is in solid solution (1,2), and the elastic modulus of Al_3Li (1,2,3). There has been no reported estimation of the elastic modulus of other phases containing Li.

This paper describes some of our preliminary results on a study of the elastic behavior of complex Al-Li-X alloys. Although the quantitative analysis is incomplete, these early results do suggest some trends and the relative importance of the manner in which Li is present in the alloy, i.e., the type of Li-containing phases present.

EXPERIMENTAL PROCEDURES

The alloys, manufactured by ingot technology, have been received from Reynolds Aluminum Company, Richmond, Virginia, in form of cross-rolled plates with a thickness of 12 mm. After solution heat treatment and cold water quenching, stretching for 2% within an hour took place. Aging was performed at 163 °C for 16, 50 and 150 hours. The ternary Al-Li-Cu alloy has been aged at 150 °C for 36 hours. More details about the investigated alloys are listed in Table 1.

Densities have been determined using the Archimedes principle, where the samples were immersed in air and CCl_4.

Table 1. Investigated alloys.

ALLOY	Li	Cu	Mg	Zr	Cu/Mg	DENSITY (g/ml)	
	w% / at%					CALC.	MEAS.
1	2.63 / 9.59	1.86 / 0.74	1.48 / 1.54	0.12 / 0.03	1.3	2.52	2.52
2	2.31 / 8.46	0.91 / 0.36	1.30 / 1.36	0.11 / 0.03	0.7	2.53	2.54
3	1.97 / 7.32	1.85 / 0.75	1.47 / 1.56	0.13 / 0.04	1.3	2.57	2.57
4	1.94 / 7.22	1.91 / 0.78	0.90 / 0.96	0.12 / 0.03	2.1	2.58	2.58
5	2.26 / 8.37	2.54 / 1.03	-	0.11 / 0.03	-	2.58	2.59

Table 2. Results for alloys aged for 50 hrs. at 163°C.

ALLOY	- (at%)	δ' (vol%)	T1 (at%)	$E_{meas.}$ (GPa)	$f_{\delta'} \cdot E_{\delta'}$ (GPa)	ΔE (GPa)	$f_{ss} \cdot E_{ss}$ (GPa)
1	"9.6"	-	-	82.9	-	-	-
2	8.46	9	0.7	81.9	9.5	72.4	72.7
3	7.32	5	0.5	81.0	5.3	75.7	73.6
4	7.22	5	0.4	80.7	5.3	75.4	73.8
5*	8.37	2.5	2.3	83.6	2.7	80.9	75.8

* 36 hrs at 150 °C

$\Delta E = E_{meas} - f_{\delta'} E_{\delta'}$

Table 3. Results for alloys aged for 150 hrs. at 163°C.

ALLOY	T1 (at%)	δ' (vol%)	T1 (at%)	$E_{meas.}$ (GPa)	$f_{\delta'} \cdot E_{\delta'}$ (GPa)	ΔE (GPa)	$f_{ss} \cdot E_{ss}$ (GPa)
1	"9.3"	-	-	82.4	-	-	-
2	8.46	4.3	1.0	79.0	4.6	74.4	74.4
3	7.32	2.7	0.1	78.6	2.9	73.7	75.6
4	7.22	3.6	0.62	77.7	3.8	75.9	74.9

$\Delta E = E_{meas} - f_{\delta'} E_{\delta'}$

Microstructural examinations were performed with optical, scanning and transmission electron microscopes. Number fractions of second phases were measured from TEM negatives with a point grid and converted into volume fractions. The foil thicknesses have been determined by convergent beam electron diffraction patterns.

The pulse echo technique was used to determine the propagation rates of elastic ultrasonic waves (10 MHz) in longitudinal and transverse modes which allowed the calculation of the elastic moduli. Testing direction was the direction of the last rolling step. The reproducibility of this method is about plus/minus 1%.

RESULTS AND DISCUSSION

Table 1 shows the compositions of the investigated alloys and a comparison of calculated and measured densities. The calculation has been performed using the following equation from Peel et al. (4):

$$D = 2.70 + 0.024Cu - 0.01Mg - 0.079Li \qquad (1)$$

where D is the density in g/ml and the atomic symbols represent the weight percent of the individual elements. In the original equation from (Peel) the density of pure aluminum was assumed to be 2.71 g/ml, but our density measurements yielded consistently a value of 2.70 for pure aluminum. For that reason the latter value was chosen in equation (1). Also the presence of zirconium has not been considered which may result in a slight underestimation of the density. The agreement between calculated and measured values is extremely good and well within experimental error.

Figure 1 shows the Young's moduli plotted versus the lithium concentration in atomic percent for the different alloys aged 16 hrs. at 163 °C. Also included is the magnesium-free ternary alloy 5, represented by a filled in circle which has been heat treated 36 hrs. at 150 °C. For the lower lithium containing quaternary alloys (star symbols) an increase in modulus with lithium levels takes place, as expected. If a linear regression analysis is applied to the data points from these lower lithium alloys a slope of 2 GPa per at.% lithium, and an intercept of 64 GPa, representing the modulus for a lithium free alloy, result. These numbers are reasonable for these alloys; however, alloys 1 and 5 do not follow this trend. The Al-Li-Cu alloy shows a much higher value and the quaternary alloy with the highest lithium content shows a value far too low. Because crystallographic texture was found to be only weak in these cross-rolled alloys, the cause for this behavior must lie in the composition, i.e., the phases present in these materials. In the Al-Li-Cu alloy which has been aged for 36 hrs. at 150 °C mainly T$_1$ (Al_2CuLi) is present in addition to delta prime. T$_1$ seems to have a large beneficial effect on modulus as we will discuss later. The quaternary 9.6 at.% Li alloy shows a value which would be expected for a lithium content of about 7.6 at.% according to this diagram. Optical microscopy clarified this apparently anomalous behavior. Figure 2 is an optical micrograph of this alloy which shows many large particles which were found to be copper and aluminum rich using X-ray energy dispersive analysis. Obviously, the solubility limits were exceeded with this composition and, therefore, large scale precipitation of insoluble primary phases occurred during casting. The exact composition of the particles and/or whether they contained lithium could not be determined. The low atomic number of lithium does not allow its detection with X-ray energy dispersive analysis. Nonetheless, the incorporation of a substantial part of the total lithium content in these large particles seems reasonable and may explain the relatively low elastic modulus of this alloy. The other alloys contained only the typical small amounts of constituent particles.

The shear moduli show the same trend as the Young's moduli as a function of lithium content. Compared to pure aluminum they show roughly the same percent increase. The poissons ratio always stayed close to 0.30.

Figure 3a, b, c and d represent the change in elastic modulus with aging time for the investigated alloys. All materials show an increase in E in the early stages of aging, i.e., from 16 to 50 hours. The maximum difference in modulus during aging is displayed by alloy 2 (2.31 wt%Li) with about 3 GPa, i.e., roughly 4%. No measurements in the solution heat treated states were performed. A decrease in Young's modulus going from 50 to 160 hours was observed for all alloys, too. The results from transmission electron microscopy, performed on the 50 and 150 hr. treatments so far, will be used to explain this behavior. The 16 hour heat treatments are still under investigation.

The initial increase in modulus with aging is attributed to the precipitation of delta prime. At 50 and 150 hrs. aging the only strengthening precipitate present in alloy 1 and 2 (high lithium contents) was delta prime. Alloy 3 which had the same copper and magnesium levels but a lower lithium content also contained S'', a precursor of the S phase (Al_2CuMg), as determined from electron diffraction patterns. In alloy 4 with the lowest Li content and the highest Cu to Mg ratio, S'' was also found to be present. The S'' phase is not expected to influence the modulus of elasticity to a great extent, since its effect is negligible in 2XXX alloys.

Table 2 lists the results of the quantitative transmission electron microscopy investigations for the 50 hr. aging treatments and the measured elastic moduli. In order to get some more quantitative information, the amount of lithium in solid solution was assumed to be 5.5 at.%, a value which has been used in binary alloys by Noble et al. (1) and which should represent an upper limit in the quaternary alloys. The measured volume fractions of delta

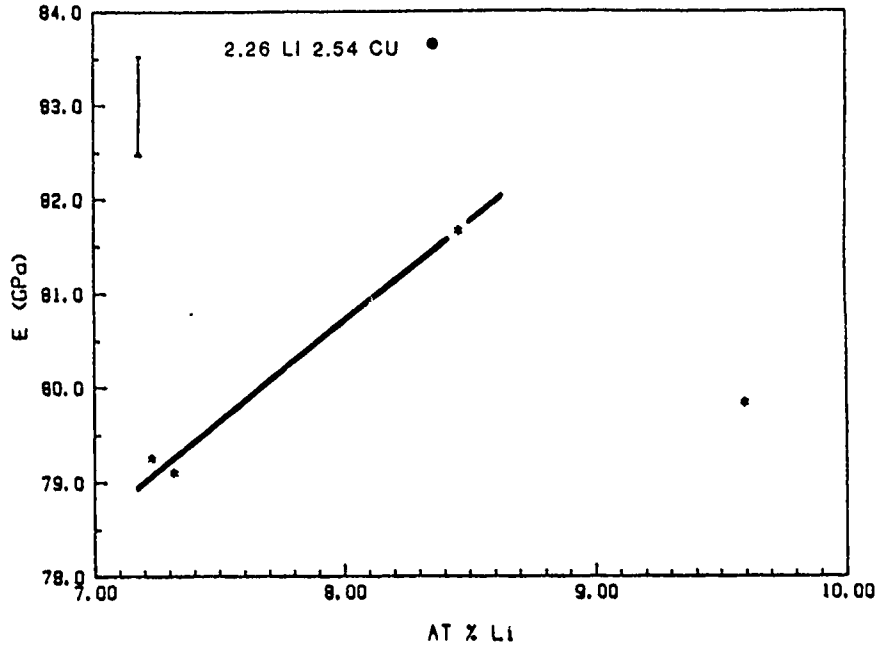

Figure 1. Young's modulus as a function of lithium concentration.

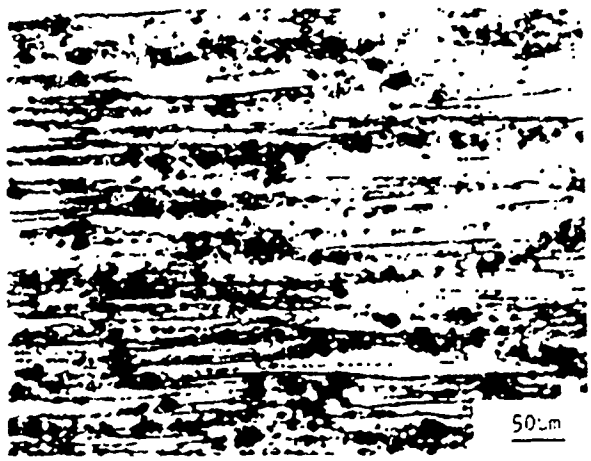

Figure 2. Optical micrograph of alloy 1 showing large particles.

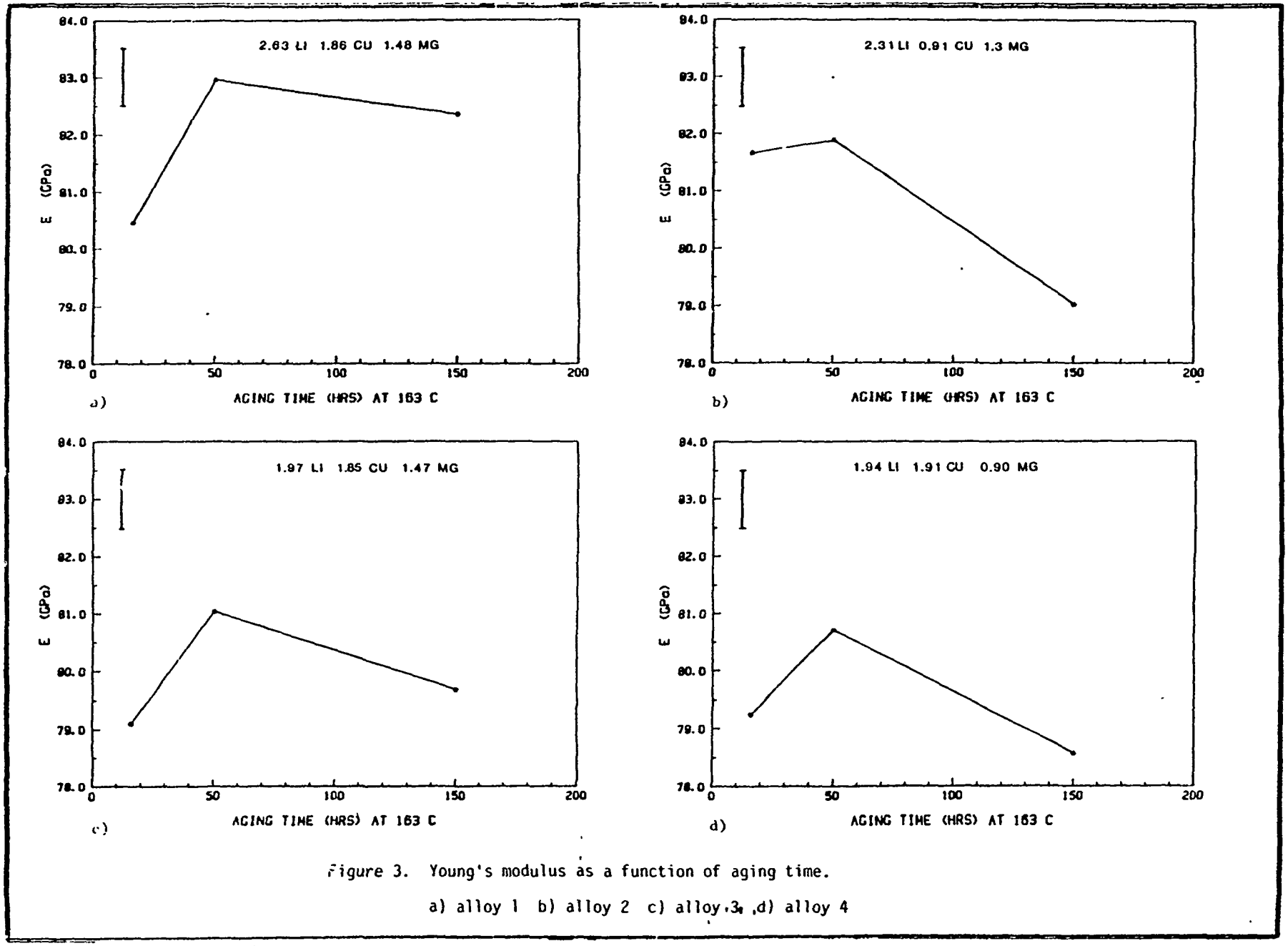

Figure 3. Young's modulus as a function of aging time.

a) alloy 1 b) alloy 2 c) alloy 3, d) alloy 4

prime have been used to calculate the amount of lithium in delta prime, and, after subtracting 5.5 at.% for solid solution, the remaining lithium content in other phases, called Li^R in Table 2, was estimated. Measurements of the δ' volume fractions in alloys 3 and 4 have yet to be performed. In alloy 1, the delta prime particles were too small to allow quantitative measurements.

The bulk modulus of an alloy can be calculated by determining the contribution of solid solution and the contribution of precipitates. The Young's modulus of the solid solution (E_{SS}) in binary aluminum-lithium alloys has been determined by Muller and Gerold (2) from experimental measurements to be:

$$E_{SS} = 71 + 1.22Li \qquad (2)$$

where E_{SS} is the solid solution modulus in GPa and Li is the atomic concentration of lithium in solid solution. Muller and Gerold also determined a value of 106 GPa for the modulus of delta prime, and the value was selected for our calculations. The way the bulk modulus of a multi-phase material can be composed of the individual contributions is:

$$E_b^m = \sum_{i=1}^{n} (f_i \cdot E_i^m) \qquad (3)$$

where E_b is the bulk modulus, f_i the volume fraction of the phase i, and E_i the modulus of the individual phase i. The exponent m equals 1 for the linear rule of mixtures, also called Voigt (5) averaging (upper bound). There the uniform strain in both phases is assumed. For the Reuss (6) method of averaging the same stress is assumed in both phases and m equals -1 (lower bound). It turns out that in our case the difference between the bounds is small and therefore the linear rule of mixtures was applied.

The contribution of delta prime to the bulk modulus was calculated using the following equation:

$$\delta'_{CONTR} = f_{\delta'} \cdot E_{\delta'} \qquad (4)$$

where $f_{\delta'}$ is the measured volume fraction of delta prime and $E_{\delta'}$ = 106 GPa according to (2). These values are also listed in Table 2. The difference between the delta prime contribution and the measured modulus is also listed in Table 2. This difference is the contribution of solid solution and other phases. The last column in Table 2 shows the calculated contribution of the solid solution to the bulk modulus under the assumption that delta prime and the solid solution are the only two phases present. It is interesting to note that the solid solution contribution, which is believed to be overestimated anyway, cannot make up the difference to the measured value. If one would consider the amounts of Cu and Mg in solid solution, both of which lower the modulus, the resulting difference will even be higher. It has yet to be determined whether or not the lithium not in delta prime and not in solid solution is incorporated in one or several phases which have a positive influence on the modulus. Further work is necessary to identify these phases. The largest contribution of precipitation other than δ' to the modulus was observed for the magnesium free ternary alloy 5. In this case we can assume the T_1 phase to be the major phase besides δ' and to be of great influence. If one assumes that all copper is tied up in T_1, the resulting volume fraction for Al_2CuLi is about 4% using a density of 3.1 g/ml for T_1. Applying the linear rule of mixtures according to equation (3) and assuming the presence of only solid solution, T_1 and δ', results in a Young's modulus of roughly 170 GPa for the T_1 phase. This value is the result of a fairly crude calculation but it stresses the point that besides delta prime there are other lithium containing phases which can contribute quite significantly to the modulus of elasticity.

In Table 3 the same analysis as in Table 2 for the quaternary alloys has been performed for the 150 hr. heat treatments. It is fair to assume that in going from 50 to 150 hours the amount of lithium in solid solution stays essentially constant, i.e., the alloys overage. Table 3 shows a decrease in delta prime volume fractions in all alloys compared to the 50 hr. treatment. It becomes obvious that the decrease in the delta prime contribution cannot alone explain the changes in measured moduli in all alloys. In alloy 2 the decrease in modulus due to a reduction in δ' volume fraction matches the reduction of the measured value. The lithium leaving the δ' particles apparently does not have a great influence on modulus. In alloy 4 the decrease in bulk modulus is less than the decrease in delta prime contribution where the opposite is true for alloy 3. In alloy 4, the lithium leaving delta prime apparently still makes a positive contribution to the overall modulus compared to alloy 3 where it makes a negative contribution. In all alloys an increase in the number of grain boundary precipitates was observed when going from 50 to 150 hours. Identification of these precipitates should aid in our understanding of the observed behavior and this analysis is currently being made.

CONCLUSIONS

- In Al-Li-Cu alloys, the T_1 phase contributes positively to the modulus of elasticity.
- Exceeding the solubility limit ties up lithium in large equilibrium particles which has a negative effect on Young's modulus.
- In Al-Li-Cu-Mg alloy, the modulus of elasticity goes through a maximum during aging.
- In Al-Li-Cu-Mg alloys the changes in modulus during aging may not be explained by changes in δ' volume fractions alone.

ACKNOWLEDGEMENTS

This work was sponsored by the Office of Naval Research, Contract No. N00014-85-K-0526, Dr. Bruce A. MacDonald, Program Manager.

REFERENCES

1. B. Noble, S.J. Harris and K. Dinsdale, J. Mat. Sci., 17 (1982), p. 461.

2. W. Müller, V. Gerold, to be published.

3. M.E. Fine, Acta Met., 15 (1981), p. 523.

4. C.J. Peel, B. Evans, C.A. Baker, D.A. Bennett, P.J. Gregson, and H.M. Flower, Aluminum-Lithium II, ed. T.H. Sanders, Jr., and E.A. Starke, Jr., TMS-AIME, Warrendale, PA, 1984, p. 363.

5. Voigt, W., Lehrbuch der Kristallphysik, B.G. Teubner, Verlag, Stuttgart, 1966.

6. Reuss, A., Z. angew. Math. Mech., 9 (1929), p. 49.

JOURNAL DE PHYSIQUE
Colloque C3, supplément au n°9, Tome 48, septembre 1987

DEPENDENCE OF ELASTIC MODULUS ON MICROSTRUCTURE IN 2090-TYPE ALLOYS

M.E. O'DOWD[1], W. RUCH, and E.A. STARKE, Jr.

Department of Materials Science, University of Virginia, Charlottesville, VA 22901, U.S.A.

ABSTRACT

The Young's modulus, shear modulus and Poisson's ratio were determined using an ultrasonic pulse echo technique. Three commercially fabricated aluminum-copper-lithium alloys and an aluminum-lithium binary alloy were examined. The elastic properties were measured as a function of aging time, aging temperature, amount of stretching and testing direction. An increase in Young's modulus due to delta prime and T1 precipitation has been measured and treated quantitatively including precipitation kinetics. A significant decrease of about 5% in the modulus of elasticity was found in the peak age condition. This decrease can be attributed to precipitation of the T2 phase. The shear modulus behaves similar to Young's modulus while the Poisson's ratio remains unchanged. There is no significant orientation dependence of the elastic properties on testing direction despite the fact that a typical rolling texture was present.

INTRODUCTION

It is well established that the addition of lithium decreases the density and increases the elastic modulus (1-4). This paper examines the important parameters which influence the elastic modulus in commercially important aluminum-lithium alloys. These parameters include solid solution concentrations, their volume fractions, and orientation effects. Industry can implement these results to produce aluminum-lithium alloys which possess an optimum elastic modulus.

EXPERIMENTAL PROCEDURE

The alloys studied in this investigation were donated by the Reynolds Metals Company, Richmond, Virginia. The material was received as hot cross-rolled plate with a thickness of 12 mm. The compositions of the alloys are given in Table I. Alloy 73 is similar in composition to ALCOA's 2090.

The alloys were solution heat treated at 550°C for 30 minutes in a salt bath and cold water quenched (CWQ). All the samples, alloys 73, 81, 82 and the binary alloy were aged at 190°C for times from 10 minutes up to 300 hours. They were all examined in the unstretched condition. Alloy 73 was also examined in a 6% stretched condition.

(1) Naval Air Development Center, Warminster, Pennsylvania, U.S.A.

Samples were machined for ultrasonic measurement from the center of the plate. The samples were rectangular, about 12 x 7 x 5 mm^3 in dimensions. Longitudinal and transverse wave velocities were measured with a 10 MHz ultrasonic pulse echo equipment.

The elastic modulus, shear modulus, and Poisson's ratio were calculated using the following equations (5):

$$R = (V_t/V_\ell)^2 \quad \text{eq. 1}$$

$$P = (2*R-1)/(2*R-2) \quad \text{eq. 2}$$

$$G = V_t{}^2*D \quad \text{eq. 3}$$

$$E = D*V_\ell{}^2*((1+P)*(1-2*P)/(1-P) \quad \text{eq. 4}$$

R - Ratio of velocities squared
P - Poisson's ratio
G - Shear Modulus (GPa)
E - Elastic Modulus (GPa)
D - Density (g/cc)
V_t - Transverse velocity (m/sec)
V_ℓ - Longitudinal velocity (m/sec)

The density of each sample was measured using Archimedes principle. The density did not change upon aging within 0.02%.

Texture analysis of the alloys was performed using a Siemens texture goniometer, set up for the Schulz reflection technique. Pole figures were obtained from each sample.

Transmission electron microscopy was performed using a Phillips 400 (120Kev) instrument. Small angle x-ray scattering (SAXS) was performed at the National Laboratory in Oak Ridge, Tennessee with $CuK\alpha$ radiation. A Huber Guinier Camera with a quartz monochromator using Cu $K\alpha_1$ radiation was used in connection with the direct comparison method to determine volume fractions of second phases.

RESULTS AND DISCUSSION

The microstructure of alloys 73, 81 and 82 display an elongated flat grain structure due to rolling. Typical dimensions are 220 x 100 x 30 μm^3. In addition there is a subgrain structure in the size range of 5 to 30 μm present. The binary alloy exhibited a fully recrystallized, equiaxed grain size ranging from 340 to 360 μm.

Figure 1 displays the results of TEM and Guinier x-ray analysis with respect to second phase precipitation at 190°C as a function of aging time. In the solution heat treated condition the matrix, δ' and Al_3Zr dispersoids were evident in the ternary alloys. The latter change neither distribution nor volume fraction during aging.

After 10 minutes aging at 190°C there is evidence of the T1 phase in alloy 73, but not in alloys 81 or 82. This can be explained by the higher Cu content of 73 resulting in a stronger driving force for T1 precipitation. The T1 phase nucleates heterogeneously at grain and subgrain boundaries. The platelets, after 10 minutes aging at 190°C, are approximately 72 nm long and 8 nm wide.

After approximately 90 minutes aging time the T1 phase is apparent in all three alloys. After 8 hours aging at 190°C, there is present in all three alloys some T2 phase which nucleates preferentially along the grain boundaries.

The volume fraction of δ' as a function of aging time was examined for alloy 81.

Table II shows that the direct comparison method yielded more consistent results than the TEM method. In the former method the integrated intensity ratio of the (200) and (100) diffraction line was measured from a Guinier camera exposure compared to the calculated value and solved for the volume fraction. At short aging times the superlattice line was too weak to be measured quantitatively and therefore a SAXS Kratky plot was used.

Figure 2 shows the δ' volume fraction in alloy 81 as a function of aging time. The SAXS data points (asterisks) have been calibrated with the direct comparison results (circles) at 40 min. aging time.

It is evident from Guinier camera and TEM results that the delta prime volume fraction remains essentially constant at longer aging times. SAXS data in Figure 2 shows an increase in volume fraction of second phases beyond 100 min., caused by T1 and T2 precipitation. The interpretation of the SAXS data in a more quantitative way is restricted due to the complicated shape and structure of T1 and T2. All ternary alloys exhibit the same (110)[$1\bar{1}2$] type texture (Figure 3). The maximum times random number of the (200) pole was 11, 7 and 10 for alloys 73, 81 and 82, respectively.

Figure 4 shows the Young's Modulus of the binary alloy as a function of aging time at 190°C. It exhibits an increase in the elastic modulus up to approximately 80 minutes aging time. The maximum modulus is approximately 80 GPa. 1 GPa is the largest overall change in modulus measured for the binary alloy where δ' and solid solution are the only phases present.

The elastic modulus versus aging time at 190°C for the ternary alloys in the unstretched condition, longitudinal direction is given in Figure 5. They reach a maximum elastic modulus at approximately 10 hours aging at 190°C. The maximum modulus of alloy 73 is 82 GPa. Alloys 81 and 82 reach a maximum modulus of approximately 80 GPa.

The shear modulus exhibits the same trends as the Young's modulus (see Figure 6). The values ranged from 29 to 31 GPa. The Poisson's ratio measurements did not exhibit any significant variation as a function of aging time. The values ranged between 0.30 and 0.33.

The variation in the elastic modulus exhibited by these alloys can be explained by changes in the microstructure. During aging, the grain size, grain orientation (texture) and density remain unchanged. Therefore, the precipitation of second phases is responsible for the changes in elastic behavior.

The change in modulus of 1 GPa exhibited by the binary alloy is due to the increasing volume fraction of delta prime. Beyond 100 minutes aging the volume fraction of delta prime remains constant. Coarsening of the delta prime has no measurable effect on the Young's modulus. This has also been reported by Broussaud and Thomas (6).

A volume fraction of 12.6 delta prime was determined using the Guinier camera on a sample which had been aged 200 hours. This corresponds well with a value of 11.5% calculated using the lever rule with the miscibility gap data reported by Cocco et al. (7).

Using a linear rule of mixtures the modulus of the delta prime can be calculated using the following equation:

$$E = f_{\delta'} E_{\delta'} + (1 - f_{\delta'})(E_{Al} + X C_{SS}^{Li}) \quad \text{. . . . . eq. 5.}$$

E - measured modulus
$f_{\delta'}$ - δ' volume fraction
$E_{\delta'}$ - modulus of delta prime
E_{Al} - modulus of aluminum
X - constant which depicts the dependence of the modulus of the matrix phase on the amount of lithium in solid solution.

C_{SS}^{Li} - Lithium concentration in solid solution (6.25 at% at metastable equilibrium)

E_{Al} and X have been determined by a linear regression of data reported by Muller et al. (8). They are 70.8 and 1.235, respectively. The modulus of delta prime calculated using the above equation with E = 80.7 GPa is 97 GPa. This value is reasonably close to 106 and 96 GPa reported elsewhere (6,8,9).

Equation 5 was also used to predict the change in modulus as a function of delta prime volume fraction. The lithium concentration in the solid solution (C_{SS}) can be related to the delta prime volume fraction according to the following equation:

$$C_{SS}^{Li} = (Y^{Li} - C_{SS}^{Li} f_{\delta'})/(1 - f_{\delta'}) \quad \ldots\ldots\ldots \text{eq. 6}$$

Y^{Li} - total atomic fraction of lithium in the alloy

$C_{\delta'}^{Li} = 0.225$ according to Cocco et al. (7).

Up to approximately 90 minutes aging, the unstretched ternary alloys can be treated as two phase materials comprised of the solid solution and delta prime phases. The aging kinetics of delta prime can be described using an equation from Turnbull (10):

$$f_{\delta'} = f_{\infty}(1 - (1 + B\,(t + t_o))^{-1/3} \quad \ldots\ldots\ldots \text{eq. 7}$$

f_{∞} - equilibrium volume fraction
$f_{\delta'}$ - volume fraction of δ' at time, t
t_o - constant
B - constant.

This equation describes well the measured change in volume fraction of delta prime up to about 100 minutes aging time. The parameters used were f = 0.2, t_0 = 2.7705 min. and B = 0.3196 min^{-1}.

Using equations 5, 6, and 7 the change in modulus for alloy 81 aged up to where Tl begins to precipitate was calculated (see Figure 7). One can see that δ' precipitation has only a weak effect on the Young's modulus.

The increase in E beyond 90 minutes is caused by Tl precipitation. A Tl volume fraction of .7% was determined after 4 hours aging using the direct comparison method. Assuming a linear rule of mixtures the modulus of Tl can be calculated using the following equation:

$$E_{Tl} = (E_{measured} - (f_{\delta'} E_{\delta'} + f_{SS} E_{SS}))/f_{Tl} \quad \ldots \text{eq. 8.}$$

Using constants from equation 5 for the modulus of the solid solution (E_{SS}) the Tl modulus calculates to about 350 GPa. This value is over two times higher than a rough approximation of the lower bound performed earlier (14).

The drop in E occurs at approximately 8 to 10 hours aging time with the precipitation of the icosahedral T2 phase. The data suggests that T2 has an extremely low intrinsic modulus because its volume fraction appears to be small. From Figure 2 follows that the volume fractio of delta prime at the longer aging times remains constant. This indicates that the T2 phase may grow somewhat at the expense of the Tl phase but not at the expense of delta prime. It may also take lithium out of solid solution, thus decreasing the modulus of the matrix phase even further.

The type of precipitates are the same in all three ternary alloys. However, the kinetics of precipitation are different. The

earlier onset of T1 precipitation in the high copper alloy, 73, shows up as an earlier increase in modulus and a larger difference between starting and peak modulus condition. The latter may be explained by a higher T1 volume fraction.

The modulus of alloy 73, stretched 6%, is 2 GPa lower than the unstretched material (Figure 8). This is due to the increased amount of dislocations in the stretched material which can result in anelastic strain effects thereby reducing the measured modulus. There is a more homogeneous precipitation of the T1 phase within the matrix at dislocation jogs (11). The increase in modulus in the stretched material occurs at a shorter age time due to the increase in the kinetics of precipitation.

Although we did not experimentally observe an influence of testing direction on the modulus, we calculated moduli for various testing directions from elastic constant data published by Muller et al. (8).

Linear regression analysis was performed to determine the elastic constants of our alloys. Using these elastic constant values the moduli are calculated and listed according to (12) in Table III, along with pure aluminum from reference (13).

The highest modulus, as expected, is in the [111] direction. The maximum theoretical difference in moduli due to testing direction (E_{max}) is only about half in aluminum-lithium alloys compared to pure aluminum. From a theoretical point of view the Al-Li solid solution alloys can be expected to be even more elastically isotropic than pure aluminum. Figure 9 shows that even during aging there is no directionality of the Young's modulus observable within experimental error despite the fact that a well pronounced rolling texture is present.

CONCLUSIONS

1. The Young's modulus increases only slightly due to the precipitation of delta prime (about 0.1 GPa/vol%).

2. The T1 phase contributes positively to the elastic modulus. Its intrinsic modulus is estimated to be approximately 350 GPa.

3. A maximum increase in E with aging time of approximately 5% can be attributed to the precipitation of T1, and to a lesser extent of δ', for the alloys examined.

4. There is a significant drop in the modulus at the peak aged condition (5%). It is associated with the precipitation of the T2 phase.

5. Al-Cu-Li alloys which have been stretched 6% will show a smaller, but faster increase in modulus upon aging. Earlier occurrence of the T1 phase and enhanced precipitation kinetics are responsible for this phenomenon.

6. There is no orientation dependence of the elastic modulus observed in these alloys.

ACKNOWLEDGEMENT

The authors would like to acknowledge the sponsorship of the Office of Naval Research, Grant #N00014-85-K0526, with Dr. Bruce MacDonald, program manager.

REFERENCES

1. E.A. Starke, Jr., T.H. Sanders, Jr., and I. Palmer, "New Approaches to Alloy Development in the Al-Li System," Journal of Metals 33 (1981) p. 24.

2. G.G. Wald, NASA Contractor Report 16576, Lockheed - California Company, Burbank, CA (May 1981).

3. W. Koster and W. Rauscher, Z. Metallkde 39 (1948) p. 111.

4. K.K. Sankaran and N.J. Grant: Aluminum-Lithium Alloys, eds. T.H. Sanders, Jr., and E.A. Starke, Jr., TMS-AIME, Warrendale, PA (1981) p. 205.

5. J. Krautkramer and H. Krautkramer, Ultrasonic Testing of Materials, 2nd ed., Springer-Verlag, New York (1977).

6. F. Broussaud and M. Thomas, "Influence of Delta Prime Phase Coalescence on Young's Modulus in an Al-2.5 wt% Li Alloy," Aluminum-Lithium Alloys III, eds. C. Baker, P.J. Gregson, S.J. Harris and C.J. Peel, Institute of Metals, London, UK (1986) p. 442.

7. G. Cocco, G. Fagherazzi and L. Schiffini, "Determination of the Delta Prime Coherent Miscibility Gap in the Al-Li System by Small-Angle X-ray Scattering," J. Appl. Cryst. 10 (1977) pp. 325-327.

8. W. Muller, E. Bubeck and V. Gerold, "Elastic Constants of Al-Li Solid Solutions and Precipitates," Aluminum-Lithium Alloys III, Institute of Metals, London, UK (1986), p. 435.

9. B. Noble, S.J. Harris, and K. Dinsdale, "The Elastic Modulus of Aluminum-Lithium Alloys," Journal of Materials Science 17 (1982) p. 461-468.

10. D. Turnbull, Solid State Physics 3 (1956) p. 226.

11. William A. Cassada, III, Ph.D. Thesis, University of Virginia, May 1987.

12. E. Kroner, Statistical Continuum Mechanics, Springer Berlin (1971).

13. C. Kittel, Introduction to Solid State Physics, 4th Edition, John Wiley and Sons, Inc., New York, NY (1971) p. 149.

14. E. Agyekum, W. Ruch, E.A. Starke, Jr., S.C. Jha and T.H. Sanders, "The Effect of Precipitate Type on the Elastic Properties of Al-Li-Cu and Al-Li-Cu-Mg Alloys", Aluminum-Lithium Alloys III, Institute of Metals, London, UK (1986) p. 448.

TABLE I. ALLOY COMPOSITIONS

ALLOY		Al	Cu	Li	Zr	Cu/Li ratio
	wt% / at%					
73		94.79 / 90.55	2.24 / 0.90	2.31 / 8.51	0.16 / 0.04	0.97 / 0.11
81		96.32 / 90.51	1.07 / 0.43	2.47 / 9.02	0.14 / 0.04	0.43 / 0.05
82		96.64 / 91.54	1.06 / 0.43	2.17 / 7.99	0.13 / 0.04	0.49 / 0.05
Binary		97.85 / 92.60		2.00 / 7.36		

TABLE II. VOLUME FRACTION OF DELTA PRIME

Alloy	Age time at 190 C	TEM Method	Direct Comparison Method
		(vol%)	
81	4 hrs		11.2
81	8 hrs	7.0	
81	8 hrs	11.0	14.0
81	8 hrs	6.5	14.0
81	20 hrs		13.8
81	20 hrs		13.9
81	100 hrs		13.9

TABLE III. THEORETICAL MODULI FOR SOLID SOLUTIONS

Alloy	Crystallographic direction <hkl>				
	<111>	<110>	<100>	<112>	E_{max}(%)
82	83.60	81.38	75.38	81.38	11%
Al	75.30	71.73	62.81	71.73	20%

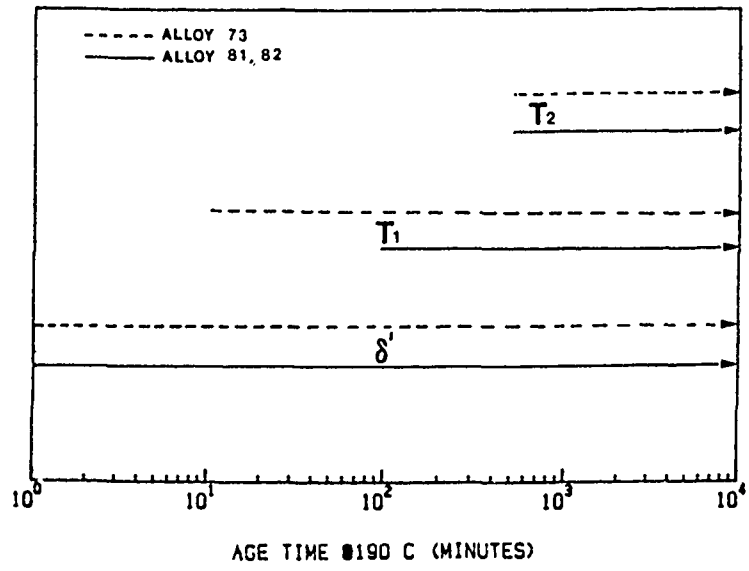

Figure 1. Profile of the occurrence of the delta prime, T1 and T2 phases in alloys 73, 81, and 82.

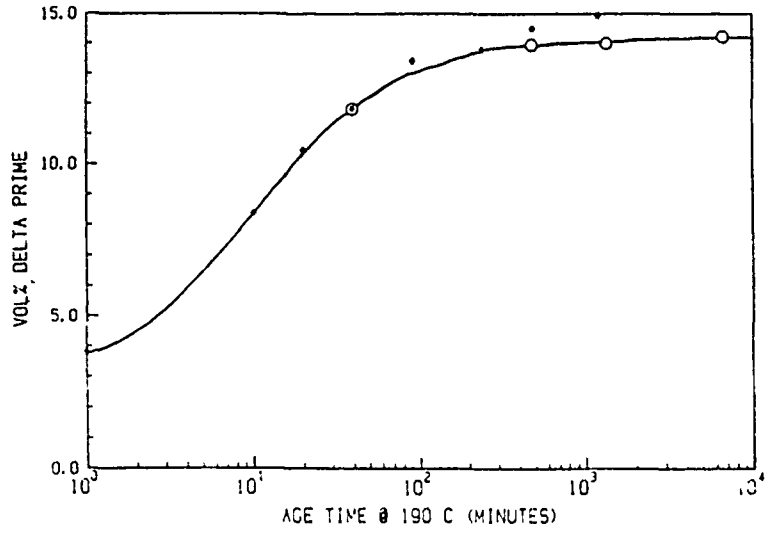

Figure 2. The volume fraction of delta prime in alloy 81 after aging at 190 C. (o) Guinier camera data; (*) SAXS data normalized.

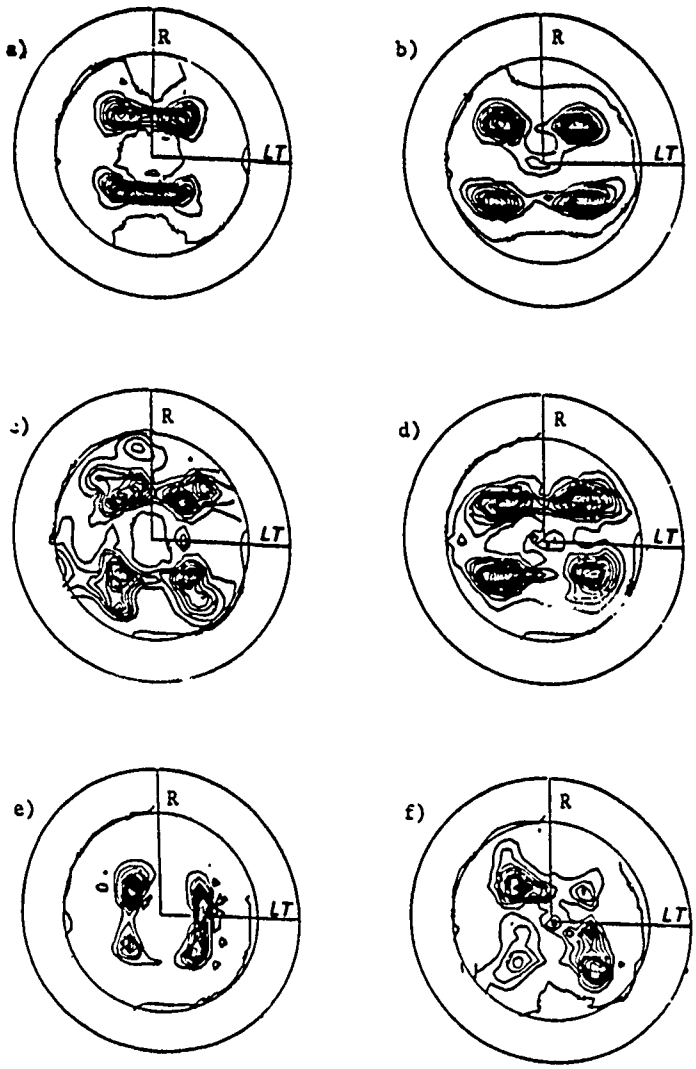

Figure 3. Pole figures a) Alloy 73 (111), b) Alloy 73 (200), c) Alloy 81 (111), d) Alloy 81 (200), e) Alloy 82 (111), and f) Alloy 32 (200).

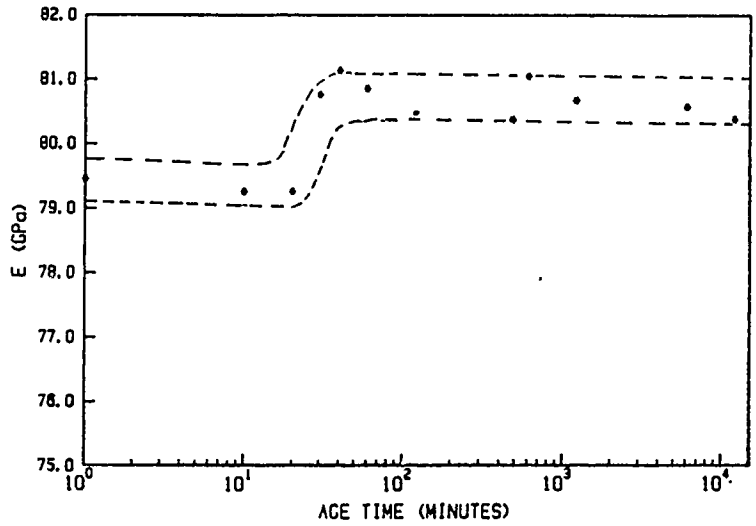

Figure 4. Elastic modulus versus aging time at 190°C of the binary alloy.

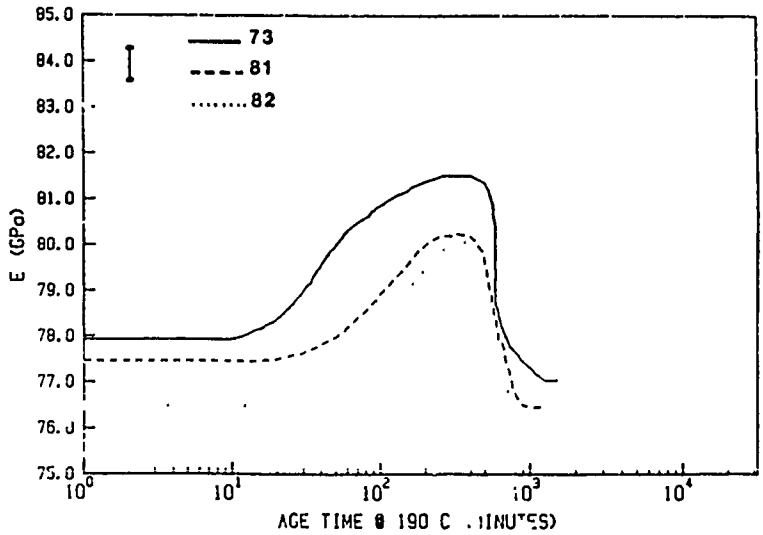

Figure 5. Young's modulus versus aging time at 190°C for alloys 73, 81 and 82 in the longitudinal testing direction.

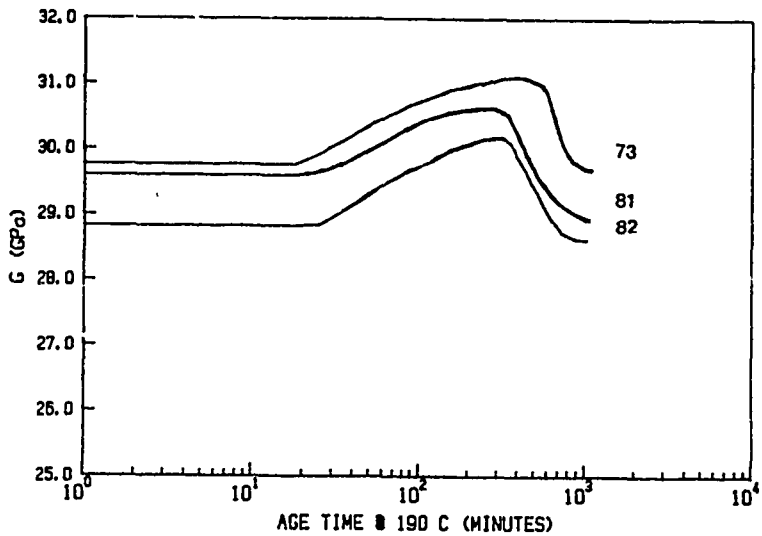

Figure 6. Shear modulus vs. aging time at 190°C for alloys 73, 81 and 82.

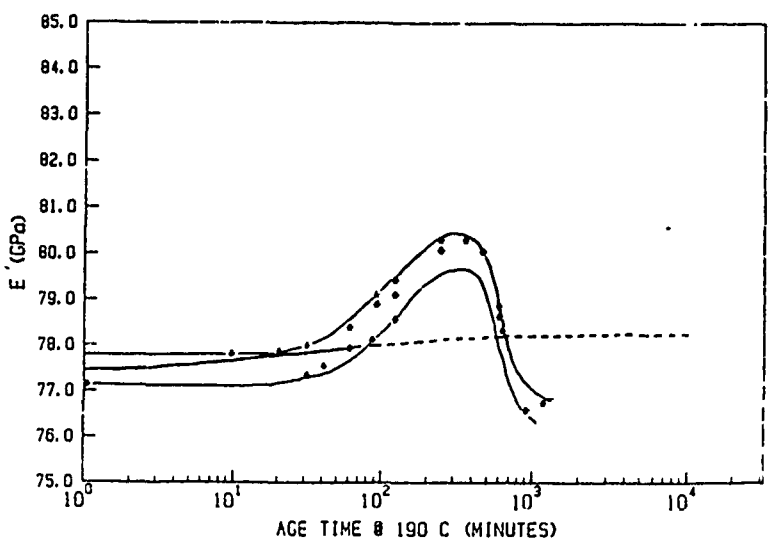

Figure 7. Elastic modulus versus aging time for alloy 81. Experimental data is compared with a theoretical prediction.

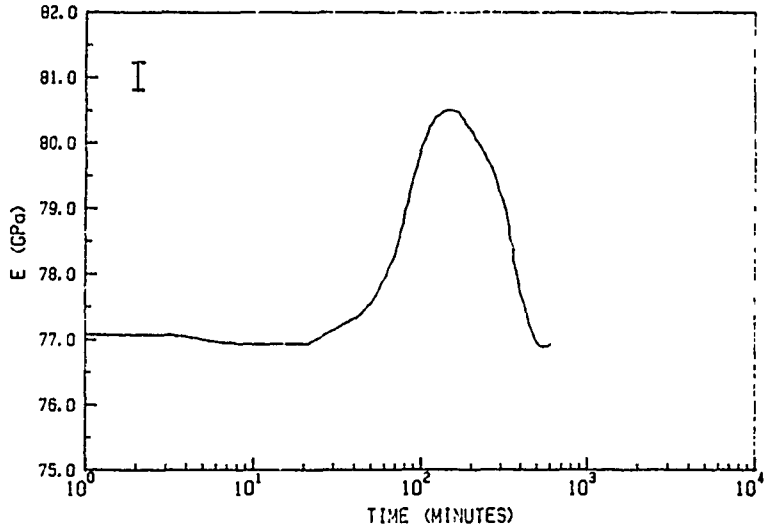

Figure 8. Young's modulus versus aging time at 190°C of alloy 73 stretched 6%.

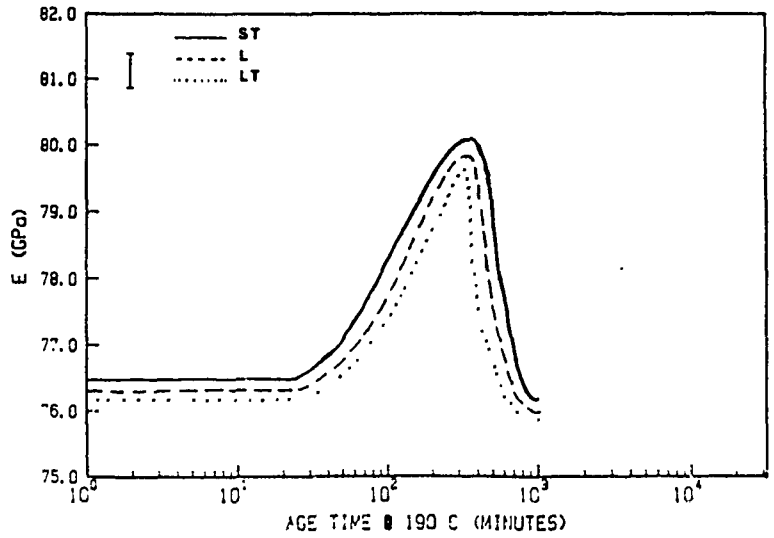

Figure 9. Young's modulus versus aging time at 190°C for the short transverse, long transverse and longitudinal directions of alloy 82.

Scripta METALLURGICA Vol. 22, pp. 1553-1556, 1988 Pergamon Press plc
Printed in the U.S.A.

FRACTURE TOUGHNESS OF Al-Li-X ALLOYS AT AMBIENT AND CRYOGENIC TEMPERATURES

K.V. Jata* and E.A. Starke, Jr.**
*University of Dayton Research Institute, Dayton, Ohio 45469
**Department of Materials Science, University of Virginia, Charlottesville, Virginia 22901

(Received June 20, 1988)
(Revised July 5, 1988)

Introduction

Recent research on the mechanical behavior of some Al-Li-X alloys indicates that the cryogenic fracture toughness in the L-T orientation could be substantially higher than at room temperature (1-5). Similar to the 2219 Al alloy (6) the yield and ultimate tensile strengths, fracture strain and strain hardening exponents at cryogenic temperatures have also been observed to be higher than at room temperature. Since there is a great interest in employing the Al-Li-X alloys in the cryogenic temperature range in some advanced aerospace vehicles, recent research has been directed towards obtaining an understanding of the mechanisms that govern the improvement of fracture toughness. Several different mechanisms have already been proposed to explain the higher fracture toughness at cryogenic temperatures. Briefly, the higher fracture toughness has been attributed to:

(1) low melting point grain boundary phases which solidify at low temperatures and remain liquid at room temperature (1,4);

(2) a larger number of crack delaminations perpendicular to the short transverse direction or perpendicular to the fracture surface in an L-T oriented specimen (2,5) and in plane crack deflections (5) at cryogenic temperatures; and

(3) higher strain hardening capacity at low temperatures (3).

Since Al-Li-X alloys are strengthened largely by coherent ordered precipitates such as Al_3Li and Al_2CuLi, planar slip is a dominant mechanism that not only governs deformation mode but also the resultant fracture (7) through transgranular shear fracture (slip band decohesion) and crack deflections (8). In a previous publication, the authors suggested that higher fracture toughness in underaged alloys is due to slip dispersal, and lower fracture toughness in near-peakage alloys is due to extensive slip localization. Depending on the aging treatment and alloy chemistry the fracture at peakage could be either transgranular or intergranular. In either case, slip bands formed by precipitate shearing largely contribute to the fracture process (7,9). Since higher fracture toughness through slip dispersal or less slip localization is expected in these alloys, it is the objective of the present study to examine the effects of slip localization and dispersal on the fracture toughness of some Al-Li-X alloys at ambient and liquid nitrogen temperatures.

Experimental Procedures

An experimental 2090 type aluminum plate, rolled to 12.7 mm thickness with actual chemical composition of 2.53Li-1.77Cu-0.5Mg-0.13Zr (Fe and Si 0.3%) was obtained from Reynolds Aluminum Company. A second plate, 8090 type, (2.28Li-

0036-9748/88 $3.00 + .00

0.86Cu-.9Mg-.13Zr-0.13Fe-.06Si) rolled to 25 mm thickness was obtained from Alcan International Ltd., U.K. The 2090 plate was solution heat treated at 823 K for one hour, stretched to 2% and then aged at 463 K for 4 and 8 hours. One set was aged for 8.5 hours without stretch. The Alcan plate was received in the T-351 condition and was aged at 463 K for 4 and 8 hours. Tension tests were performed at a strain rate of $1*10^{-4}$ s^{-1}, and 10.5 mm thick compact tension specimens were tested with a crack opening displacement gauge both at ambient and liquid nitrogen temperatures. Although the thickness criterion was met in some specimens, some stable crack growth was also observed in those specimens, and thus the fracture toughness is designated as K_Q. Thin foils from fractured tensile samples were examined under <110> and <112> zone axis and a (111) 2-beam condition to obtain slip band width and slip band spacing from at least twenty sets of micrographs. Fracture surfaces were analyzed with a scanning electron microscope.

Results and Discussion

Mechanical property data of 2090 and 8090 alloys at 300 and 77 K (Table 1) clearly show an increase in the fracture toughness and the accompanied increase in the strength, strain hardening exponent n and fracture strain.

TABLE 1
Mechanical Property Data at Ambient and Liquid Nitrogen Temperatures

Alloy + Aging	YS (MPa) 300K	YS (MPa) 77K	UTS (MPa) 300K	UTS (MPa) 77K	K_Q ($MPa\sqrt{m}$) 300K	K_Q ($MPa\sqrt{m}$) 77K	%el. 300K	%el. 77K	n 300K	n 77K
2090										
4 h	503	525	548	619	23	37	14	17	.06	.10
8 h	507	564	542	630	20	33	12	15	.04	.07
T-6										
8 h	407	478	493	627	24	38	13	23	.09	.15
8090										
4 h	387	392	456	542	35	56	9.4	16	.08	.09
8 h	406	411	464	566	32	52	9.4	16	.07	.10

As shown in Figure 1, the fracture toughness samples at liquid nitrogen temperature exhibit deeper and larger numbers of delaminations normal to the crack plane at all aging conditions and in both alloys. Fractography of the samples reveals the fracture mechanism to be slip band decohesion at both ambient and liquid nitrogen temperatures. However, as shown in the micrographs Figure 2 (a) and (b), the transgranular shear or slip band facets are observed to be consistently wider at 77 K. Transmission electron microscopy of thin foils obtained from fractured tensile samples showed wider slip bands and smaller slip band spacing at 77 K, Table 2. These results are consistent with the observations made before on Al-Li-X alloys, where higher strain hardening exponents and wider slip bands (SBW) with smaller spacing (SBS) resulted in higher fracture toughness (7).

The present results suggest that the fracture toughness improvement at liquid nitrogen temperature could be explained by the deformation processes that occur in the Al-Li-X alloys. From Tables 1 and 2, it is clear that the increase in strain hardening capacity and total elongation at 77 K is related to wider slip bands and smaller slip band spacings. At 300 K where slip localization is more prevalent, i.e., narrower slip bands and larger spacings, a decrease in the strain hardening exponent and fracture strain occurs. In notched specimens, such as a compact tension specimen, the crack initiation process is controlled by the

FIG. 1. Fracture surfaces of compact tensions tested at (a) 300 K and (b) 77 K.

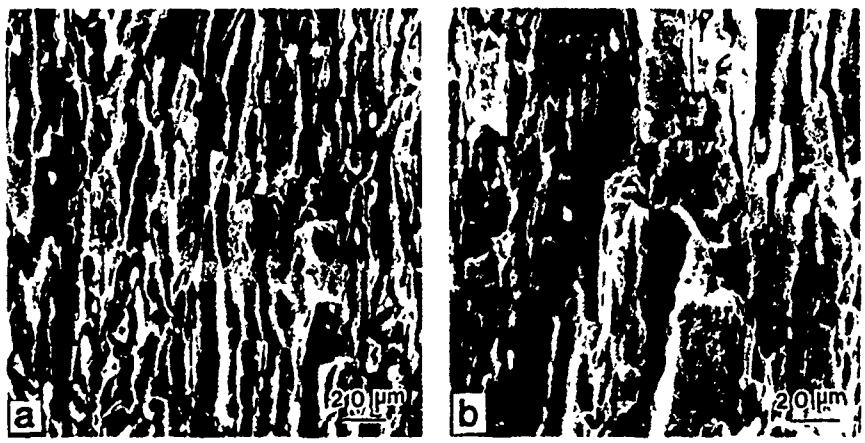

FIG. 2. Fractography of compact tension specimens tested at (a) 300 K and (b) 77 K.

deformation process ahead of the crack tip. For a critical strain controlled fracture process, the ability to concentrate strain in the slip bands is a critical factor. When slip is dispersed, such as at 77 K, larger numbers of wider slip bands accommodate strain whereas at 300 K when slip is localized, fewer and narrower slip bands (Table 2) accommodate strain. Thus at 77 K, the critical strain in one of the potential slip bands where cracks initiate is reached at a later stage when compared to that at 300 K. Following a previous model for fracture toughness of Al-Li alloys (7) in terms of slip band width (SBW) and slip band spacing (SBS), fracture toughness at 300 and 77 K is calculated for the 2090 alloy using

$$K_{1c} = \left[8 \, \mathrm{Sin}\alpha \, E \, \sigma_{ys} \, D \, \left(\frac{SBW}{SBS}\right) \, (\varepsilon)_F^C\right]^{1/2}$$

where E is the Youngs modulus, σ_{ys} is the yield stress, D is the plastic zone width, SBW is the slip band width and SBS is the slip band spacing and $(\varepsilon)_F^C$ is the critical fracture strain.

Although delaminations exist in samples tested at 77 K the material between the delaminations still acts as a notched fracture specimen except that it is now in the plane stress condition due to reduced thickness. The deformation processes that control the fracture toughness in the Al-Li-X alloys, as described in detail in cf. (7) are still applicable. The previous model (7) has been used here to calculate the fracture toughness values and are shown in Table 2.

TABLE 2
Calculated and Experimental Fracture Toughness Values

Alloy + Aging	SBS 300K	SBS 77K	SBW 300K	SBW 77K	K_Q(meas.) 300K MPam$^{1/2}$	K_Q(meas.) 77K MPam$^{1/2}$	K_Q(calc.) 300K MPam$^{1/2}$	K_Q(calc.) 77K MPam$^{1/2}$
2090								
4 h	1.8	1.07	.26	.45	23	37	19.3	47
8 h	2.1	1.22	.20	.36	20	33	12	34
T6								
8 h	1.25	.75	.29	.58	25	38	32	56

Conclusions

The fracture toughness of 2090 and 8090 alloys increases at liquid nitrogen temperature. This is accompanied by an increase in yield and ultimate tensile stress, strain hardening exponent, and fracture strain. A larger number of delaminations occur at liquid nitrogen temperature. These delaminations cause the specimen to behave as if it were under plane stress. However, the deformation processes, i.e., less slip localization at liquid nitrogen temperature when compared to intense slip localization at room temperature, still control the fracture process. Less slip localization at 77 K results in wider and closely spaced slip bands, whereas at 300 K slip bands are narrower and widely spaced. The fracture mechanism at both temperatures is slip band decohesion with larger facets at 77 K and smaller facets at 300 K.

Acknowledgement

This work was sponsored by the U.S. Office of Naval Research under Contract No. N00014-85-5-0526, Dr. Donald Polk, Contract Monitor.

References

1. D. Webster: Al-Li Alloys III, C. Baker, P.J. Gregson, S.J. Harris and C.J. Peel, eds., Institute of Metals, London, U.K., 1986, pp.602-609.
2. R.C. Dorward: Scripta Metall., 1986, 20, pp. 1379-83.
3. J. Glazer, S.L. Verzasconi, R.R. Sawtell and J.W. Morris: Met. Trans. A, 1987, vol. 18A, pp. 1695-1701.
4. D. Webster: Met. Trans. A, 1987, vol. 18A, pp. 2181-93.
5. K.T. Venkateswara Rao, H.F. Hayashigatani, W. Yu and R.O. Ritchie: Scripta Metall., 1988, vol. 22, pp. 93-98.
6. F.G. Nelson and G.J. Kauffman: in Fracture Toughness Testing at Cryogenic Temperatures, ASTM STP 496, American Society for Testing of Materials, Philadelphia, PA, 1971, pp. 27-39.
7. K.V. Jata and E.A. Starke: Met. Trans. A, 1986, vol. 17A, pp. 1011-26.
8. S. Suresh, A.K. Vasudevan, M. Tosten and P.R. Howell: Acta. Metall., 1987, pp. 25-46.
9. T.H. Sanders and E.A. Starke: Acta Metall., 1982, vol. 36, p. 927-937.

Scripta METALLURGICA et MATERIALIA
Vol. 24, pp. 421-426, 1990
Printed in the U.S.A.

EFFECTS OF TEXTURE ON DELAMINATION BEHAVIOR OF A 8090-TYPE Al-Li ALLOY AT CRYOGENIC AND ROOM TEMPERATURE

H.J. Roven*, E.A. Starke, Jr.*, Ø. Sødahl**, and J. Hjelen**
*Dept. of Materials Science, University of Virginia, Charlottesville, VA 22901, USA
**SINTEF, Dept. of Metallurgy, 7034 Trondheim, Norway

(Received December 14, 1989)

Introduction

The high strength, low density Al-Li-X alloys have been considered for aircraft and space vehicle applications, including cryogenic tankage, during recent years (1-5). Rolled plate of 2090- and 8090-type Al-Li alloys may have a tendency to form delamination cracks extending in the rolling direction during fracture (3-7). Some authors have suggested that the delamination phenomena increases the conventional fracture toughness due to 'delamination toughening' (7), i.e., the L-T, L-S and T-S oriented specimens show higher fracture toughness than S-L and S-T specimens. Moreover, recent research indicates that the cryogenic fracture toughness in the L-T orientation is higher than at room temperature (3-6) and is accompanied by an increase in the yield strength, UTS, strain to fracture and the strain hardening exponent (3-5).

The objective of the present work is to examine the influence of precipitate free zones (PFZs) and variations in the relative misorientations between grains in the S-direction on the delamination behavior of an 8090-type alloy at cryogenic and room temperature. Two conditions are investigated, i.e., one condition having a wide PFZ and the other condition with no PFZ. The recently developed (8) and modified EBSP technique in the SEM (9) is employed for micro-texture measurements. This technique is unique since it makes direct correlations between the microstructure and the crystallographic orientation possible on a macroscopic specimen (9).

Experimental

A rolled 8090-type aluminum plate with 25 mm thickness having an actual chemical composition of Al-2.58Li-1.36Cu-0.86Mg-0.14Zr was used for the present study. Two heat treatments were examined: Condition A, for which the alloy was solution heat treated for 1 hour at 803 K (heating rate 10 K/h between 793 K - 803 K), quenched and aged for 38 h at 450 K. This treatment resulted in a pronounced PFZ. Condition B, was obtained by solution heat treatment, quenching and then giving the alloy a 7% stretch before aging at 394 K for 96 h. No PFZ was present in this condition. The two conditions had an identical hardness of 82 HRB (100kg) equal to the peak hardness for condition A and about 3% below the peak hardness value for condition B.

Standard, flat tension specimens were taken both parallel and perpendicular to the rolling direction and tested both at 298 K and immersed in liquid nitrogen (77 K). Two specimens were tested for each variable. Standard CT specimens (W=25.4 mm and B=12.7mm) with L-T orientation were prepared from

0036-9748/90 $3.00 + .00

the plate mid-section and tested in accordance to standard procedure (10) at room temperature and at 77 K. Fracture surfaces were investigated in the SEM. The spacing between fracture surface delaminations were carefully measured in a stereo light microscope at 35λ magnification. All delaminations across the specimen in the crack initiation area were examined on each specimen. From this extensive database, delamination spacings were calculated for each condition.

The relative misorientations between neighbor grains in the S-direction on planes containing the S and L directions were processed by using the modified EBSP technique. A total of 543 and 255 grains were analyzed for conditions A and B, respectively. Since there exists 24 possible solutions to describe the misorientation between two FCC crystals, the relative misorientation angle picked in each case was that of the smallest value. From the crystallographic information obtained (100) micro-pole figures were generated.

Results and Discussion

Optical microscopy of the two conditions revealed a predominately unrecrystallized grain structure which in sections containing the S and L directions consisted of pancake-shaped grains aligned in the rolling direction. The average grain size in the S-direction was 12.9 μm, and the grains consisted of equiaxed subgrains having a size in the range 2-6 μm. The mechanical properties obtained for the two conditions at room and liquid nitrogen temperature are listed in Table 1.

Table 1: Mechanical properties of conditions A and B at room temperature and at liquid nitrogen temperature.

Cond.	YS [MPa]		UTS [MPa]		%el. -		n -		K_{Q_Y} [MPa-$m^{½}$]		K_{max}	
	77K	RT	77K	RT	77K	RT	77K	RT	77K	RT	77K	RT
COND.A												
L/L-T	490	453	658	577	15.5	7.6	.124	.096	36	25	41	33
T	436	426	534	539	16.0	7.4	.111	.100	-	-	-	-
COND.B												
L/L-T	483	466	679	548	21.2	5.7	.135	.084	36	36	48	43
T	429	420	608	522	15.0	8.0	.140	.085	-	-	-	-

These data clearly show an increase in yield strength, ultimate tensile strength, the strain to fracture, the strain hardening exponent, and fracture toughness for both conditions at 77 K compared to room temperature tests. This is in general agreement to literature data obtained on similar materials (3-5). Condition A had somewhat higher RT strength and work hardening capability than condition B, but the opposite appeared at 77 K. It is worthwhile to note that the increase in the n-exponent for condition B was much higher than for condition A as the test temperature decreased to 77 K. Further, the RT ductility was about the same for both conditions, while the PFZ-free condition tended to have higher ductility at 77 K, especially in the L direction. Literature data on mechanical properties for PFZ vs. no PFZ containing materials are very limited and a further interpretation of these observations must incorporate many experimental observations, i.e., fracture toughness and fatigue data, slip localization behavior, precipitate structures and texture (11).

Further, in accordance with earlier reported findings, i.e. (5), the strength for both conditions was highest in the L direction for both RT and 77 K.

Another anisotropic behavior was reflected through the macroscopic fracture mode, i.e., the L orientation showed a 45 degree shear fracture whereas the T direction had a planar crack profile. These anisotropic phenomena can probably be related to the deformation texture and the aligned microstructure.

The fracture toughness in terms of K_{max} or K_Q was higher for condition B than for condition A at RT and the same seemed to apply at 77 K. This is in agreement with Charpy impact test results on a similarly aged 8090 alloy (1). Detailed examinations showed that the delamination could be described by a 'fine delamination' whose spacing and frequency were independent of both aging treatment and testing temperature and a 'coarse delamination' whose spacing and frequency were dependent on both aging treatment and testing temperature (Table 2).

TABLE 2: Average delamination spacings for conditions A and B at room temperature and 77 K.

	Condition A		Condition B	
	RT	77 K	RT	77 K
'Coarse delamination ' spacing (mm)	0.55 +/-.19	1.00 +/-.22	2.20 +/-.78	1.04 +/-.15
'Fine delamination ' spacing (mm)	0.25 +/-.13	0.25 +/-.01	0.27 +/-.06	0.22 +/-.06

The relative misorientations between neighbor grains in the S-direction towards the plate center are plotted for both conditions in Figure 1. These curves were obtained using the cubic spline function fit. For both conditions it is seen that the curve drops to a low from a high misorientation angle (or rises from a low to a high misorientation angle) in some sort of periodic manner. The average spacing between these periodic events was 0.24 mm and 0.21 mm for conditions A and B, respectively (i.e. 'event'= the fitted curve is respectively above and below the upper and lower standard deviations). The 'fine delamination' having an average spacing of 0.25 mm, correlated very closely to periodical events of high to low relative misorientations of grains in the S direction. Although the coarse delamination spacing is quite different for the two aging conditions at room temperature, it is roughly the same at liquid nitrogen temperature. This may be explained by the different contribution of the Peierls stress at room and liquid nitrogen temperatures (11).

Fractographic work and studies of the electropolished surface of tensile specimens showed that condition A tended to deform both by intense slip localization in slip bands but also in the PFZs. Intergranular failure, including intersubgranular crack growth, occurred at both room temperature and at 77 K. The intergranular mode seemed to be more important to the fracture processes than the decohesion of slip bands. Condition B with no PFZ seemed to fracture more along slip bands than by ductile growth processes along grain boundaries. The fractographic studies of condition B showed domination of slip band decohesion both at room and cryogenic temperatures. In general the slip line patterns showed an increased homogeneity at 77 K in both conditions.

The delamination fracture surfaces reflected the general deformation processes, i.e., intergranular growth plus slip localization, and slip localization, causing slip band decohesion for conditions A and B, respectively (Figure 2). However, some delamination cracks in condition B

were also associated with intergranular processes, but most tended to be of the slip band decohesion type of failure.

As seen from the {100} pole figures (Figure 3), the texture consisted of three components, i.e., the brass, Cu and S components. A more detailed study of the development of the texture going from t/4 towards t/2 (half plate thickness) indicated that the brass component tended to be more developed in the plate center region than at t/4. This is in agreement with findings on a 8090-type of alloy recently reported (12). In general, the texture seemed to be more pronounced in positions close to the plate center than at the quarter plate thickness position.

Conclusions

The present study on a 8090-type Al-Li alloy shows that the tensile, fracture and strain hardening properties increase as the test temperature decreases from room temperature to 77 K. The delamination behavior can be characterized by (i) a 'fine delamination' whose spacing is independent of both aging condition and test temperature, i.e., 77 K and room temperature, and (ii) a 'coarse delamination' whose spacing varies both with aging condition and test temperature (RT and 77 K). However, the coarse spacing is roughly equal for the two conditions at 77 K. The spacing of the 'fine delaminations' correlates very closely to periodical events of high to low relative misorientations of grains in the S direction. The fracture processes of the PFZ-containing condition includes slip localization both in slip bands and in the PFZs giving intergranular failure. In the PFZ-free condition the fracture process is dominated by slip localization in slip bands giving slip band decohesion. The latter condition has better cryogenic properties than the PFZ-containing microstructure.

Acknowledgement

This work was sponsored by the U.S. Office of Naval Research under contract no. N00014-85-5-0526. The authors would like to thank contract monitor Dr. George Yoder for his interest and support.

References

1. E.A. Starke, Jr., ICAS Proceedings 1986, eds. P. Santini and R. Staufenbiel, American Institute of Aeronautics and Astronautics, Inc., New York, p. 934 (1986).
2. W.E. Quist, G.H. Narayanan and A.L. Wingert, Aluminum-Lithium Alloys, eds. T.H. Sanders, Jr., and E.A. Starke, Jr., AIME, Warrendale, PA, p. 313 (1981).
3. K. Jata and E. Starke, Jr., Scripta Met. 22, 1553 (1988).
4. J.W. Morris, Jr., and J. Glazer, Lecture at the 1988 Int. Cryogenic Mater. Conf., Shenyang, China (1988).
5. J. Glazer, PhD Thesis, Lawrence Berkeley Lab., University of California, July 1989.
6. K.T. Vankateswara Rao, H.F. Hayashigatani, W. Yu and R.O. Ritchie, Scripta Met., 22, 93 (1988).
7. K.T. Vankateswara Rao, W. Yu, and R.O. Ritchie, Met. Trans. 20A, 485 (1989).
8. D.J. Dingley, Scanning El. Micr. 2, 569 (1984).
9. J. Hjelen and E. Nes, Proc. 8th Int. Conf. on Textures of Materials, AIME, Warrendale, PA, p. 597 (1988).
10. Standard ASTM E399-83.
11. H.J. Roven and E.A. Starke, Jr., "Effects of PFZs, Deformation Mode and Texture on Mech. Prop. of 8090-type Al-Li alloys at Cryogenic and Room Temp.," to be published.
12. A.W. Bowen and P. Holdway, Proc. 10th Riso Int. Symp. on Mat. Sci., Denmark, p. 283 (1989).

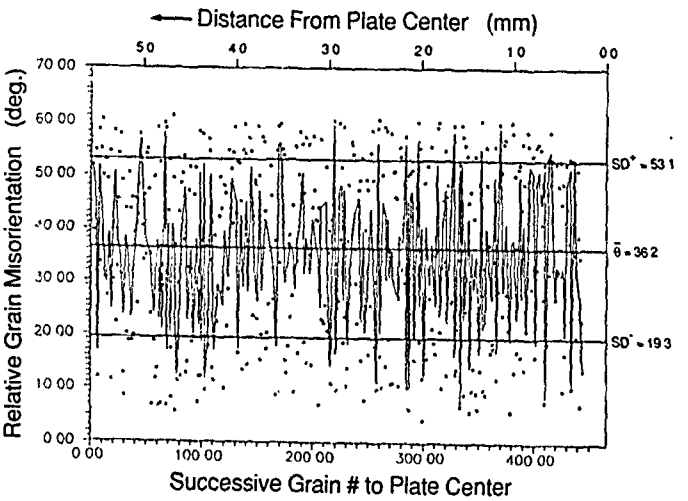

(a)

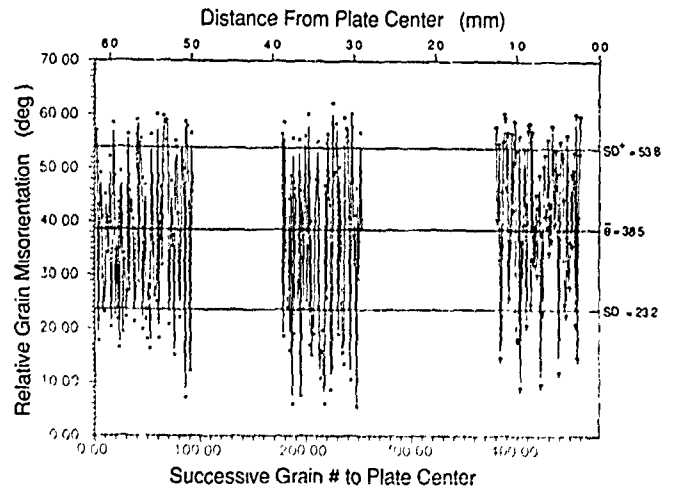

(b)

Figure 1 : Relative misorientation between grains in the S direction vs distance towards the plate center (obtained from section containing S and L directions). (a) Condition A, and (b) Condition B.

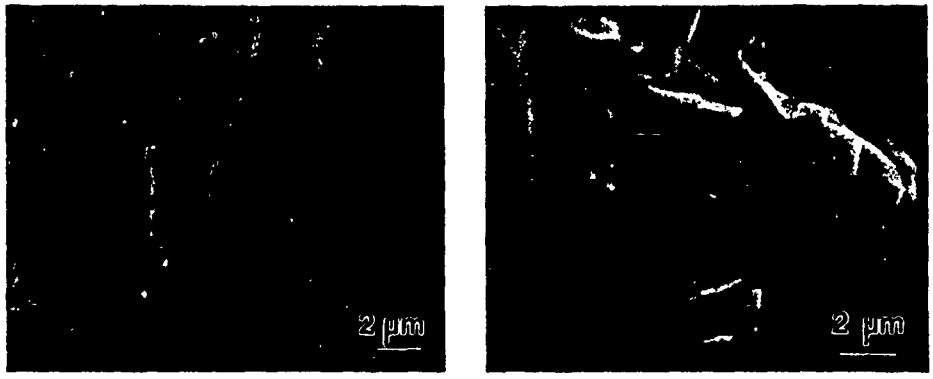

(a) (b)

Figure 2: Delamination fracture surfaces viewed with specimen tilted 35 degrees. Liquid nitrogen test temperature. (a) Condition A: intergranular ductile void growth plus intense slip localization. (b) Condition B: intense slip localization and decohesion.

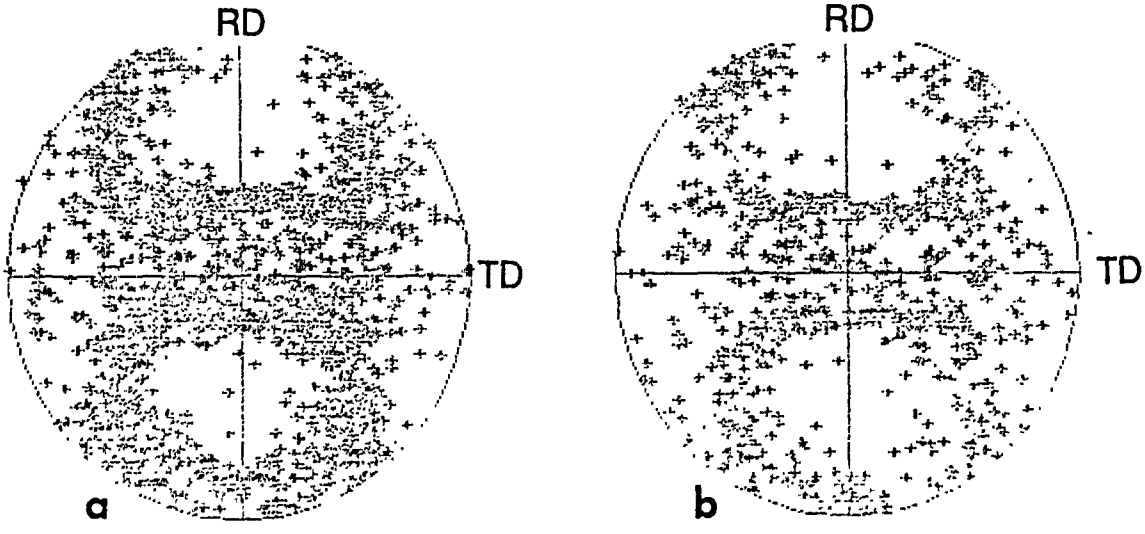

Figure 3: (100) pole figures obtained from the EBSP technique.
(a) Condition A; 543 grains (b) Condition B; 255 grains.

FATIGUE 90

Volume II

Editors
H. KITAGAWA and T. TANAKA.

Proceedings of the Fourth International Conference on Fatigue and Fatigue Thresholds held 15-20 July, 1990.

Materials and Component Engineering Publications Ltd
P. O. Box 1550
Edgbaston
Birmingham B15 2JZ (UK)
Tel: 021 - 456 - 3088

THE FRACTURE AND FATIGUE BEHAVIOR OF Al-Li-X ALLOYS

C.P. Blankenship, Jr.,* H.J. Roven** & E.A. Starke, Jr.*

During recent years, the high strength, low density Al-Li-X alloys have been considered for aircraft and space vehicle applications, including cryogenic tankage. Historically, these alloys have had lower than desirable ductility and fracture toughness, especially in the short transverse direction, but their fatigue crack growth resistance is usually superior to other high strength aluminum alloys. The low ductility and fracture toughness is usually associated with strain localization resulting from shearable strengthening precipitates, coarse grain boundary precipitates and coupled precipitate free zones. However, texture also plays an important role in the fracture behavior, especially in the short transverse direction. Strain localization is the primary reason for the excellent fatigue crack growth resistance and when strain localization is minimized by alloying or heat treatment the fatigue crack growth resistance is reduced.

BACKGROUND

The chemical compositions and alloy designations of the new lithium-containing aluminum alloys are listed in Table 1. In addition, alloys are under development which show improved corrosion resistance and post-weld properties. One of these, a high strength, weldable Al-5.0Cu-1.3Li-0.4Mg-0.4Ag-0.1Zr alloy, Weldalite 049, was developed specifically for cryogenic tanks [1]. The Fe and Si contents are kept to a minimum in these alloys to prevent the formation of coarse constituent phases which have an adverse effect on fracture toughness. As noted in the Table, Zr is the dispersoid forming element of choice to control grain structure and recrystalliza-

*Dept. of Materials Science, University of Virginia, Charlottesville, VA 22901; **SINTEF, Dept. of Metallurgy, 7034-Trondheim, NORWAY

tion during primary processing. The Zr precipitates as the small, coherent, metastable phase, Al_3Zr, which may be sheared by dislocations during plastic deformation.

TABLE 1. Current Al-Li Alloys and Compositions

Alloy / Element*	2090 Alcoa 8/6/84	2091 C Pechiney 4/8/85	8090 Alcan and C Pechiney May 1985	8090A Alcoa (Late 1985)	8091 Alcan 3/29/85	X8092 Alcoa May 1985	X8192 Alcoa Aug 1985
Si	0.10	0.20	0.20	0.10	0.30	0.10	0.10
Fe	0.12	0.30	0.30	0.15	0.50	0.15	0.15
Cu	2.4-3.0	1.8-2.5	1.0-1.6	1.1-1.6	1.8-2.2	0.5-0.8	0.4-0.7
Mn	0.05	0.10	0.10	0.05	0.10	0.05	0.05
Mg	0.25	1.1-1.9	0.6 to 1.3	0.8-1.4	0.5-1.2	0.9-1.4	0.9-1.4
Cr	0.05	0.10	0.10	0.05	0.10	0.05	0.05
Ni	—	—	—	—	—	—	—
Zn	0.10	0.25	0.25	0.10	0.25	0.10	0.10
Ti	0.15	0.10	0.10	0.15	0.10	0.15	0.15
Li	1.9-2.6	1.7-2.3	2.2-2.7	2.1-2.7	2.4-2.8	2.1-2.7	2.3-2.9
Zr	0.08-0.15	0.04-0.16	0.04-0.18	0.08-0.15	0.08-0.16	0.08-1.5	0.08-1.5
Other Each	0.05	0.05	0.05	0.05	0.05	0.05	0.05
Total	0.15	0.15	0.15	0.15	0.15	0.15	0.15

*Numbers Shown Are Either Maximums or Ranges

A schematic representation of the various phases found in basic as well as the more complex Al-Li-X systems is shown in Figure 1 [2]. The δ and T_2 phases are equilibrium phases that nucleate and grow on grain boundaries and therefore do not affect the deformation behavior. However, grain boundary precipitation results in precipitate free zones (PFZ's) along the grain boundaries which, along with the grain boundary precipitates, affect the fracture behavior. The δ', θ', T_1 and S' phases are the strengthening phases that precipitate in the matrix. The δ' phase is sheared by dislocations during plastic deformation. Early work by Price and Kelly [3] on Al-Cu single crystals aged to precipitate θ' indicated that θ' is not sheared but is looped and bypassed by moving dislocations in accordance with the Orowan model of strengthening. However, Starke and Lin [4] clearly showed that when the Al-Cu-Li alloy 2020 is aged to peak strength, where both θ' and δ' are present, deformation occurs by coarse planar slip indicating that θ' is sheared, at least when δ' is present.

There is also some controversy over the shearability of the T_1 phase. Huang and Ardell [5] obtained indirect evidence that T_1 is looped and bypassed by glissile dislocations, confirming an earlier suggestion by Sainfort and Guyot [6]. The former authors aged an Al-Li-Cu alloy to produce δ' and T_1 and then applied a reversion treatment to eliminate δ'. However, Jata and Starke [7] showed direct evidence of T_1 shearing in an Al-Li-Cu alloy which also contained θ' and δ' precipitates. Howe et al. [8] used high resolution electron microscopy to study the structure and deformation behavior of T_1 plates in an Al-2Li-1Cu alloy and showed conclusively that T_1 plates are cut by dislocations during deformation. Shearing of T_1 and θ' when δ' is present may result from superdislocations associated with δ' having a pileup force sufficient to shear these partially coherent precipitates.

When Mg is added to Al-Li alloys containing Cu, matrix precipitation of S' may occur. Crooks et al. [9] and Crooks and Starke [10] have shown that when S' is present in Al-Li-Cu-Mg alloys strain localization is suppressed indicating that the precipitate is not sheared by glissile dislocations. These observations were later confirmed by Gregson and Flower [11]. The S' precipitates do not have densely packed slip planes parallel to the matrix slip planes and are, therefore, unlikely to be penetrated by dislocations [11].

DEFORMATION AND FRACTURE BEHAVIOR

Precipitate shearing, such as occurs in Al-Li alloys, leads to strain localization. The precipitate free zone that results from preferential grain boundary precipitation of equilibrium phases is weaker than the precipitation-hardened matrix and can also be a region of concentrated slip. Both types of concentrated slip produce stress concentrations at grain boundaries and at grain-boundary triple junctions and low-energy intergranular or intersubgranular fracture. The grain boundary precipitates also have a major detrimental effect on fracture resistance since they are the sites for microvoid nucleation, which occurs at small macroscopic strains when deformation is localized in the PFZ. The failure modes described are shown schematically in Figure 2.

Since the deformation behavior of age-hardened alloy is determined by the nature of the interaction of dislocations with the strengthening precipitates, it can

be modified by changes in the type, size, coherency, and distribution of the precipitates present. Cassada et al. [12] showed that the ductility of Al-Li alloys could be significantly increased by the addition of an element that formed small incoherent precipitates which dispersed slip. The addition of Mg to Al-Li-Cu alloys has been shown to have a similar effect when the S' phase is precipitated. Although significant improvement in the ductility and fracture toughness of Al-Li alloys has been obtained by alloying and heat treatments that improve the homogeneity of deformation, most still suffer from a 'delamination' problem.

Rolled plate and extrusions of 2090- and 8090-type Al-Li alloys have a tendency to form delamination cracks extending in the processing direction during fracture and a low fracture toughness in the short transverse direction [13]. The spacing of the delamination cracks appears to be periodic, and although they are associated with grain boundaries, all grain boundaries do not fracture. Consequently, the mechanism of delamination cracking must involve features other than grain boundary precipitates and PFZ's, although these latter microstructural features may play a significant role in the fracture process.

We have studied the delamination behavior of an 8090-type alloy at cryogenic (77K) and room temperature (RT). Two conditions were investigated, i.e., one condition having a wide PFZ and grain boundary precipitates and one condition having no PFZ. The first, condition A, was obtained after a solution heat treatment of one hour at 803K, quench, and holding for 38 hours at 450K. The second, condition B, was obtained after a solution heat treatment of one hour at 803K, quench, a 7% stretch, and holding for 96 hours at 394K. Condition A had large grain boundary precipitates of the T_2 phase and δ' and S' in the matrix, Figure 3(a,b). Condition B did not contain grain boundary precipitates or a PFZ, Figure 4. The matrix precipitate structure consisted of a very fine distribution of δ' with almost no S'.

The mechanical properties obtained for the two conditions at RT and 77K are listed in Table 2. These data clearly show an increase in yield strength, ultimate tensile strength, the strain to fracture, the strain hardening exponent, and fracture toughness for both conditions at 77K compared to RT tests. This is in general agreement to literature data obtained on similar materials [13,14]. Condition A had a somewhat higher RT strength and work hardening capability than condition B,

but the opposite was true at 77K. It is worthwhile to note that the increase in the n-exponent for condition B was much higher than for condition A as the test temperature decreased to 77K. Further, the RT ductility was about the same for both conditions, while the PFZ-free condition tended to have higher ductility at 77K, especially in the L direction. A detailed examination of the fracture surfaces showed that the delamination could be described by a 'fine delamination' which had a spacing and frequency independent of both aging treatment and testing temperature and a 'coarse delamination' which had a spacing and frequency dependent on both aging treatment and testing temperature, Table 3.

TABLE 2. Mechanical properties of conditions A and B at room temperature and at liquid nitrogen temperature.

Cond.	YS [MPa]		UTS [MPa]		%el. -		n -		K_Q [MPa-m^{½}]		K_{max}	
	77K	RT	77K	RT	77K	RT	77K	RT	77K	RT	77K	RT
COND.A												
L/L-T	490	453	658	577	15.5	7.6	.124	.096	36	25	41	33
T	436	426	534	539	16.0	7.4	.111	.100	-	-	-	-
COND.B												
L/L-T	483	466	679	548	21.2	5.7	.135	.084	36	36	48	43
T	429	420	608	522	15.0	8.0	.140	.085	-	-	-	-

TABLE 3. Average delamination spacings for conditions A and B at room temperature and 77 K.

	Condition A		Condition B	
	RT	77 K	RT	77 K
'Coarse delamination' spacing (mm)	0.55 +/-.19	1.00 +/-.22	2.20 +/-.78	1.04 +/-.15
'Fine delamination' spacing (mm)	0.25 +/-.13	0.25 +/-.01	0.27 +/-.06	0.22 +/-.06

Transmission electron microscopy of deformed samples showed that deformation was essentially homogeneous at 77K for both treatments, with condition A, Figure 5(a), being slightly more homogeneous than condition B, Figure 5(b). The deformation of the RT samples was more inhomogeneous than the 77K samples and condition B, Figure 5(c) was slightly more inhomogeneous than condition A, Figure 5(d). Coarse slip bands were observed on the fracture surfaces of condition B but not on those of condition A, supporting the TEM results and the conclusion that deformation of condition B was more inhomogeneous than for condition A.

The relative misorientations between neighbor grains in the S-direction on planes containing the S and L directions were processed by using the modified EBSP technique [15]. A total of 543 and 255 grains were analyzed for conditions A and B, respectively. Since there exists 24 possible solutions to describe the misorientation between two FCC crystals, the relative misorientation angle picked in each case was that of the smallest value. The relative misorientations between neighbor grains in the S-directions towards the plate center are plotted for both conditions in Figure 6. These curves were obtained using the cubic spline function fit. The curve drops to a low from a high misorientation angle (or rises from a low to a high misorientation angle) for both conditions in some sort of periodic manner. The average spacing between these periodic events was 0.24 mm and 0.21 mm for conditions A and B respectively. (Note: the average grain dimension in this direction was a much smaller 13 mm). The spacing of the 'fine delamination' correlated very closely to the periodic events of high to low relative misorientations of grains in the S direction. This suggests that the 'fine delamination' may be associated with strain incompatibility across boundaries of high misorientation and is thus a 'texture' phenomenon. Whether or not this unique through-thickness texture is a result of the presence of the Al_3Zr dispersoid (and possibly the lithium addition) is not known at this time.

The 'coarse delamination' spacing may be related to the slip behavior. At 77K the deformation behavior of the two treatments was essentially the same, i.e., homogeneous, and the coarse delamination spacing was the same. Similar deformation behavior at low temperature is most likely due to an increased contribution of the Peierls stress as the temperature is decreased. At RT the coarse delamination spacing of condition B was four times larger than condition A. The delamination fracture

surfaces reflected the general deformation processes, i.e., grain boundary fracture associated with the more homogeneous matrix deformation, localized deformation in PFZ's and void nucleation at grain boundary precipitates for condition A, and slip band fracture associated with the more inhomogeneous matrix deformation and the lack of PFZ's and grain boundary precipitates, for condition B.

FATIGUE CRACK GROWTH BEHAVIOR

The superior fatigue crack growth resistance that has been observed for Al-Li-X alloys may be associated with one or more of the following: a higher elastic modulus due to the lithium addition, a higher slip reversibility associated with intense planar slip, and a higher degree of crack deflection and roughness-induced closure [16], when compared with conventional aluminum alloys.

Gayle and coworkers [17] have shown that in the naturally-aged temper the strengthening phases of Weldalite 049 are shearable δ' and GP zones, and in the artificially aged T6 and T8 tempers, the strengthening phase is T_1. Unlike other commercially available Al-Li-X alloys there is little or no δ' present in the T6 and T8 tempers. Since shearable precipitates enhance slip reversibility [18] and strain localization which contributes to crack deflection and roughness-induced closure [19-21], and since the T_1 phase may not be shearable when δ' is not absent, Weldalite 049 appeared to be an excellent material with which to examine the reasons for the superior fatigue crack growth resistance of Al-Li-X alloys.

TEM studies of deformed Weldalite samples showed that the naturally aged T3 material deformed by intense localized planar slip, Figure 7a, while deformation was relatively homogeneous for the artificially aged T8 material, Figure 7b. Fatigue crack growth tests were performed on compact tension samples taken from an extruded plate of Weldalite in both the T3 and T8 tempers. Samples were tested from the T-L and L-T orientations. Load shedding was accomplished via computer control, and crack length was monitored using the compliance technique. Intrinsic crack propagation was studied using a decreasing ΔK at constant K_{max} = 9.5 MPa $m^{\prime}$ mode of operation. Closure effects were studied using a decreasing ΔK constant load ratio, R = 0.1. Optical microscopy was used to characterize crack

tortuosity. Since the elastic modulus was the same for both tempers [22], that parameter could be eliminated as a cause for any difference in FCGR observed in this study.

Intrinsic fatigue crack growth rates are shown in Figures 8a and 8b, along with crack growth rates at R = 0.1. The T3 and T8 tempers showed intrinsic thresholds of $\Delta K = 2.0$ MPa $m^{\frac{1}{2}}$ (R = 0.79), and $\Delta K = 1.3$ MPa $m^{\frac{1}{2}}$ (R = 0.86), respectively. In both tempers, there was virtually no difference between the data generated for the T-L and L-T orientations. The T8 temper has an intrinsic fatigue resistance similar to the 2XXX series alloys and slightly superior to the conventionally processed 7XXX alloys. The T3 temper has a higher intrinsic fatigue resistance than conventionally processed aluminum alloys.

In order to explain these results, the mechanism of damage accumulation must be investigated. Plastic strain is accumulated by slip ahead of the crack tip. The T3 temper contains shearable coherent precipitates that allow for eased slip reversibility as discussed by Hornbogen and Zum Gahr [18]. The dislocations can glide in both directions on the slip plane with ease due to decreased resistance from sheared precipitates and the fact that precipitate shearing enhances planar slip. Planar slip often leads to crack branching and crack deflection [19,20], and a significant amount of branching and deflection was observed for the T3 temper. These avenues for energy release reduce the driving force for crack propagation, which partially explains the unusually high intrinsic threshold measured for the T3 temper. The T8 condition contains a fine dispersion of T_1 plates and deforms in a predominately homogeneous manner. Dislocation looping mechanisms, tangles, and cross slip associated with near-homogeneous deformation hinders slip reversibility. This situation leads to a higher accumulation of plastic strain in the T8 temper for the same number of cycles [23]. Therefore, the T8 material should exhibit faster crack growth than the T3 material at any given ΔK, which is observed experimentally.

Although the effect of environment on the fatigue crack propagation behavior was not evaluated in this study, it is well-known that strain localization increases environmental sensitivity in age hardenable aluminum alloys [24]. This effect is normally associated with a hydrogen embrittlement mechanism for corrosion fatigue which relates the degree of susceptibility to

slip planarity [25-27]. However, the surface oxide film which forms in air also hinders slip reversibility [23]. In either case, one would expect that the T3 temper would be more environmentally sensitive than the T8 temper and that the T3 temper would show an even larger crack growth resistance, compared with the T8 temper, in vacuum.

In addition to contributing to intrinsic crack growth rates, the deformation mode determines the amount of extrinsic shielding mechanisms such as roughness-induced closure. The planar slip microstructure of the T3 temper makes a significant contribution to extrinsic effects by causing crack branching, crack deflection, and fracture surface roughness. Fracture occurred along slip bands, and an optical micrograph of the tortuous crack path is shown in Figure 9(a). SEM analysis indicated that branching and deflection occurred throughout the specimen thickness. All of these effects reduce the ΔK experienced at the crack tip and thus reduce the driving force for crack propagation. The role of crack deflection as an extrinsic shielding mechanism was investigated using equations developed by Suresh [20]. The ΔK at the deflected crack tip was found to be 2% lower than the nominal value, and the fatigue crack growth rate was found to be 4% lower than for an undeflected crack. These results suggest that crack deflection does not significantly affect the crack propagation rate. Therefore, the high intrinsic threshold measured for the T3 temper must be attributed to either slip reversibility, closure (even at high R), or crack branching. Since the T3 temper has a high level of roughness-induced closure, some permanent mode II displacement must occur, i.e., complete slip reversibility does not take place during unloading. As shown in Figure 10a, the T3 specimens exhibited tortuous crack paths. In the presence of Mode II displacements, crack tip openings are not large enough to assure closure-free testing even at high R, e.g. 0.8. Consequently, the high threshold is most likely associated with crack branching and closure. Although these are considered extrinsic shielding mechanisms, they are caused by the deformation mode of the alloy which is controlled by the microstructure.

Closure effects in the T8 temper are small, as would be expected from its deformation behavior. Figure 9(b) shows the straight crack profile associated with the T8 temper. Fracture was predominately intersubgranular, and there were no mechanisms for energy release other than the extension of the crack perpendicular to the loading

direction. Fatigue crack profiles shown in Figure 9 are representative of both constant K_{max} and R = 0.1 test conditions.

Figure 10 is a direct comparison of near threshold fatigue crack growth rates for Weldalite-T3 and 2024-T3 [28]. The enhanced crack growth resistance of Weldalite under constant K_{max} and R = 0.1 conditions cannot be attributed to the 6% improvement in elastic modulus and is most likely associated with extrinsic effects such as crack branching. Weldalite may have a higher propensity for planar slip and slip reversibility due to the presence of δ'; however, it seems logical to credit branching and closure effects for most of the improvement in resistance to fatigue crack growth compared to 2024-T3.

CONCLUSIONS

1. The delaminations that occur in the longitudinal direction during fracture of Al-Li-X alloys can be described by 'fine delamination' and 'coarse delamination'. The 'fine delamination correlates very closely to periodic high to low relative misorientations of grains in the S direction. The 'coarse delamination' is correlated both with the texture variation and with slip localization and strain incompatibility across these high angle grain boundaries.

2. The superior fatigue crack growth resistance of Al-Li-X alloys is primarily associated with the coarse planar slip that occurs in most of these materials. This strain localization leads to crack branching, crack deflection and fracture surface roughness, features which result in high closure levels. When strain localization is eliminated, either by alloying or heat treatment, the fatigue crack growth resistance is comparable to other high strength aluminum alloys.

ACKNOWLEDGMENT

This work was sponsored by the U.S. Office of Naval Research under Contract N00014-85-5-0526. The authors would like to thank our contract monitor Dr. George Yoder for his interest and support. Special thanks are expressed to Dr. Ashim Mukhopadhyay for his help with the transmission electron microscopy.

REFERENCES

1. J.R. Pickens, F.H. Heubaum, T.J. Langan and L.S. Kramer in Aluminum-Lithium Alloys V, edited by T.H. Sanders, Jr., and E.A. Starke, Jr., Vol. III, MCE Publications Ltd., Birmingham, UK, 1989, p. 1397.

2. W.E. Quist and G.H. Narayanan, in Aluminum Alloys - Contemporary Research and Applications, edited by A.K. Vasudevan and R.D. Doherty, Academic Press, Inc., 1989, p. 219.

3. R.J. Price and A. Kelly, Acta Met. 12, 1964, p. 159.

4. E.A. Starke, Jr., and F.S. Lin, Metall. Trans. 13A, 1982, p. 2259.

5. J.C. Huang and A.J. Ardell, 4th International Aluminum Lithium Conference, edited by G. Champier, B. Dubost, D. Miannay, and L. Sabetay, J. de. Physique, Colloque C3, 1987, p. C3-373.

6. P. Sainfort and P. Guyot, in Aluminum-Lithium Alloys III, ed. by C. Baker, P.J. Gregson, S.J. Harris and C.J. Peel, Inst. of Metals, London, 1986, p. 420.

7. K.V. Jata and E.A. Starke, Jr., Metall. Trans. 17A, 1986, p. 1011.

8. J.M. Howe, J. Lee and A.K. Vasudevan, Metall. Trans. 19A, 1988, p. 2911.

9. R.E. Crooks, E.A. Kenik and E.A. Starke, Jr., Scripta Met. 17, 1983, p. 643.

10. R.E. Crooks and E.A. Starke, Jr., Metall. Trans. 15A, 1984, p. 1367.

11. P.J. Gregson and H.M. Flower, Acta Met. 33, 1985, p. 527.

12. W.A. Cassada, G.J. Shiflet and E.A. Starke, Jr., Acta Met. 34, 1986, p. 367.

13. K. Jata and E.A. Starke, Jr., Scripta Met. 22, 1988, p. 1553.

14. J. Glazer, Ph.D. Thesis, Lawrence Berkeley Lab., University of California, July, 1989.

15. J. Hjelen and E. Nes, Proc. 8th Int. Conf. on Textures of Materials, AIME, Warrendale, PA, 1988, p. 597.

16. E.J. Coyne, T.H. Sanders, Jr. and E.A. Starke, Jr., in Aluminum-Lithium Alloys, ed. by T.H. Sanders, Jr. and E.A. Starke, Jr., AIME, Warrendale, PA., 1981, p. 293.

17. F.W. Gayle, F.H. Heubaum and J.R. Pickens, in Aluminum-Lithium V, ed. by T.H. Sanders, Jr. and E.A. Starke, Jr., Vol. II, MCE Publications Ltd., Birmingham, UK, 1989, p. 701.

18. E. Hornbogen and K.H. Zum Gahr, Acta Met. 24, 1976, p. 581.

19. F.S. Lin and E.A. Starke, Jr., Mater. Sci. and Engr. 43, 1980, p. 65.

20. S. Suresh, Metall. Trans. 14A, 1983, p. 2375.

21. S. Suresh, Metall. Trans. 16A, 1985, p. 249.

22. Frank Heubaum, Martin Marietta Laboratories, Baltimore, MD, private communication, 1989.

23. E.A. Starke, Jr. and J.C. Williams, in Fracture Mechanics: Perspectives and Directions, ASTM STP 1020, ed. by R.P. Wei and R.P. Gangloff, ASTM, Philadelphia, PA, 1989, p. 184.

24. F.S. Lin and E.A. Starke, Jr., in Hydrogen Effects in Metals, ed. by I.M. Bernstein and A.W. Thompson, AIME, Warrendale, PA, 1980, p. 485.

25. J.A. Donovan, Metall. Trans. 7A, 1976, p. 1677.

26. M.R. Louthan, Jr., G.R. Caskey, Jr., J.A. Donovan, and D.E. Rawl, Jr., Mater. Sci. and Engr. 10, 1972, p. 357.

27. R.P. Wei, in Fatigue '87, ed. by R.O. Ritchie and E.A. Starke, Jr., EMAS, West Midlands, United Kingdom, 1987, p. 1541.

28. W.A. Herman, R.W. Hertzberg, and R. Jaccard, Fatigue Fract. Engr. Mater. Struct. 11, 1988, p. 303.

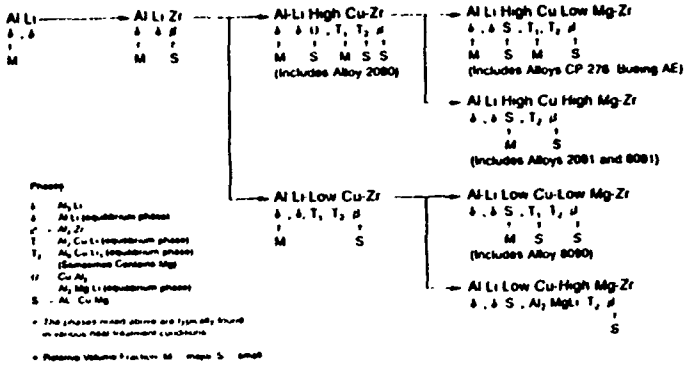

Figure 1. Schematic representation of the various phases found in Al-Li-X alloys. From reference 2.

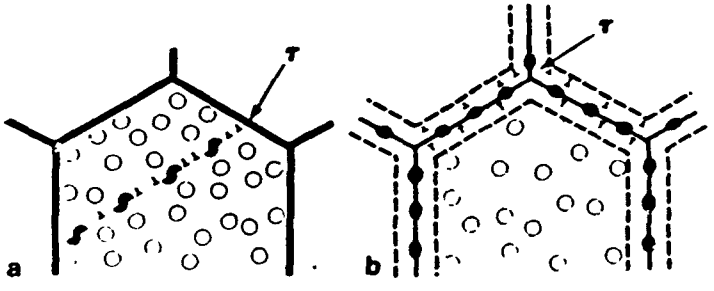

Figure 2. Schematic of the failure modes associated with strain localization in Al-Li-X alloys, (a) strain localization in the matrix and (b) strain localization in the PFZ and void nucleation at GB precipitates.

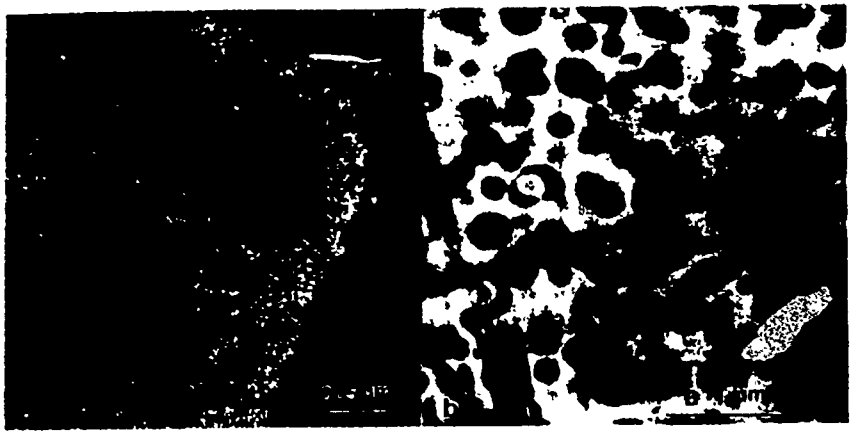

Figure 3. TEM's of condition A showing (a) grain boundary region, PFZ and GB precipitates and (b) matrix precipitate structure of δ' and S'.

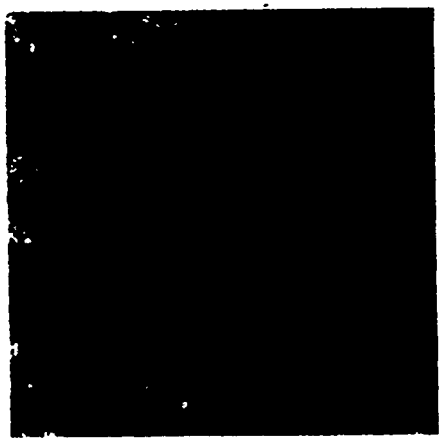

Figure 4. TEM of condition B showing grain boundary region and matri. precipitate structure of δ'.

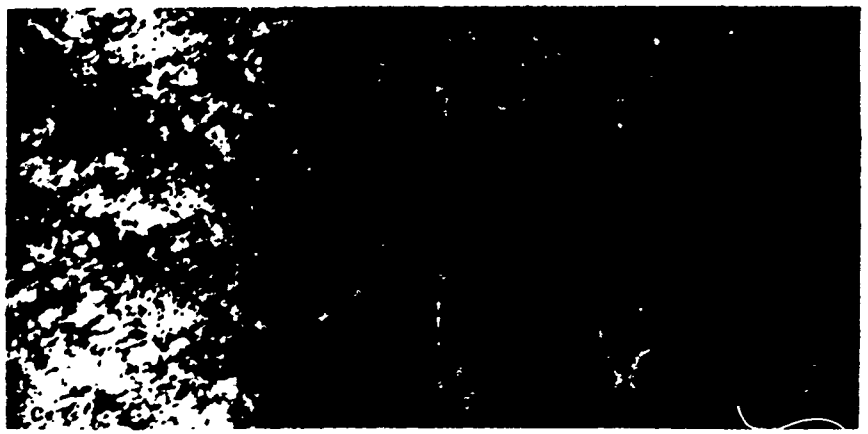

Figure 5. TEM's of deformed samples of (a) condition A at 77K, (b) condition B at 77K, (c) condition B at RT and (d) condition A at RT.

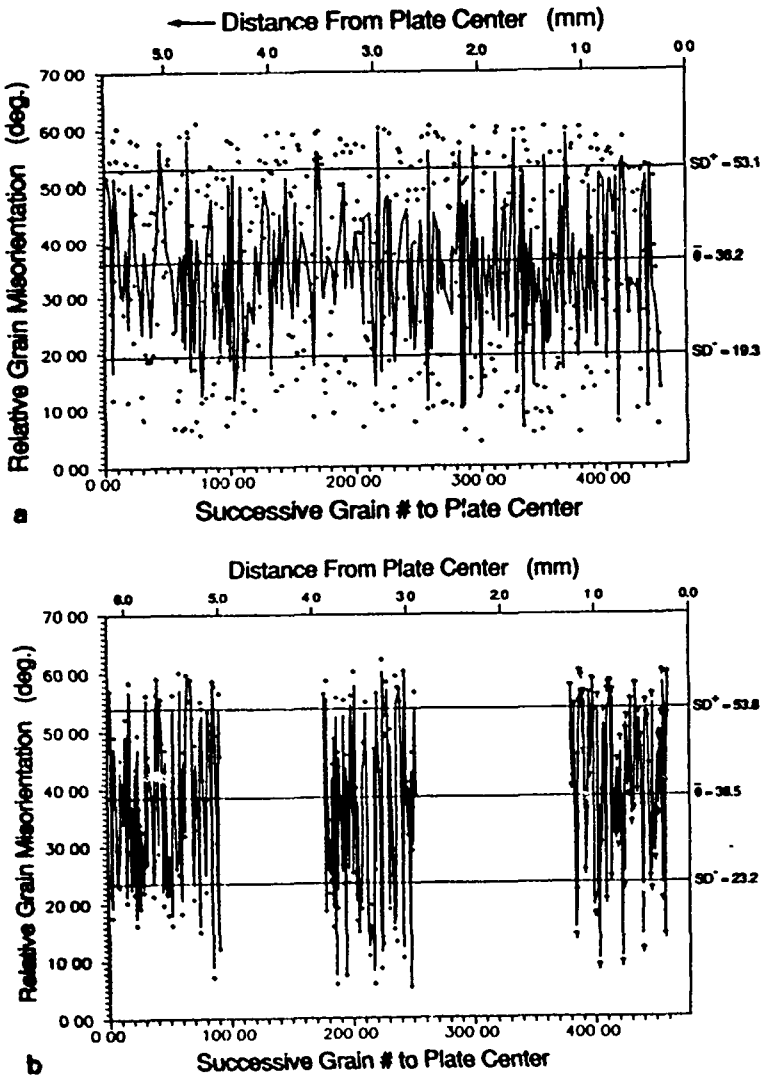

Figure 6. Relative misorientation between grains in the S direction vs. distance towards the plate center (obtained from section containing S and L directions); (a) condition A, and (b) condition B.

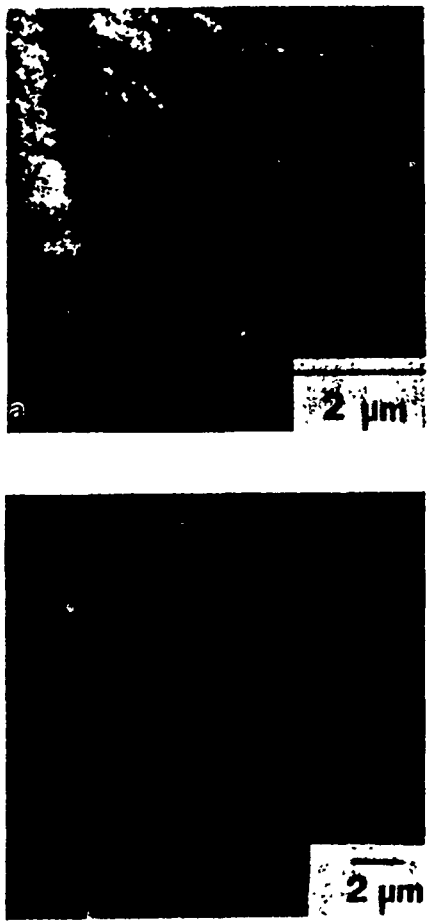

Figure 7. TEM's of deformed Weldalite samples showing (a) localized deformation in the T3 temper, and (b) more homogeneous deformation in the T8 temper.

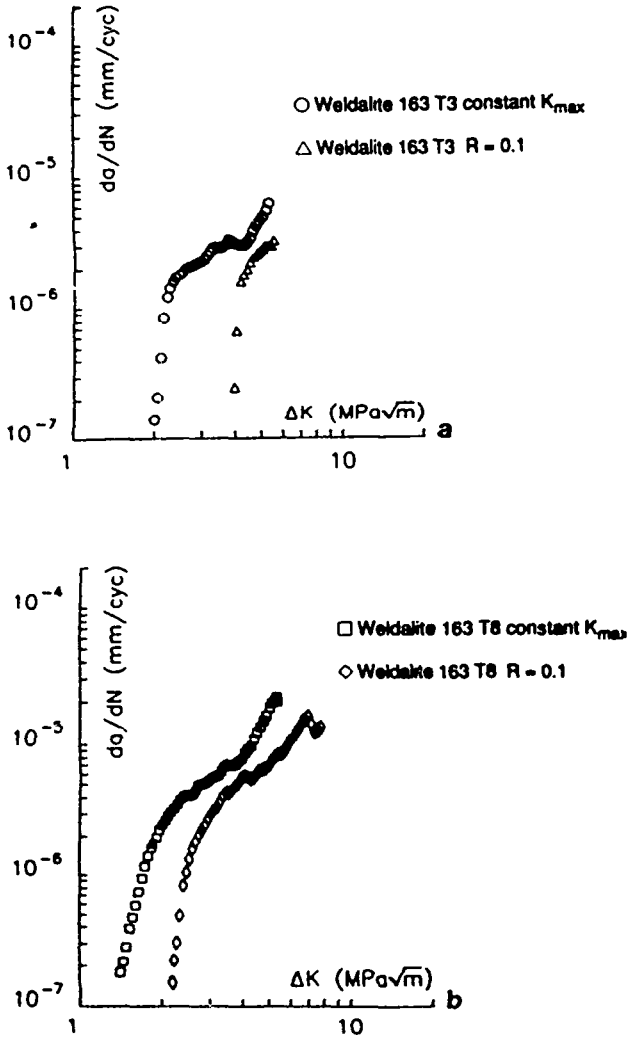

Figure 8. Fatigue crack growth rates for the (a) T3 and (b) T8 tempers, constant K_{max} and R = 0.1.

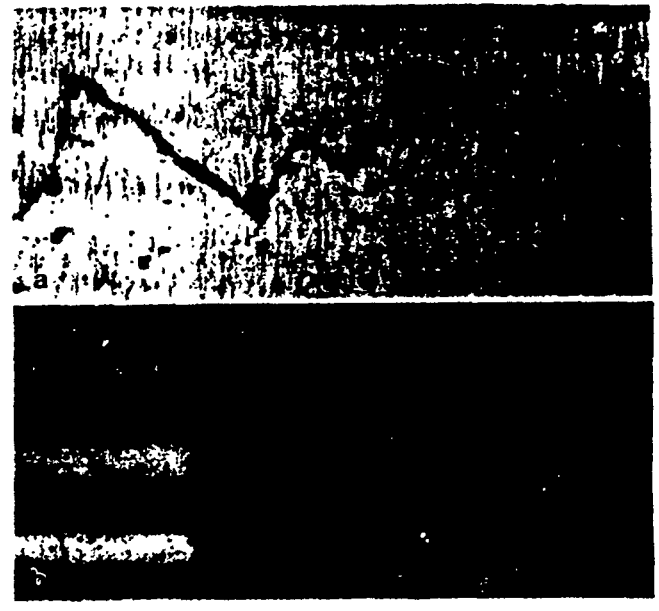

Figure 9. Fatigue crack profiles for the (a) T3, and (b) T8 tempers, constant K_{max}. Taken from regions of low ΔK.

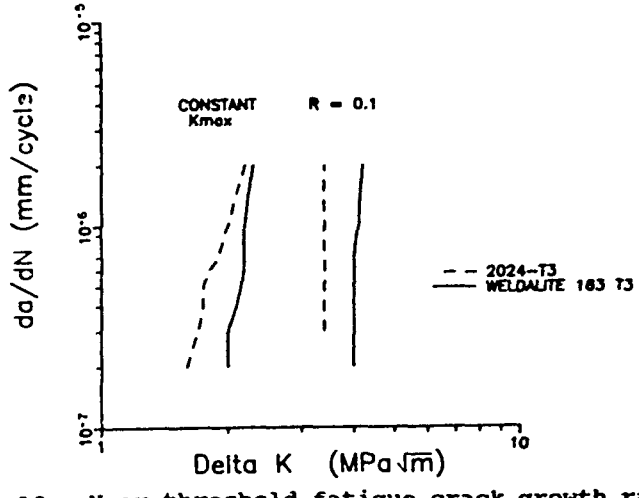

Figure 10. Near threshold fatigue crack growth rates of Weldalite T3 compared to 2024-T3 (after W.A. Herman et al., reference 28), constant K_{max} and R = 0.1.

THE ROLE OF TRACE ALLOY ADDITIONS ON PRECIPITATION IN AGE–HARDENABLE ALUMINUM ALLOYS

A. K. Mukhopadhyay, G. J. Shiflet and E. A. Starke, Jr.

Department of Materials Science

University of Virginia, Charlottesville, VA 22903

Abstract

The application of most age–hardenable aluminum alloys requires that they have both high strength and fracture toughness. Studies have shown that this is best accomplished when the strengthening phases are fine and uniformly distributed throughout the matrix and there is a minimum of coarse grain boundary precipitates. Often a preaging deformation is applied to promote nucleation of the strengthening phases by providing nucleation sites in the form of dislocation structures. The preaging deformation also affects the aging kinetics in such a way that the time at the aging temperature can be reduced which reduces the volume fraction and size of the deleterious grain boundary precipitates. For some alloy systems and/or product forms a preaging deformation is impractical and other methods must be utilized. In many aluminum alloys trace element additions may stimulate nucleation of finer dispersions of strengthening precipitates. Such potential benefits have been known for many years although there is no consistent theory to explain the effect of such additions to aluminum alloys. This paper reviews the results of previous research on trace additions and catalogs the results according to the specific role that the trace addition plays on the precipitation process.

Introduction

Since the recognition of the age hardening capability of an aluminum alloy containing copper and magnesium by Wilm in 1906 (1) and subsequently of the major principles responsible for such phenomena by Merica et al. in 1911 (2), many complex aluminum–based alloys have been developed. Our current understanding of structure–property relationships suggests that optimization of the grain structure, the presence of fine and uniformly distributed appropriate strengthening phases in the matrix, and a minimal presence of coarse grain boundary precipitates in the final heat treated microstructure are keys towards obtaining attractive combinations of mechanical properties. While the grain structure may largely be controlled by a suitable combination of dispersoids and mechanical and thermal processing, attempts to control the precipitate structure via variations of the heat treatment conditions are often not feasible. Often a preage deformation stretch is used to promote nucleation of the appropriate strengthening phases by providing nucleation sites in the form of dislocation structures. The utilization of a preage strength, however, has limitations on various product forms and with various forming operations. An alternative approach may be the use of suitable trace alloying additions to stimulate nucleation of the strengthening phases.

A number of studies on the effects associated with trace additions to different Al–based alloys have been reported in the past several years, although the exact mechanisms responsible for the catalytic role of many of these trace additions are still undetermined. Consequently, no decisive rules are available to predict which trace element may be chosen for a specific purpose. As was noted by Kelly and Nicholson (3), "the effect of the trace additions are qualitatively understood but their mode of action is unknown", or as was noted by Hardy (4), "it is necessary to discover whether or not trace element effects in precipitation reactions are specific to certain precipitates". A complete understanding of trace element effects in precipitation hardening systems requires that many systems be identified and investigated.

Role of Nucleation

In the formation of new phases (in this case precipitates) nucleation can be homogeneous or heterogeneous. Unless the new phase can be proven to be homogeneously nucleated it should be considered to be formed heterogeneously. This is particularly true if there is a change of lattice parameter and/or a matrix:precipitate misfit >2%. As common nucleation sites are grain boundaries, dislocations and interphase boundaries, it would be necessary to examine the effect of trace elements on these defects. Although some trace additions (e.g. Cu in Al–Mg–Si alloys), by preferential interactions with vacancies, may reduce the rate of nucleation we will only consider the case where trace elements greatly increase the number of a specific precipitate type that already exists at the same temperature and chemistry without the trace addition. The emphasis of trace element effects on nucleation would seem to be a safe assumption since the increase in density of the particles is a result of nucleation kinetics and not growth kinetics.

What are the mechanisms available to small solute additions in increasing nucleation rates? They should revolve around reducing ΔG^*, the barrier to an embryo achieving critical size, and increasing N, the number of available nucleation sites. In $\Delta G^*$the primary parameters include the interfacial energy, the volume free energy, ΔG_v, and the volume strain energy, W.

Alloying additions can alter the misfit between the precipitate and matrix, e.g. in Ni–Al and Al–Zn–Mg alloys. This effect is due to incorporation of solute into the emerging embryo which changes its lattice parameter, and hence its misfit strain. This can affect interfacial energy as well as volume strain energy, leading to a reduction of ΔG^*. Further, trace additions in the embryo may increase nucleation kinetics through electronic contributions (e/a ratio, to be discussed later). If the altered phase is a latter part of a sequence of metastable precipitates (e.g. θ') or the equilibrium phase, more of the available volume free energy will be consumed. Because nucleation is based on the statistical fluctuation of atoms it is probably not correct to refer to the diffusional segregation of a trace element to the embryo interface to

Morris E. Fine Symposium
Edited by Peter K. Liaw, J. R. Weertman,
Harris L. Marcus and Joseph S. Santner
The Minerals, Metals & Materials Society, 1991

reduce its interfacial energy as a basis of invoking homogeneous nucleation. On the other hand, this mechanism can surely alter growth kinetics.

Dislocations can accommodate a high density of nuclei, as much as 10^6 on a cm. of dislocation line (5). The main attribute of dislocations in encouraging precipitation is in reducing the volume strain energy, W, associated with the new phase. Because the strain energy associated with an edge dislocation is higher than that for screw dislocations, edge dislocations are more effective nucleation sites. However, as supersaturation increases, the effect is less pronounced. Since the elastic strain field has an important effect on nucleation, trace element segregation to dislocations may amend this strain field which can favor certain precipitate misfit strains. As embryos should all be coherent, minimization of volume strain energy occurs. Depending on the sign of the misfit, precipitates will form on the compressional or dilatational side of an edge dislocation, at an appropriate distance from the core.

Dislocations can influence nucleation in another way. Precipitates that grow via the separation of $a/2\{110\}$ dislocations to partials $a/6\{112\}$ (in aluminum, e.g., γ' in Al–Ag and T_1 in Al–Cu–Li, referred to as the stacking fault mechanism) might also be affected by trace alloying additions since they may change the local stacking fault energy. An increase of several orders of magnitude of T_1 precipitate densities can occur in Al–Cu–Li by initially plastically deforming the material before heat treatment (6). The reason for the large increase is not so much because of a higher dislocation density due to the plastic deformation, but rather, the increase in kinks in the dislocations because of dislocation interaction that can lead to embryo formation. It might be possible that trace elements segregate to the dislocation and increase the number of kinks and therefore the number of nucleation sites.

A proven effect of trace additions on heterogeneous nucleation is the formation of small precipitates (10–100 Angstroms) uniformly in the matrix. The differences in crystal structure between the particle and matrix insure a relatively high energy interface at least at some fraction of the phase boundary. If the supersaturation, ΔG_{v_1} is everywhere the same in the matrix then these sites become ideal locations for the nucleation of the equilibrium (or metastable) precipitate. This is the mechanism observed for In additions to Al–Cu. For reasons similar to nucleation on grain boundaries, interphase boundaries provide a means to reduce ΔG^* through the destruction of the original interface.

It therefore seems that what the addition of trace elements may do is to encourage two or more heterogeneous mechanisms to operate simultaneously. Site selection is strongly dependent on undercooling and as supersaturation increases an increased number of heterogeneous nucleation sites are utilized.

Previous Work on the Role of Trace Alloying Additions in Al–based Alloys

The catalytic effects of trace additions of solute elements on the precipitation processes in Al–based alloys are reviewed. Table I summarizes such results. For the purpose of this review, trace alloying additions of about 0.1 atomic percent are considered.

Al–Cu Alloys

The first published account of the role of trace alloying additions in age–hardenable Al–based alloys was due to Sully, Hardy and Heal (7). They reported that the addition of 0.05 $\omega t\%$ Sn to a commercial purity Al–4.5 $\omega t\%$ Cu alloy showed a much lower response to natural aging but a marked increase in properties after artificial aging. The authors suggested that the increased rate of artificial aging was associated with initial precipitation of Sn particles which subsequently acted as nuclei for the Cu–rich phase. However, the authors were unable to explain the slower natural aging. The influence of the elements closely adjacent to Sn in the periodic table on the aging characteristics of Al–Cu alloys was examined by a number of investigators who found that small additions ($\sim$ 0.012 at%) of Cd and In to an Al–4.5 $\omega t\%$ Cu alloy had the same general effects (8). Age hardening curves shown in Figure 1 depict the catalytic effects of In on an Al–Cu alloy; the increase in both the rate of aging and the magnitude of hardening at two different aging temperatures is significant (9). The catalytic action of the trace element Sn on the θ' nucleation in Al–Cu alloys was supported by the calorimetric measurements of Polmear and Hardy (10), and Boyd and Nicholson (11). A major shift in the exothermic specific heat peak associated with θ' to a lower temperature when Sn was present suggested that θ' nucleation rates were increased by the presence of Sn in the alloy (10). Boyd and Nicholson (11) later showed that the addition of Cd to an Al–Cu alloy reduces the specific interfacial enthalpy for θ' by a factor of approximately six.

Several explanations were provided for the two distinct effects, i.e. suppression of GP zone formation and acceleration of θ' nucleation, which were thought to be the typical features associated with the trace alloying additions to Al–Cu alloys. For the former effect, Hardy (4,9) first suggested that the large trace element atoms act as traps for the small solute atoms (owing to the strain energy effects) thereby decreasing the number available for GP zone formation. However, as was later pointed out by Kelly and Nicholson (3). there are two objections to these theories: firstly, such a cluster of solute atoms would act as a nucleus for a GP zone and secondly the relative concentration of the elements in the alloy require that each trace element atom must trap several hundred Cu atoms. An alternative explanation by Silcock (12) was that the presence of strong trace element–vacancy binding prevents excess vacancies from accelerating the diffusion rate of copper at ambient temperature. The high Sn–vacancy binding energy concept was supported by resistivity measurements of Kimura and Hasiguti (13) and transmission electron microscopy studies of Nuyten (14). Silcock's interpretation is realistic since the concentrations of vacancies and trace element atoms are comparable.

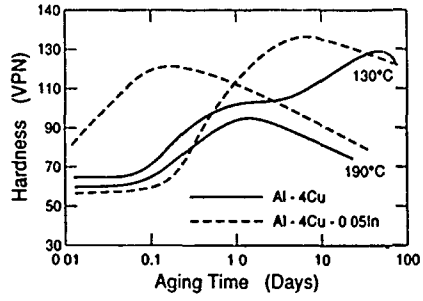

Fig. 1. Age hardening curves for Al-4Cu and Al-4Cu-0.05 wt.%In alloys at 130 C and 190 C (9).

Hardy (9) and Silcock et al. (15) reported that although the tensile strength of Al–Cu alloys is enhanced by cold work before artificial aging, the Al–Cu alloys containing trace additions show the very unusual characteristic that their tensile properties are diminished. They suggested that a high density of dislocations introduced during cold work could interfere with the normal action of trace additions in two ways: firstly, the trace element atoms may be adsorbed along dislocations, and secondly, a rapid heterogeneous precipitation of trace elements upon dislocations, which would be non–coherent, may occur. This implies that prior matrix precipitation of the trace elements is necessary in a form that

is capable of influencing the θ' nucleation. The presence of a high density of dislocations in the matrix may also act as sinks for the vacancies which would further hinder the matrix precipitation of the trace elements.

There have been numerous attempts to explain the accelerated aging response at higher than ambient temperatures. Nuyten observed that during artificial aging θ' nucleated heterogeneously on the dislocation loops that resulted from the Cd additions. Other investigators (16,17) suggested a similar mechanism associated with Cu/Cd/vacancy clusters. Hardy (8,9) and Silcock (12) suggested that prior precipitation of Cd, In, and Sn particles could act as heterogeneous nucleation sites for the θ' phase. Using X-ray diffraction, Silcock et al. (15) showed that during elevated temperature aging, the precipitation of θ' in Al–Cu alloys containing minor additions is accompanied by the appearance of some anomalous diffraction effects (designated P and In'). The P diffraction effects increased in intensity continuously until the ternary alloys (Al–Cu–In,Cd,Sn) reached peak hardness, whilst aging to beyond peak hardness increased the size of the θ' platelets, removed the P diffraction, and increased the In' diffraction intensity. The authors suggested that the P diffraction effects were associated with a new interface structure between θ' and the matrix which formed by the absorption of the trace element atoms: "if the ternary atoms were concentrated close to the surface of disregistry of the θ' platelets with the matrix, i.e. the surface parallel to [100] θ', it is very reasonable to assume that they would enter into the θ' (or the aluminum) lattice to allow improved registry between the matrix and θ' planes" (15). The authors did note, however, that the origin of the P diffraction effects were unclear and those from the tin-containing alloys (P_{Sn}) were different from those of the alloys with Cd and In additions.

Sankaran and Laird (18) provided direct evidence for the presence of Cd, In and Sn particles at the edges of θ' plates. The authors suggested that the trace elements first segregate and subsequently precipitate at the edges of the θ' plates. It may, however, be noted that no direct evidence for the segregation of trace element atoms to the edges of θ' plates, which is rather difficult to obtain, was provided by the authors. Other investigators (19–22) using TEM and EDX microanalysis showed that at the very early stages of aging (200°C for 1 minute) very fine In (Cd & Sn) precipitates form. The authors found no evidence for the segregation of trace element atoms around the periphery of θ' precipitates; rather, it was shown that upon subsequent aging these fine precipitates act as heterogeneous nucleation sites for the θ' phase. Our recent research (23) has supported this analysis.

Figure 2 shows the precipitate morphology in an Al–4.0 Cu–0.15 ωt%In alloy which has been aged for 5 minutes at 200°C after solution treatment and quenching. Association of many of the θ' precipitates with fine "dark spots" (arrowed in the micrograph) is noteworthy, and such observations are similar to those reported by Suzuki et al. (19) in a similarly treated material. Qualitative EDX–microanalysis on one such "dark spot" revealed spectra of Al, Cu and In suggesting that the "dark spots" are In–bearing precipitates (23).

Our experimental studies, along with those of others, suggest the following explanation for the role of trace additions of Cd, In and Sn in Al–Cu alloys. These elements (Cd,In & Sn) have a higher binding energy with vacancies than either Al or Cu and trap the vacancies during quenching. Since the vacancies are associated with the trace elements they are not available to aid the nucleation of Cu–rich clusters at ambient temperature. During subsequent artificial aging fine precipitates of the trace elements form throughout the matrix and the vacancies are released. The vacancies now become associated with the Cu atoms, accelerating their diffusion kinetics. The interfaces of the trace element particles serve as heterogeneous nucleation sites for θ' precipitation. The binary aging sequence , i.e. GPZ (discs) → θ'' (discs) → θ' (plates) → θ (Al_2Cu), begins with θ' since heterogeneous sites are provided by particle:matrix interfaces. This also yields a larger volume free energy change than if GPZ or θ'' had precipitated.

Fig. 2. Precipitation morphology in the heat treated (200 C for 5 mins.) Al-4Cu-0.15 wt.%In alloy. <011> aluminum orientation. (23)

Al–Cu–Mg Alloys

The effects of trace elements on the precipitation in Al–Cu–Mg alloys were studied by Brook and Hatt (24) using alloys containing aluminum of different purities. They observed that high purity Al(3.3–4.0)Cu–0.2 ωt% Mg alloys harden appreciably at 30°C by formation of both GP and ternary GPB zones but at 165°C peak hardness is associated with θ'' precipitation. In a comparable alloy, but containing 0.1 at.% Si as an impurity, a smaller amount of GP zones and no GPB zones were formed at 30°C. During aging at 165°C, θ'' precipitation was followed after 16h by θ' precipitation and P diffraction effects similar to those discussed earlier for Al–Cu–In alloys. Brook and Hatt associated this observation with an electrochemical interaction between Mg and Si leading to the formation of the Mg_2Si phase (24). These results led the authors to add Ge (0.19 at%) to the ternary Al–Cu–Mg alloy, as the binary phase Mg_2Ge also involves high enthalpy of formation. Although the amount of Ge (0.19 at%) used was higher than the usual amount of trace alloying element (i.e. $\leq$ 0.1 at%) being added, it is worth mentioning that compared to silicon, the Ge addition was found to have a much superior influence on the artificial aging response of the Al–Cu–Mg alloys. The electron diffraction effects obtained from the artificially aged Al–Cu–Mg–Ge alloy were also found to bea striking similarity with those found in similarly treated Al–Cu–In alloys (15). These results indicate that the role of the Mg_2Ge particles in θ' nucleation may be similar to that of the In–particles in Al–Cu–In alloys (19). Further studies by Brook and Hatt (24) revealed that the strength properties in Ge bearing alloys remain almost unaffected by cold work prior to aging at 165°C, and that the presence of a much lower amount of Ge (~ 0.02 at%) in the material also accelerated the nucleation process.

Later work on trace element effects in Al–Cu–Mg alloys involved studies of the effects of trace additions of Ag (~ 0.1 at%) on Al–Cu–Mg alloys of varying (Cu+Mg) concentrations and Cu:Mg ratios. In ternary Al–Cu–Mg based alloys of commercial interest, hardening results from GP (Cu,Mg) zone (i.e., GPB zone) formation and heterogeneous nucleation of the S phase on dislocation loops, helixes and dislocation structures.

Siver additions to these alloys enhance the formation of more stable GPB zones (25) implying that Ag has the effect of promoting the ordering processes within the zones; the latter causes an increment in hardening of the precipitates. In addition, Ag has the remarkable effect of inducing nucleation of a homogeneously distributed cubic T phase in the material, rather than the S phase (25–27). The particles of T phase initially grow with increasing aging time but ultimately dissolve in favor of S precipitates which are more finely distributed in the microstructure compared to that in the similarly treated Ag–free alloys (25–27).

Further studies revealed that the influence of Ag additions on the ternary Al–Cu–Mg alloys is sensitive to alloy composition (Fig. 3) (28). For example, when the alloy composition lies in the $(\alpha + \theta + S)$ phase field, Ag additions induce nucleation of a new phase (29–39). Auld and Vietz (29) reported that in an Al–2.5 Cu–0.5 Mg–0.5 ωt% Ag alloy aged for various times in the range 150–350°C, the principal precipitating phase (later designated 'Ω') is in the form of thin hexagonal–shaped plates lying on the {111}Al planes which could be indexed as HCP with a = 4.96 Å and c = 8.48 Å. Recent work by Knowles and Stobbs (38), and Muddle and Polmear (39), however, showed that the Ω phase is in fact orthorhombic with a = 4.96, b = 8.59 and c = 8.48 Å. The Ω phase is believed to be a slightly distorted and chemically modified coherent form of θ (30,38).

Several theories have been proposed regarding the formation of the Ω phase in the Ag bearing Al–Cu–Mg alloys. Muddle and Polmear (39) pointed out that it is the combined action of Mg and Ag which is effective in promoting the formation of the Ω phase. Kerry and Scott (31) and Scott et al. (33) suggested that Mg and Ag lower the stacking fault energy of aluminum and that stacking faults on $\{111\}_{Al}$ planes provide nucleation sites for the Ω phase. Also, Taylor et al. (34) suggested that Mg and Ag may segregate to {111} planes forming fine scale particles of the hexagonal Mg_3Ag phase, which serve both to nucleate the Ω phase and determine the morphology. Muddle and Polmear (39) further pointed out that Ag partitions to the Ω phase, and it is possible that Ag segregates to the Ω/α interface, thus facilitating the Ω nucleation. However, Garg et al. (40) showed that the Ω phase forms in Al–4 Cu–0.5 Mg alloys during aging at higher temperatures, and therefore, Ag is not required for precipitation of the Ω phase. The presence of Ag does, however, greatly enhance the precipitation of Ω at the expense of θ'. The role of Ag on the Ω nucleation in high Cu:Mg alloys is not known.

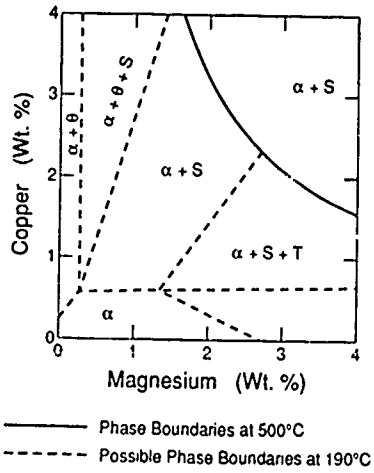

Fig. 3. Isothermal section of the Al-Cu-Mg system (28).

Al–Cu–Li Alloys

Studies of the trace element effects in Al–Cu–Li alloys were first performed by Hardy (4). It was reported that the tensile properties of commercial purity Al–(4–4.5)Cu–1 ωt% Li alloys were greatly enhanced by trace additions of Cd and In, and were affected to a lesser extent by Sn. It was suggested that besides the preferential nucleation of θ' in the Al–θ system by Cd, it is highly likely that Cd exerts a dominant catalytic influence on T_1 (Al_2CuLi) nucleation (4). The T_B phase was not found to be influenced by Cd and this led Hardy (9) to conclude that the ability of Cd to bring about preferential nucleation in Al–Cu–Li alloys is specific to certain precipitates, e.g. to the structural relationships between the precipitates and the matrix. The author (4) further showed that precipitation in an Al–4.4Cu–1 ωt%Li alloy was appreciably influenced by trace additions (~ 0.1 ωt%) of Ga. Later work by Silcock (41) showed that the aging characteristics of Cd bearing Al–Cu–Li alloys are sensitive to the lithium content in the material: additions of small quantities of Li (< 0.1 ωt%) reduce the number of the θ' precipitates, suppresses the P_{Cd} diffraction spots and gives rise to a small increase in the number of the θ'' precipitates. The decrease in the numbers of the θ' precipitates occurs only with small additions of Li up to 0.1%. The amount of θ' increases with further additions of Li and there is only a little difference in the quantity of θ' between an alloy containing no lithium and one containing 0.5 ωt% Li (41).

The first commercial Al–Cu–Li alloy, Alcoa's 2020, utilized the effect of minor alloy additions of Cd to enhance the precipitation of θ' thus negating the need for a stretch prior to aging. Le Baron (42) showed that the strength of Al–Cu alloys increased when lithium was added in combination with a variety of trace additions, particularly Cd, but also Zn, Hg, Ag, Sn, and In. The nominal composition of 2020 was Al–4.5Cu–1.1Li–0.5Mn–0.2 ωt%Cd and the major strengthening phase was θ'.

Silcock pointed out that in high Li–alloys (2–3 ωt%), both Cd–free and Cd–containing alloys form approximately the same quantity of T_1, δ' and θ' precipitates after aging at 165°C. These results suggest that Cd does not have any catalytic influence on precipitate nucleation in these high lithium alloys when aged at 165°C. These effects coincide with the absence of any Cd–precipitate in Al–Li–Cd alloys containing δ' or δ precipitates (41). Implications of the above results are that prior formation of Cd–precipitates during aging is necessary for any acceleration in the aging response to be observed in these alloys, and that Cd additions to commercial high lithium Al–Li–Cu alloys would not therefore be beneficial. The latter interpretation is supported by the more recent work of Blackburn and Starke (43) that Cd additions to an Al–Li–Cu based AA 2090 alloy do not affect the aging behavior of the alloy. The authors (43) further showed that Sn additions to these alloys are also without any influence, whilst In additions do improve the peak–aged strength properties significantly by increasing the number density and homogeneity of both T_1 and θ' precipitates. Our recent results (23) suggest that In plays the same role in the nucleation of T_1 in Al–Li–Cu alloys as it does in the nucleation of θ' in Al–Cu alloys.

The microstructure developed in an AA 2090 alloy with In additions aged at 250°C for 5 minutes is shown in Figure 4. In addition to the spherical Al_3Li δ' phase, the micrograph shows the presence of Al_3Zr (β') and T_1 phases. Close examination of the micrograph reveals that many of the T_1 precipitates are associated with the fine "dark spots". EDX–microanalysis on one spot suggested that they are In–bearing precipitates. Given the existence of a ternary Al–Li–In phase (44), the In–bearing precipitates observed are likely to be different from those found in Al–Cu–In or Al–Cu alloys. However, the present observations, i.e. association of the T_1 phase with the In–precipitates, suggest that In–bearing precipitates act as effective nucleation sites for the T_1 phase.

Such an interpretation is supported by the results of Blackburn and Starke (43) that trace amounts of In in 2090 greatly increase the number density of T_1 precipitates. We suggest that the mechanism is very similar to that which occurs in Al–Cu alloys containing In and/or Cd.

One recent study of trace element effects in Al–Cu–Li–(Mg) alloys explained the influence of Ag additions (0.4 ωt%) on the aging characteristics of Al–4 Cu–(0.13–2.5) Li – 0.3 ωt% Mg alloys (45). Polmear and Chester showed that the hardness of these alloys (at 200°C) is very sensitive to the Li content in the material and that the hardness increases progressively with increasing amounts of Li up to 1 ωt%. A smaller response to hardening was observed in the alloy containing 2.5 ωt% Li. This study showed that Li additions to Al–Cu–Mg–Ag alloys always have the effect of reducing the number density of the Ω phase, whereas at Li levels $\leq$ 1 ωt%, θ' plates are more finely distributed compared to those in the Li free alloy. Lorgan and Pickens (46) investigated the effect of Li concentration on an Al–6.3 Cu–0.4 Ag–0.4 Mg–0.14 Zr–Xωt% Li alloy and observed that peak strength occurred at a Li concentration of ~1.3 ωt.%. The major strengthening in the 1.3% Li alloy was T_1 which precipitated uniformly throughout the matrix. Cold work prior to aging had very little effect on the T_1 phase in the alloy studied. The role that Ag may play in increasing the nucleation frequency of some strengthening precipitates in aluminum alloys will be discussed in detail in the next section.

Fig. 4. Precipitate morphology in the heat treated (250 C for 5 mins.) AA 2090 alloy containing indium. <001> aluminum orientation. (23)

Al–Zn–Mg Alloys

Following the early work of trace element effects in Al–Cu alloys, similar investigations were extended to cover a wide range of potential Al–based alloys. In Al–Cu alloys, effects of Cd additions were found not to be influenced by the presence of magnesium and, therefore, Cd additions were made to 7000 series Al–based alloys. However, Hardy (47) observed that Cd additions did not affect the aging of wrought Al–Zn–Mg and Al–Zn–Mg–Cu alloys. Indium and Sn additions were also found to have no catalytic influence on Al–Zn–Mg based alloys (48,49). These results led Hardy (4) to conclude that if an alloy's strength is increased only slightly or moderately by aging, but raised appreciably by cold work followed by aging then trace additions may enhance the aging response in the absence of preage cold work. The implication was that nucleation is already easy in alloys (e.g. in Al–Zn–Mg alloys) whose response to aging is high and whose strength is unaffected by prior cold work, so that large effects are not expected from the introduction of trace elements (4). However, Hardy's conclusion implies that trace additions only affect strain and/or interfacial energies and not the volume free energy or stability of the precipitate.

Polmear (50–54) showed that trace additions of Ag to Al–Zn–Mg alloys (of varying compositions) enhances the aging response, particularly at high aging temperatures, furthermore, the effect of Ag is not destroyed by cold work prior to aging as in Al–Cu–Cd (In,Sn) alloys. Ag additions to Al–Cu alloys, on the other hand, were also found to have no "trace element" effects (55). It was then realized that the action of Ag in Al–Zn–Mg alloys is different from those of Cd, In and Sn in Al–Cu alloys. The distinctive effects of Ag in Al–Zn–Mg alloys may further be described as follows: a) compared to Cd, In or Sn, a relatively higher amount of Ag is required to obtain the relevant trace element effects. b) Ag additions to Al–Zn–Mg alloys do not suppress GP zone formation, rather, Ag is known to be absorbed into the zones and produces an acceleration of aging with stimulation of the formation of the intermediate η' phase. c) Overaging is reduced, and higher strength is obtained at higher temperature ranges. d) η' precipitates are refined and the PFZs adjacent to the grain boundaries are greatly reduced. These results point out that the role of Ag in Al–Zn–Mg alloys is to enhance both the nucleation frequency, as well as the stability of the η' precipitates.

As was described earlier in this paper, the efficiency of the GP zones to act as the nucleation sites for more stable precipitates in the aging cycle depends on the stability of the GP zones at the aging temperature of interest. The reduction in PFZs adjacent to the grain boundaries in Ag–bearing alloys, therefore, implies greater stability of the GP zones nucleated near the grain boundary region and that excess vacancies are not necessary for homogeneous nucleation at temperatures higher than the critical temperature, T_c in Ag–free alloys (56). Such an interpretation is consistent with the findings of Parker (57) that the upper temperature limit of stability of these zones is raised to 200°C from 120–140°C. The reason for the greater stability of the GP zones is understood to be due to the promotion of internal ordering within the zones in the presence of Ag (58): a higher Ag–Mg bond energy arising out of the electrochemical effects is likely to play a key role in this process. Precise mechanisms responsible for the ability of silver to stimulate nucleation and guarantee the stability of η' at higher temperatures in Al–Zn–Mg alloys are not fully understood, although these effects have been suggested to originate in an interaction between Ag atoms, Mg atoms and vacancies because of the observed sensitivity of these alloys to small changes in Mg:Ag or Mg:Zn ratios (52).

The aging sequence in Al–Zn–Mg alloys, e.g. 7075, is: GPZ (spheres) → η' (plates) → η ($MgZn_2$) (plates or rods). The $MgZn_2$ precipitate (which contain Al and Cu in 7075) is a HCP Laves–type phase. Laves (59) and Laves and Witte (60) have shown that the size and valencies of the elements associated with the compound are important factors in determining the compound's stability. The most important factor appears to be the number of valence electrons/number of atoms in the compound. According to Engel (61,62) and Brewer (63), each crystal structure is characterized by a definite (s+p) electron to atom ratio. The energy of a crystal structure is determined by the promotion energies of electrons to the appropriate (s+p) configuration and the bonding energies of all the (s+p) and unpaired d electrons. The structure with minimum energy represents the stable structure. The importance of e/a ratio on the stability of Laves phases of particular crystal structure types may, therefore, be understood.

The e/a ratio in the $MgZn_2$ phase is 2.0. This implies that the stability of this phase is maximum at an e/a ratio of 2.0. Both Mg and Zn are divalent, so, the presence of a third element within the $MgZn_2$ phase having valency other than 2 would tend to destabilize the phase. Aluminum can dissolve into the $MgZn_2$ phase and hence in Al–Mg–Zn alloys the

presence of trivalent Al in the $MgZn_2$ phase would tend to increase the e/a ratio. Now, in the presence of monovalent Ag in the Al–Mg–Zn alloys, Ag also enters the $MgZn_2$ phase and would, therefore, restore the ideal e/a ratio. In other words, any increase in the e/a ratio in the $MgZn_2$ phase due to trivalent Al would be compensated via a similar decrease in the e/a ratio by monovalent Ag. The presence of Ag in Al–Zn–Mg alloys would, therefore, increase the stability of the $MgZn_2$–based η' phase.

Al–Mg

The poor aging response of binary Al–Mg based alloys is quite marked when compared with the similar behavior of other age–hardenable Al–based alloys. Polmear and Sargent (64) showed that small amounts (0.025–0.08 at%) of Ag may, however, induce hardening in several wrought Al–Mg based alloys which normally do not age–harden. Also, the effects of Ag additions to binary Al–Mg alloys containing higher Mg contents (7ωt%), which age harden, were found to increase both the rate of aging as well as the level of hardening. These effects were evident in the medium temperature range i.e. 120–200°C (64–66). Using X–ray diffraction methods, Auld (66) later investigated the structural changes associated with aging of Al–5 Mg–(0.5–1) ωt% Ag alloys. It was found that at lower temperatures and shorter times, the hardening is due to the formation of spherical Mg–Ag zones (having an AuCuI type structure), and at higher temperatures hardening is due to the precipitation of a ternary T phase, $Mg_{32}(Al,Ag)_{49}$ (66,67). These results reconfirmed the earlier work of Wheeler et al. (68), who, however, pointed out that the Al–Mg alloys with even small additions of Ag should be regarded as ternary precipitation hardening alloys rather than alloys in which Ag had a trace–element effect.

Effects of Cd additions (0.2 ωt%) to Al–10ωt% Mg and Al–10 Mg–0.2 ωt% Ag alloys were studied by Kievits and Zuithoff (69). The authors presented age–hardening curves showing that Cd additions to the binary Al–Mg alloy do not affect the aging behavior of the alloys whereas combined additions of Cd and Ag to the Al–Mg alloy markedly increase the aging response of the material compared to that obtained by an addition of 0.2 ωt% Ag alone. The exact cause of these effects, however, remains unknown.

Al–Zr

In binary Al–(0.1–0.2) ωt% Zr alloys, the nucleation of the metastable cubic Al_3Zr phase (having $L1_2$ structure) of commercial interest is a sluggish process, and requires prolonged aging treatments at higher temperatures for any reasonable distribution of these precipitates to be obtained in the microstructure (70,71). However, a small addition of Si (0.1 ωt%) to these Al–Zr alloys has been found to increase both the rate of aging as well as the level of hardening (72–74) by increasing the nucleation frequency of the coherent Al_3Zr phase. The exact mechanisms by which Si influences the Al_3Zr nucleation, however, are not known.

Al–Li

In Al–Li based alloys, the major strengthening is due to the precipitation of ordered ($L1_2$ type) and coherent δ' (Al_3Li) phases which form during or immediately after quenching throughout the matrix. Occasional nucleation of δ' upon matrix dislocations, and at low angle subgrain boundaries in unrecrystallized wrought alloys has also been observed. In the presence of trace additions of Zr, which is a common addition to Al–Li–X alloys for grain refining purposes, δ' precipitates form heterogeneously on coherent Al_3Zr ($L1_2$ type) precipitates (75,76) resulting in an apparent acceleration of the aging process. The submicron intermetallic compounds, e.g. Al_3Zr, which are utilized to control the grain structure in commercial aluminum alloys frequently provide interfaces for heterogeneous nucleation of precipitates. Often this has a deleterious effect in that it increases the "quench sensitivity" of the alloys. For example large Mg_2Si phases often precipitate on Al_6Mn in Al–Mg–Si alloys and the Mg(ZnCuAl) η phase nucleates on the $Al_{12}Mg_2Cr$ dispersoid particles during slow cooling of Al–Zn–Mg–Cu alloys; both of these reactions remove solute and decrease the amount of strengthening precipitate that forms during subsequent aging.

Trace amounts of Ge in an Al–2 ωt.% Li highlight a second effect (other than influencing nucleation sites) of alloyed precipitates (77). Figure 5a illustrates intense slip bands in the matrix of a binary Al–2.2 ωt.% Li alloy. At

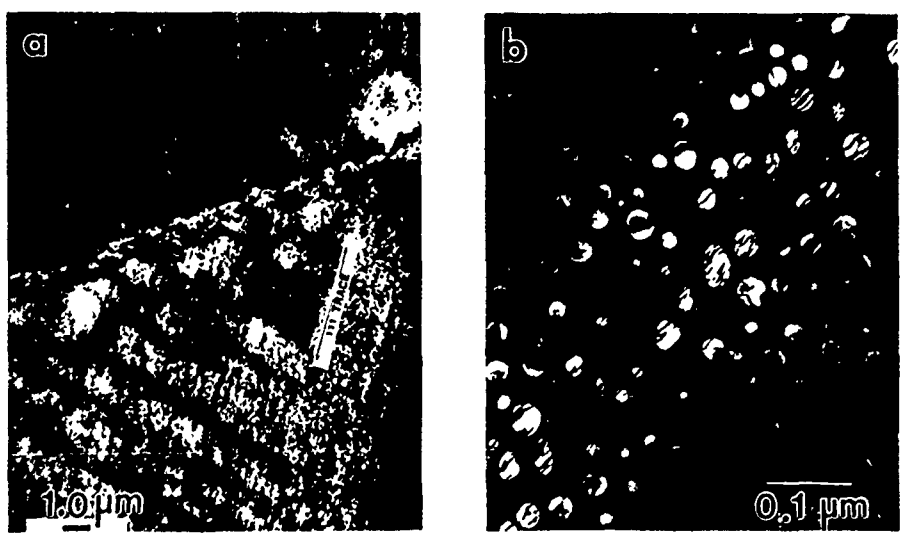

Fig. 5. Deformation structure near the fracture surface of an Al-2 wt%Li alloy. (a) Strain localization in vicinity of grain boundary. (b) Sheared Al_3Li precipitates within slip band. (77)

TABLE I

Effect of Trace Additions (≤0.1 at%) of Solute Elements on Precipitate Nucleation in Al-Based Alloys

Alloy System / Precipitate Influenced	Trace Element Effects						
	Cd	In	Sn	Ag	Si	Zr	Ga
Al-Cu (θ')	Large	Large	Large	-	-	Small	-
Al-Cu-Li (T_1)	Large (in the absence of δ')	Large	-	Not Known	-	Small	Medium
Al-Cu-Mg (Ω)	-	-	-	Large	-	-	-
Al-Zn-Mg (η')	-	-	-	Large	-	Nega-tive	-
Al-Li (δ')	-	-	-	-	-	Large	-
Al-Zr (β')	-	-	-	-	Large	-	-

higher magnification the shearing of δ′ along straight slip lines (Figure 5b) demonstrates slip localization. When 0.2 *wt.*% Ge is added to the alloy the strain is uniformly distributed throughout the matrix (Figure 6a). Pinning of dislocations is apparent in Figure 6b, and is due to the high density of evenly distributed Ge particles in the matrix, which because of significant misfit effectively block dislocation motion.

Summary

The preceding review confirms that trace element additions in aluminum alloys can have a profound effect on the rates at which precipitates form. Also, the effect on nucleation rates is not due to a single mechanism but involves augmenting several heterogeneous sites in the matrix simultaneously. One of the primary mechanisms associated with the trace element effects in Al–based alloys is that the trace elements first precipitate out early in the heat treatment cycle as elemental, or as binary or ternary precipitates (depending on the alloy systems) and these precipitates in turn act as the potential heterogeneous nucleation sites for the intermediate phases of interest during the aging heat treatments. This can allow the bypass of one or more metastable precipitates and thus a more rapid decrease in supersaturation.

This is demonstrated in the role of In in Al–Cu–Li based alloys together with the earlier results of the trace element effects in Al–Cu–Cd (/In or Sn) and in Al–Cu–Mg–Si (/Ge). Results show that aging enhancement in alloys containing trace elements is caused by the preferential nucleation of the intermediate phases of interest at numerous

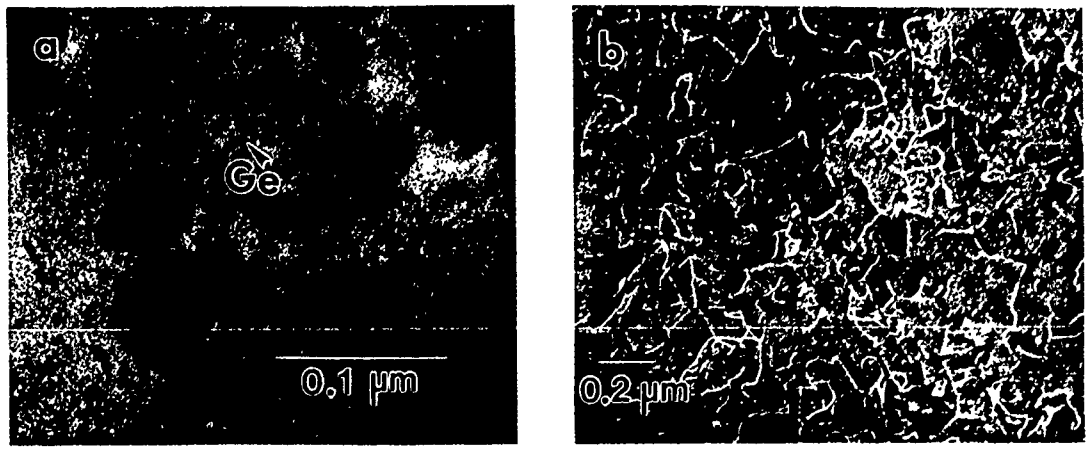

Fig. 6. (a) Transmission electron micrograph showing germanium particles in Al-2.0Li-0.2Ge after aging 3 h at 200 C. (b) Dark field TEM image of deformation structure in the matrix after stretching 2%. Note homogeneous dislocation structure and dislocations pinned at the germanium particles. (77)

fine trace element–bearing precipitates which form at the early stages of the aging cycle.

Trace additions can alter nucleation rates through electronic contributions (e/a ratios). In Al–Cu–Mg alloys Ag additions promote ordering in GPB zones as well as inducing nucleation of the T phase over the S phase, while the effect of Ag in Al–Zn–Mg alloys is to enhance both the nucleation rate, as well as the stability of η' precipitates through modification of the electronic structure.

Finally trace elements, such as Ge, can precipitate directly and affect the properties directly by effectively blocking dislocation motion and homogenizing strain.

Acknowledgements

EAS and AKM wish to acknowledge support from the Office of Naval Research, Contract #85–K–0526, Program Monitor, Dr. George R. Yoder. GJS acknowledges support from the Department of Energy through grant DE–FG05–89ER45389.

References

1. A. Wilm, Metallrgie, 8, p 225, 1911.
2. P. D. Merica, R. G. Waltenberg and H. Scott, Scientific papers of the Bureau of Standards, 15, (347), p 271, 1919.
3. A. Kelly and R. B. Nicholson, Prog. in Mat. Sci., 10, p 48, 1963.
4. H. K. Hardy, JIM, 84, p 429, 1955–56.
5. G.W. Lorimer and R.B. Nicholson, in "The Mechanism of Phase Transf. in Cryst. Solids," Inst. of Metals, London, p 36, 1069.
6. W.A. Cassada, G.J. Shiflet and E.A. Starke, Jr., Jnl. de Physique, colloq. C3, 48, p 397, 1987.
7. A. H. Sully, H. K. Hardy and T. J. Heal, JIM, 76, p 269, 1949.
8. H. K. Hardy, JIM, 78, p 169, 1950–51.
9. H. K. Hardy, JIM, 80, p 483, 1951–52.
10. I. J. Polmear and H. K. Hardy, JIM, 83, p 393, 1954–55.
11. J. D. Boyd and R. B. Nicholson, Acta Met., 19, p 1101, 1971.
12. J. M. Silcock, Phil. Mag. (8), 4, p 1187, 1959.
13. H. Kimura and R. R. Hasiguti, Acta Met., 9, p 1076, 1961.
14. J. B. M. Nuyten, Acta Met., 15, p 1765, 1967.
15. J. M. Silcock, T. J. Heal and H. K. Hardy, JIM, 84, p 23, 1955–56.
16. E. Holmes and B. Noble, JIM, 95, p 106, 1967.
17. B. Noble, Acta Met., 16, p 393, 1968.
18. R. Sankaran and C. Laird, Mat. Sci. & Engn., 14, p 271, 1974.
19. H. Suzuki, M. Kanno and O Kanoh, J. Jpn. Inst. Light Metals, 44, p 1139, 1980.
20. H. Suzuki, M. Kanno and K. Fukunaga, J. Jpn. Inst. Light Metals, 25, p 413, 1975.
21. H. Suzuki, M. Kanno and O. Kanoh, J. Jpn. Inst. Light Metals, 29, p 223, 1979.
22. H. Suzuki, M. Kanno and M. Fujii, J. Jpn. Inst. Light Metals, 26, p 391, 1976.
23. A.K. Mukhopadhyay, G.J. Shiflet, and E.A. Starke, Jr., unpublished research, University of Virginia.
24. G. B. Brook and B. A. Hatt, in "The Mechanism of Phase Transfs. in Crystalline Solids," Monograph No. 33, Institute of Metals, p 82, 1969.
25. N. Sen and D. R. F. West, in Ref. 32, p 59.
26. J. H. Auld, J. T. Vietz and I. J. Polmear, Nature, 209, p 703, 1966.
27. J.T. Vietz and I.J. Polmear, JIM, 94, p 410, 1966.
28. J.M. Silcock and B. A. Parsons, Fulmer Res. Inst. Report, R 10/67, 1958.
29. J.H. Auld and J.T. Vietz in Ref. 32, p 77.
30. J.H. Auld, Acta cryst. A28, 598, 1972.
31. S. Kerry and V.D. Scott, Metal Science, 18, p 289, 1984.
32. J.H. Auld, Mat. Sci. Technol., 2, p 784, 1986.
33. V.D. Scott, S Kerry and R.L. Trumper, Mat. Sci. Technol., 3, p 827, 1987.
34. J. A. Taylor, B. A. Parker and I. J. Polmear, Met. Sci., 12, p 478, 1978.
35. R. J. Chester and I. J. Polmear, Micron, 10, p 311, 1980.
36. R. J. Chester and I. J. Polmear, The Metallurgy of Light Alloys, Inst. Met., London, p 75, 1983.
37. I.J. Polmear and M.J. Couper, Met. Trans., 19A, p 1027, 1988.
38. K. M. Knowles and W. M. Stobbs, Act. Cryst., B 44, p 207, 1988.
39. B. C. Muddle and I. J. Polmear, Acta. Metall., 37, (3), p 777, 1989.
40. A. Garg, Y. C. Chang and J. M. Howe, Scr. Metall., 24, (4), p 677, 1990.
41. J. M. Silcock, JIM, 88, p 357, 1959–60.
42. I.M. Le Baron, U.S. Patent no. 2,381,219, Application date 1942, Granted 1945.
43. L. Blackburn and E.A. Starke Jr. in Vol. II, Proc. Al–Li V, (ed. T.H. Sanders, Jr. and E.A. Starke, Jr.), p 751, 1989.
44. M. Yahagi, K. Kuriyama and K. Uwamura, Jpn. J. Appl. Phys., 14 (3), p 405, 1975.
45. I. J. Polmear and R. J. Chester, Scr. Metall., 23, p 1213, 1989.

46. T.J. Langar and R. Pickens, in Aluminum–Lithium Alloys V, eds. T.H. Sanders and E.A. Starke, Jr., Materials Component Engineering Publs. Ltd, Birmingham, UK, Vol II, p 701, 1989.

47. H. K. Hardy, JIM, p 657, 1951.

48. L. F. Mondolfo, "Aluminum Alloys: Structure and Properties", Butterworths, London, p 859, 1976.

49. Y. Baba, Trans. JIM, 2, p 406, 1970.

50. I. J. Polmear, Nature, 186, p 303, 1960.

51. I. J. Polmear, JIM, 89, p 51, 1960–61.

52. I. J. Polmear, JIM, 89, p 193, 1960–61.

53. J. T. Vietz, K. R. Sargant and I. J. Polmear, JIM, 92, p 327, 1963–64.

54. I.J. Polmear, J. Aust. Inst. Metals (JAIM), 17, p 1, 1972.

55. Y. Baba, Sumitomo Light Metal Tech. Rep., 10, (2), p 9–17, 1968.

56. E.A. Starke, Jr. Jnl. Metals, Jan. 1970, p 54, 1970.

57. B. A. Parker, JAIM, 17, p 31, 1972.

58. I. J. Polmear, Materials Science Forum, Volumes 13/14, p 195, 1987.

59. F. Laves, Crystal Structure and Atomic Size, in Theory of Alloy Phases, ASM Seminar, Metals Park, OH, 1955.

60. F. Laves and H. Witte, Metallwirtschaft, 14, p 645, 1935; 15, p 840, 1936.

61. N. Engle, Amer. Soc. Metals, Trans. Quart., 57, p 610, 1964.

62. N. Engle, Acta Met., 15, p 557, 1967.

63. L. Brewer, in Alloying, eds. J. Walter, M. Jackson, and C. Sims, ASM Inter., Metals Park, OH, p 1, 1988.

64. I. J. Polmear and K. R. Sargant, Nature, 200, p 669, 1963.

65. I. J. Polmear, Trans. Met. Soc. AIME, 230, p 1331, 1964.

66. J. H. Auld, Acta Met., 16, p 97, 1968.

67. J.H. Auld and B.E. Williams, Acta cryst., 21, p 830, 1966.

68. M. J. Wheeler, G. Blankenburgs and R. W. Staddon, Nature, 207, p 746, 1965.

69. J. Kievits and A. J. Zuithoff, JIM, 93, p 517, 1964–65.

70. W. Dahl, W. Gruhl, W. G. Burchard, G. Ibe and C. Dumitrescu, Z. Metallkd., 68, (3), p 188, 1977.

71. S. Hori, S. Saji and T. Kobayashi, J. Jpn. Inst. Met., 37, (10), p 1134, 1973.

72. S. Hori, T. Kondo and S. Ikeno, J. Jpn. Inst. Light Met., 28, (2), p 79, 1978.

73. S. Hori, S. Saji and Y. Higaki, J. Jpn. Inst. Light Met., 25, (7), p 246, 1975.

74. H. Westengen, O. Reiso and L. Auran, Aluminum, 56, (12), p 768, 1980.

75. F. W. Gayle and J. B. Vanderande, Scr. Metall., 18, p 473, 1984.

76. P. J. Gregson and H. M. Flower, J. Mat. Sci. Lett., 3, p 829, 1984.

77. W.A. Cassada, G.J. Shiflet, and E.A. Starke, Jr., Acta Met., 34, p 367, 1986.

DISTRIBUTION LIST

1 - 3 Office of Naval Research
800 N. Quincy Street
Arlington, VA 22217-5000

Attention: Dr. George R. Yoder, Program Manager
Materials Division, Code 1131

4 - 9 Director
Naval Research Laboratory
Washington, DC 20375

Attention: Code 2627

10 - 21 Defense Technical Information Center, S47031
Building 5, Cameron Station
Alexandria, VA 22314

22 Mr. Michael McCracken
Administrative Contracting Officer
Office of Naval Research Resident Representative
Code N66002
National Academy of Sciences
2135 Wisconsin Avenue, N.W., Suite 102
Washington, DC 20007

23 - 24 E. A. Starke, Jr.

25 - 26 E. H. Pancake, Clark Hall

27 SEAS Preaward Administration Files

JO#3927:ph